ScuDo
Scuola di Dottorato ~ Doctoral School
WHAT YOU ARE, TAKES YOU FAR

Doctoral Dissertation
Doctoral Program in Chemical Engineering (30th Cycle)

Renewable Power to Fuels: Dynamic Modeling of Slurry Bubble Column Reactor in Lab-scale for Fischer-Tropsch Synthesis under variable loads of synthesis gas

By

Siavash Seyednejadian

******

Supervisor(s):
Prof. S. Bensaid
Prof. G. Saracco

Doctoral Examination Committee:
Prof. Stefano Cimino, Istituto Di Ricerche Sulla Combustione Irc-Cnr
Prof. Salvatore Abate, Universita degli studi di Messina

Politecnico di Torino
2018

Declaration

I hereby declare that, the contents and organization of this dissertation constitute my own original work and does not compromise in any way the rights of third parties, including those relating to the security of personal data.

Siavash Seyednejadian

2018

* This dissertation is presented in partial fulfillment of the requirements for **Ph.D. degree** in the Graduate School of Politecnico di Torino (ScuDo).

I would like to dedicate this thesis to my lovely family

Acknowledgment

First of all, I would like to thank my supervisor, Prof. Samir Bensaid for all his supports, helps and patience during the past three years. Further, I would like to thank Prof. Guido Saracco for helping me kindly during my work in Polytechnic University of Turin.

I also would like to thank Prof. Reinhard Rauch and Prof. Hermann Hofbauer in Karlsruher Institute of Technology (KIT) and Technical University of Vienna (TU Wien) for giving me the possibility to work at TU Wien as a research scholar for 6 months, during my Ph.D. research.

Abstract

In recent years, Renewable Power to Fuels technology is becoming a vitally important pathway from the value-added products point of view. This electricity-to-fuel transformation is regarded as an efficient way not only to preserve renewable energy (i.e. wind and solar) and to offset the fluctuating nature of these sources but also to generate synthesis fuels with respect to the demand for, the capacity limitation and the existing infrastructure of the targeted products. In this sense, many E.U. countries are transforming CO_2 into clean and the carbon-free products to achieve the targets of greenhouse gas (GHG) emissions. With regards to the renewable energy action plan, each E.U. country has a contribution target to reach by 2020: Italy's overall target is to reach 17% of contribution, and it has already surpassed this (it reached 17.5% by the end of 2015). Germany is aiming for 35%, whereas Austria has a targeted of 34% [1].

In this study, two main scenarios through Power to Fuels conversion are considered: 1) Power to Gas (PtG) technology (methanation process); 2) Power to Liquid (PtL) technology based on Dimethyl ether (DME), a direct one-step process, and Low Temperature Fischer Tropsch (LTFT) process. Therefore, the conceptual design of all three processes based on a Solid Oxide Electrolysis Cell (SOEC) is analyzed. In the optimized configuration of methanation, a methane fraction of 95% at the outlet is achieved, which is compatible with the existing pipeline network. The main challenge of this technology is the lack of accurate and explicit kinetic data for its catalyst. Also, the heat released from methantion and its utilization for providing the heat required for electrolysis is another issue in the latest configuration of methanation. In DME synthesis, four explicit Langmuir Hinshelwood Hougen Watson (LHHW) kinetics were implemented in Software Aspen plus. The main challenge in one-step direct DME synthesis (based on renewable energy) is the low value of yield and selectivity of the DME product (15% and 78% in the once-through process, respectively). However, the separation process and recycling of unreacted syngas in order to achieve high purity of the DME product is quite complex due to the presence of the unreacted syngas and the CO_2 produced in the one-step synthesis process. Above all, it leads to higher operational costs. In the optimized configuration of LTFT based on renewable energy, a comprehensive simulation was conducted. To model an FT reactor, an external subroutine within an Excel spreadsheet through USER2 MODEL on the simulator was implemented. It was found that total efficiency of the system was achieved at 76.6 %. However, the main challenge of this

configuration is the low value of liquid products due to the low capacity of the SOEC.

Having considered the challenges and limitations of each process, it is concluded that FT synthesis is more interesting to model due to the complexity of the products and the more highly developed catalyst and reactor used. As a consequence, this dissertation mainly focuses on the dynamic modeling of a Fischer-Tropsch Slurry Bubble Column Reactor (FT-SBCR), which is considered as the best candidate for Fischer-Tropsch synthesis. In the dynamic modeling of FT-SBCR, a comprehensive computer model was developed to investigate flexible reactor operation. This flexibility was performed by a step-change of syngas flow rate load (3.5, 5, 7.5 m^3/h) in a low-temperature Fischer–Tropsch synthesis. It was found that the dynamic simulation is not only able to predict all Fischer–Tropsch components over the reactor bed but can also describe the behavior of superficial gas velocity as a sub-model using the overall gas mass balance. The effects of a step-change volumetric syngas flow on the performance of the FT slurry reactor, CO conversion and α-value, as well as information about the inside of reactor were investigated. The results show that the temperature distribution of the slurry reactor remains constant under base load and change load conditions. It is concluded that load change conditions do not have a negative influence on the temperature distribution inside the reactor and the dynamic model of the slurry reactor presented responds quite well to the load change conditions.

Contents

List of Figures

List of Tables

Chapter 1

Introduction

1.1 Overview

Many European countries are transforming CO_2 into clean and carbon-free products to achieve the targets of greenhouse gas (GHG) emissions. This is due to a number of factors: the proliferation of renewable energy, increasing CO_2 emissions, dwindling oil resources and environmental issues. Concerns over CO_2 reduction require a switch from Renewable Energy Sources (RES) to storable energy initiating carbon capture and storage/usage (CCS/U) projects and ensuring sufficient sustainable energy sources [2]. Potential CO_2 sources include biogas facilities, biomass gasification, and blast furnace off gases or atmosphere [3]. In this respect, the EU's renewable energy action plan has set a target of at least 20% final energy consumption from renewable sources by 2020. Each E.U. country has a contribution target: Italy's overall target by 2020 is to reach 17% of contribution, and it has already surpassed its target (it reached 17.5% by the end of 2015). Germany is aiming for 35% whereas Austria stands at 34% [1].

This transformation of electric energy-to-fuel can be considered as an efficient way not only to conserve renewable energy (i.e. wind and solar) and to offset the fluctuating nature of these sources but also to generate synthesis fuels with regards to the demand for, the capacity limitation and the existing infrastructure (transport and end-use) of targeted products. In this sense, installed capacity and demand for hydrogen are moderately small compared with liquid fuel such as gasoline, naphtha and diesel. Furthermore, increasing petroleum

prices tend to promote more production of synthesis fuel from renewable resources [4].

The basic challenge is how to deal with stable molecule CO_2 through potential CO_2 dissociation technologies, preferably in zero-net carbon emissions process. In general, there are three energy sources for CO_2 reduction: 1) heat 2) electricity 3) light, each of which has several process pathways to obtain sustainable liquid hydrocarbons. For instance, Artificial Photosynthesis is a potential technology which has a capability to use light as an energy source for CO_2 dissociation. However, this method is limited by low capacity and efficiency. In this dissertation, we focus on Electricity source coming from Renewable Energy (RE). Figure 1 illustrates a close CO_2 loop utilizing emitted CO_2 (and water) back into synthetic hydrocarbons as fuel. [5] In this way, if hydrogen comes from a carbon-neutral source i.e. electrolysis coupled with renewable energy, then it is possible to assert a virtually 100% carbon conversion in the final utilization. However, hydrogen produced from a carbon source such as steam reforming of methane (SRM) is still an attractive and viable option due to its capability for operation in large-scale production. Hydrogen from carbon-free sources is hindered by the considerable investment cost attributed to solar panels, wind turbines and electrolysis [6].

The product of this CO_2 dissociation is synthesis gas (syn-gas) which is composed largely of H_2 and CO plus some impurities depending on the source of syn-gas generation. After its generation, the downstream of fuel production is required. The desired Products are methane, methanol, Dimethyl Ether (DME) and other practical liquid fuels in the transport sector such as gasoline, diesel and kerosene.

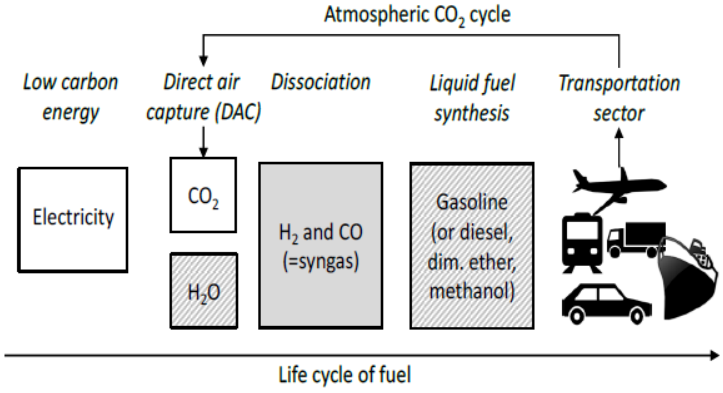

Figure 1: A schematic view of Carbon-Neutral Free Process [5].

These liquid products are referred to with the term “drop-in”. This means they can be directly used in the existing internal combustion engine hybrids and fuel cells without any modification in the infrastructure of downstream of fuel production [5]. The main process of drop-in fuel production from syngas with usage ratio (H_2/CO=2) under catalyst Co or Fe in low temperature range (between 220 to 260 $^{\circ}$C) is known as the Fischer-Tropsch process which was developed by two German scientists named Franz Fischer and Hans Tropsch in 1925. In recent years, FT synthesis gathered significant attention in reactor modeling, process design and optimizing product selectivity.

In general, this variety of products (Gaseous and Liquid) arises from two main scenarios through fuel conversions:

1) Power to gas technology (PtG) (Products: Methane during methanation process)
2) Power to liquid technology (PtL) (Products: DME and drop-in fuels respectively, during dehydration of methanol and Fischer-Tropsch synthesis)

With PtG and PtL technologies, entire elements of the final energy mix (feedstock, gaseous and liquid products, and electricity) at the final utilization can be successfully obtained while substantially reducing CO_2 emissions [7].

The main challenge of renewable power grids arises from the fluctuating nature of power generation e.g. wind power and photovoltaic and decentralized capacities of the electricity distribution system. To overcome this intermittent behavior, chemical storage and transport technologies are considered as fundamental solutions for providing storage capacities and stabilizing seasonal imbalances. One approach to improve the recovery of CO_2 and produce liquid and gases fuel is to use this electricity. One highlight of this method is that the long-time storage of high energy density resources is more feasible [2]. The major benefit of PtG and PtL is the fact that they relax the main limit of large scale transport by converting renewable energy into liquid and gaseous mediums [7].

1.2 Power to Gas Technology (PtG)

PtG utilizes electricity to energize an energy carrier such as carbon or hydrogen to manufacture hydrocarbon gas or pure hydrogen. As a case in point, coupling high temperature electrolysis (SOEC[1]-based) with methanation is a promising approach because it exploits heat released from exothermal methanation to supply steam for electrolysis. Since the reaction is extremely exothermic the heat must be managed in order to prevent catalyst degradation and thermodynamic limitation of the process. At small scales of Power-to-gas processes isothermal reactors are usually preferred due to coolant fluid which directly cools the reactors. However, in large scale applications temperature control is achieved by a series of adiabatic fixed bed reactors with inter-cooling of the stream between each reactor [8]. Amongst these technologies, the integration of methanation section with two isothermal and adiabatic reactors in T=300 k and P=30 bar is considered as a very efficient and cost-optimized process because the vaporization of heat required for high-T electrolysis can be provided by the exothermal methanation. This project (HELMETH) has recently been financed by European Union's seventh Framework program. (http://www.helmeth.eu)

Figure 2 illustrates the schematic diagram of power to gas technology. Electric power is employed in an efficient way if the available grid capacities are sufficient. Electric power utilization can be elevated by producing higher demands. If supply takes over power demand, renewable power stations (wind and photovoltaic) need to be shut down and the proper full capacity of the plant would not be met. Therefore, transport and storage technology becomes indispensable by the continuous increase in usage of renewable energies. In a practical way, analyzing total efficiency can be performed by reconversion of Substitute Natural Gas (SNG) into power and heat. This shifting of electricity is realized as Power to Power (P2P) in Combined Cycle Power Plant (CCPP) or Combined heat and power (CHP) [9]. Therefore, repowering of hydrogen or methane to electricity in Combined Cycle Plants closes the loop of power-SNG-power and generates the potential to produce electricity power in regions not close to the sources, however connected with a gas grid. The spread of this re-shifting for providing electricity demand is hindered by loss of efficiency and high costs. [10].

[1] Solid Oxide Electrolysis Cell

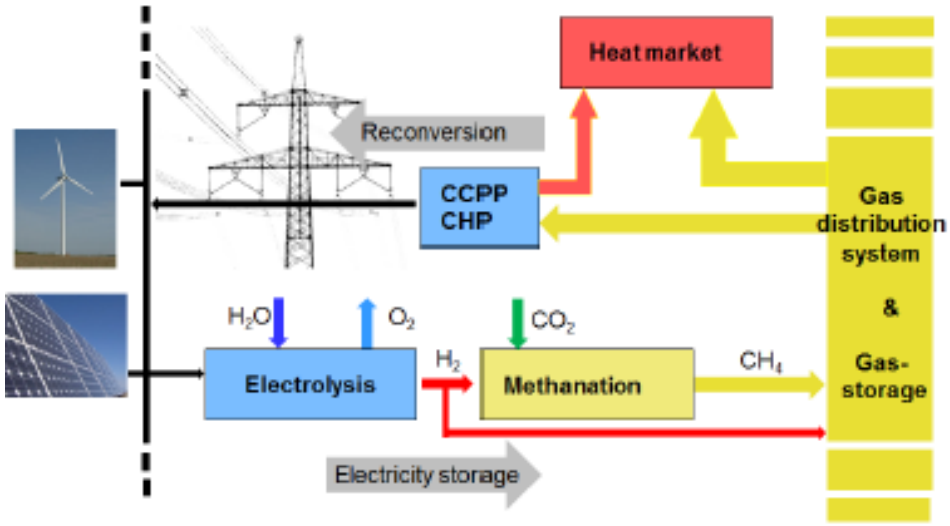

Figure 2: Power to Gas technology Diagram including reconvention into electrical power [9].

1.3 Power to Liquid Technology (PtL)

PtL technology has attracted a lot of attention in transforming syngas to synthetic fuel products because there is no loss during long-term storage, it has wide-ranging applications in the transport sector and high energy density with existing infrastructures [11]. There are two main pathways in PtL scenario, the Fischer-Tropsch (FT) pathway and the Dimethyl Ether (DME) pathway.

In the Fischer-Tropsch process, liquid fuel such as gasoline, diesel, naphtha, jet fuels and other chemicals from synthesis gas are produced through an appropriately engineered catalyst and reaction conditions. Conventionally, synthesis gas is generated by biomass or coal gasification (CtL) or Steam Methane Reforming (SMR). The former process generates significant amounts of CO_2, whereas SMR requires a considerable amount of heat energy input [7]. In this conventional FT process Carbon Conversion Efficiency (CCE) reaches only from 25 to 50 % [12]. However, hydrogen produced from SOEC with the aid of renewable energy and CO_2 reduction in reverse water gas shift (RWGS) can achieve efficiency of up to 70 % in the Fischer Tropsch reactor [6]. The source of CO_2 can be provided from the atmosphere by the direct CO_2 capture equipment (designed by Swiss firm Climworks AG [13]). Figure 3 demonstrates a rig converting water and CO_2 into high purity liquid fuel (petrol, diesel, kerosene). Firstly, hydrogen is produced using steam in SOEC with the aid of renewable electricity then, the yielded hydrogen reduces CO_2 to reverse water gas shift (RWGS). Afterwards, synthesis gas produced from RWGS enters the FT reactor to produce transportation products.

The capability of this process is to obtain an almost-100 % conversion of the carbon feedstock using hydrogen that has been derived from non carbon source. This enables coupling RES power connected with electrolysis which provides carbon free cycle in the final utilization [13]. Small scale FT facilities can cut capital costs by reducing the capacity; however it could decrease productivity. This trade-off relatively depends on the syngas sources. For instance, in biomass-to-liquid (BtL) conversion the capacity of the plant is considered undersized due to biomass transportation expenses, quantity constraints and logistic issues. It could also be profitable to utilize smaller sized facilities for waste-to-liquid (WtL) transformation, enabling decentralized solid waste processing. On the contrary, syngas derived from autothermal reforming or gasification technology with air separation unit must be employed in large scale FT facilities which have the further benefit of generating a high syngas ratio (H_2/CO) [14].

In the DME pathway, the syngas generated is converted to methanol and its dehydrated counterpart Dimethyl Ether (DME). The currently-used fuel delivery system can be enhanced by integrating this pathway in an economical manner and could be utilized for internal combustion engines as well as gas turbines and fuel cells to generate power in combined cycle plants [15]. Details of this process come in next chapters.

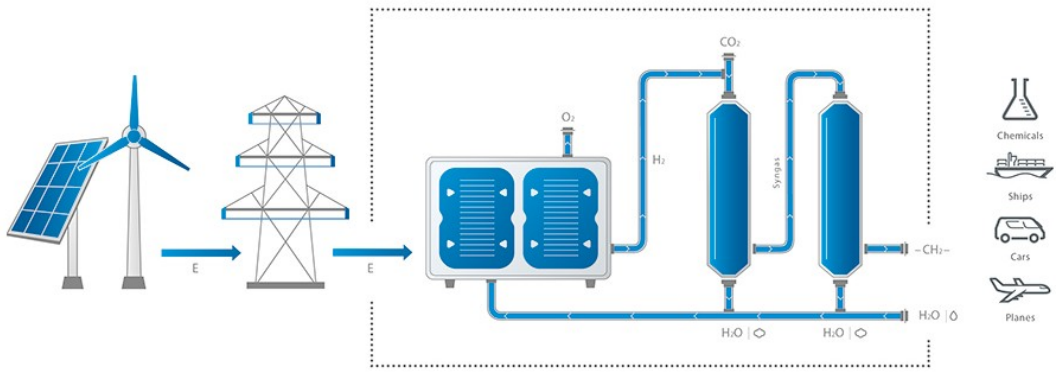

Figure 3: Power to liquid technology proposed by Sunfire Company [13].

Fuels derived from renewable Fischer-Tropsch technology has some advantages compared to other processes such as crude oil-derived fuels and Methanol-to-gasoline (MTG process). One is the absence of impurities, which deactivates the catalyst quickly. Moreover, a large amount of energy is saved in FT because it does not require the energy and hydrogen needed for heavy crude oil [14]. There is also a significant advantage in the FT technology compared to conversion of natural gas into liquid fuel, because more natural gas has been discovered in far-off locations where gas pipelines are not cost-effective [12]. Another benefit of FT liquid fuels compared to H_2 production is the availability of an existing market for these fuels. There are two costs involved in this process. Firstly, the direct costs for producing drop-in fuels which involves more sub-processes for conversion and upgrading leading to higher costs than producing hydrogen from electrolysis. Moreover, the costs for transport to the end-user and constructing the required transportation infrastructures could be a hindering factor compared to the extra costs for gasoline and diesel fuels [16].

1.4 Types of Fischer-Tropsch Reactor

Designing of all types of Fischer-Tropsch reactors deals with the complex nature of FT synthesis as well as the difficulty to manage the thermophysical aspects of the FT reaction blend. Since the reactor is considered as the heart of PtL process, well-designed reactors make the process more efficient with higher productivity. In general, there are four types of FT reactor: 1) Multi-tublar Fixed Bed, 2) Fixed Fluidized bed 3) Circulating Fluidized bed, 4) Slurry Bed Reactors. In this respect, each new design for an FT reactor aims to overcome weaknesses in previous models. Figure 4 illustrates the schematic view of each reactor [17].

The first generation of FT reactors at industrial scale was the multitublar fixed-bed reactor which faced major challenges of releasing reaction heat due to highly exothermic reaction. This hurdle led to a new design to control temperature profile over the reactor bed and remove heat efficiently by locating high capacity heat exchangers to cool down the reactor length. This limitation made Sasol Company introduce a Circulating Fluidized Bed (CFB) which operates under bubbling flow pattern whilst the reaction heat is pulled out by cooling tube over the catalyst bed (see figure 4-c). The improved version of FT fluidized bed technology was designed by Sasol Company in 1991 which named it the fixed-fluidized bed reactor, have several benefits over CFB [18]. In general, FT fluidized bed helps to resolve difficulties surrounding temperature control. However, the major drawback of the fluidized beds is wax formation during fluidization process which creates catalyst agglomeration. To eliminate this shortcoming, the fluidized bed reactor needed to be operated at high temperatures causing low selectivity towards desired liquid products (middle distillate and diesel fuel fraction). This constrained motivated reactor designers to take a step forward over FT reactor technology to introduce one of the latest FT reactor technologies known as the Slurry phase distillate (SPD) reactor. In general, there are two types of operations for slurry reactors: 1) mechanically agitated reactors which are mostly employed for semi-batch operation [19] have efficient mass and heat transfer whilst their applications are hindered due to backmixing of the liquid phase and catalyst attrition. 2) Slurry Bubble Column Reactors are normally operated as semi-isothermal modes due to appropriate heat transfer within the well mixed slurry phase. The dispersion of catalyst and liquid (slurry) is performed by means of a gas distributor at the bottom of the column [20]. In addition, this slurry type operates at relatively moderate temperatures which favor the production of clean diesel fuel and middle distillate fraction. These main benefits of slurry reactors with regards to the challenges of previous reactors,

make the slurry reactor the best option in the application of power to liquid fuel technologies.

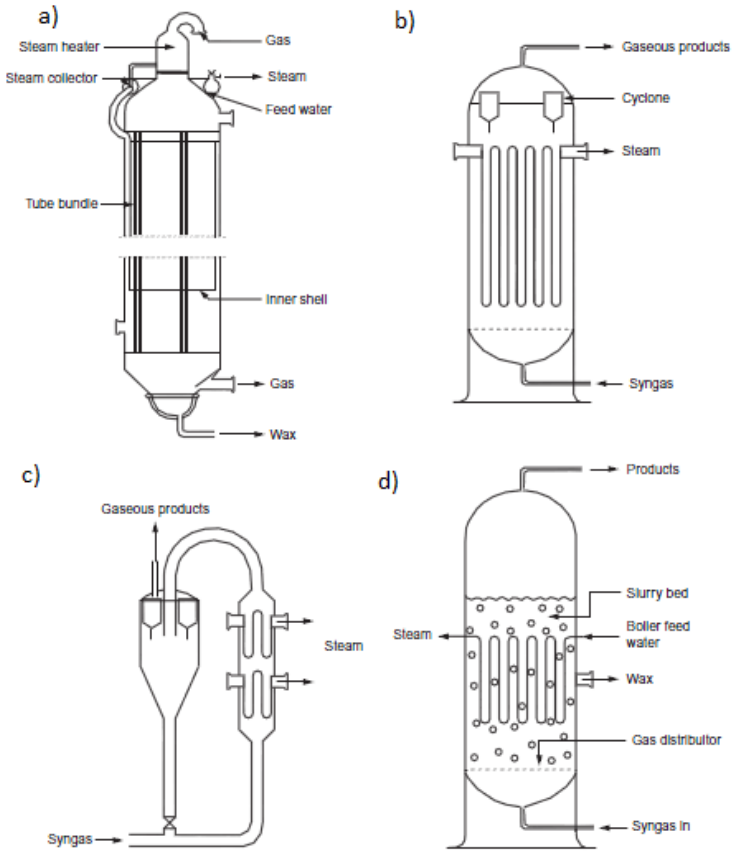

Figure 4: The scheme of four types of Fischer-Tropsch Reactor: a) Multi-tublar Fixed Bed Reactor, b) Fixed Fluidized Bed, c) Circulating Fluidized Bed, d) Slurry Bed Reactor

Table 1: Advantages and Disadvantages of different type of FT Reactor [14][17][21].

Reactors	Advantages	Disadvantages
Multi-tublar Fixed bed reactor	1-easy to operate and scale up	1-High tendency of carbon deposition
	2-simple construction	2-difficulty in temperature control and poor heat transfer inside the reactor
	3-easy separation wax from catalyst	3-elevated pressure drop
	4- Being resistant to syn-gas contaminants such as H_2S.	4-low effectiveness factor due to use of fairly large catalyst pellets.
Fixed fluidized bed	1-Low construction, operating and maintenance cost	1-Poor temperature control
	2-considerable throughput for a single reactor	2-Possibility of clogging the reactor and sintering the catalyst due to uniform & fairly large catalyst particles
	3-low overall catalyst consumption compared to CFB	3-limited application (Generally used for slow and non-deactivating catalysts)
Circulate fluidized bed	1-continuous regeneration of catalyst pellets when catalyst is rapidly deactivated	1-Back-mixing because of random movement of particles leading to loss of selectivity
	2-low possibility of thermal instability, hot spot and runaway	2-Severe erosion of pipes, internals and vessels due to particle abrasion
	3-Efficient solid & gas contacting	3-the entrainment of particles and installation a cyclone for separating purpose

Reactors	Advantages	Disadvantages
Slurry Bed Reactor	1-Excellent heat transfer and flexible temperature control. 2-Efficient inter-phase contacting resulting in a higher productivity 3-Significant catalyst area which leads to better catalyst utilization 4-low pressure drop (Four time less than in FBR)	1-Difficulty in scale up due to complex hydrodynamic features. 2-High possibility of catalyst attrition and erosion 3-Back-mixing of gas phase leading to significant drop in conversion per pass. 4-Difficulty and elevating separation cost of catalyst.

Table 1 lists the advantages and disadvantages of each FT reactor. The main challenge in Multi-tublar fixed bed reactor is the efficient removal of reaction heat and maintenance of a suitable temperature distribution through the length of reactor. To redress this drawback, there are a number of solutions which includes: 1) reducing the tube diameters in order to decrease heat transfer resistance; 2) using catalyst dilution with inert materials [22]; 3) recycling off-gas which increases reaction rate leading to higher overall conversion along the catalyst bed. However, this solution tends to increase operating costs related to recycle reactors e.g. advanced separation units, and high compressor energy demand [14, 23].

The concerning point in Slurry FT reactor is: 1) how to deal with scale up because of the complexity of hydrodynamic features; 2) difficulty with solid/liquid separation design. Above all, there is the issue of maldistribution of the catalyst particles, gas and the liquid phases (back-mixing) affecting the mass transfer and productivity of the reactor, which makes this type of FT reactor attractive to design [14, 21].

1.5 Possibility of flexible operation in FT reactors

In the field of power to fuel technology, flexible analysis of a Low Temperature Fischer-Tropsch (LTFT) reactor under variable operating conditions presents more challenges compared to other value-added processes such as methanation and the Dimethyl ether process. These challenges involve more complexity in FT product selectivity and lower feasibility in the dynamic analysis of an LTFT reactor compared to methanation and the DME synthesis [24].

In this respect, the most suitable FT reactors for analyzing under flexible operation are the Multi-tubular Fixed Bed Reactor and the Slurry Bubble Column Reactor. In the Fixed Bed Reactor (FBR), dynamic analysis addresses the feasibility of reducing the size of H_2 storage and optimizing the temperature profile along the catalyst bed [23], whereas, in the FT Slurry type, the analysis is focused on improving mass transfer phenomena (gas-to-liquid contact and interfacial mass transfer area), leading to enhanced selectivity and catalyst performance with regard to complex hydrodynamic features and scale up issues [25]. During recent years, the Slurry Bubble Column Reactor has been identified as the best option for Fischer-Tropsch synthesis due to its many advantages compared to the other reactors. These advantages include 1) flexible temperature control and excellent heat transfer; 2) efficient inter-phase contacting which results in higher productivity; 3) low pressure drop leading to reduced compression costs; 4) better use of catalyst surface (fine particles less than 100 μm) allowing suitable liquid-solid mass transfer [23, 26].

1.6 Motivations and Thesis Objectives

Given this framework, this dissertation presents the conceptual design of three possible catalytic processes for renewable power to gaseous and liquid fuels (Methanation, Direct Dimethyl Ether (DME) and Low Temperature Fischer-Tropsch synthesis) which are independently simulated by Aspen plus commercial software. This analysis highlights several challenges and limitations of each process when integrating a Solid Oxide Electrolysis Cell (SOEC). With the aim of improving these processes, using the Aspen plus software simulation of the last optimized configuration of three processes based on renewable energy with aid of an SOEC are performed. In methanation, by considering the main product (methane) as a storable energy carrier to stabilize seasonal imbalances in renewable power, the goal is to reach the desired value of methane fraction (95%) at the outlet which is fully compatible with the quality requirements of the natural gas grid. On the other hand, in DME and FT synthesis the objective is to obtain green renewable products with the lowest amount of aromatics and impurities within optimized configurations. In this context, the main focus of this thesis is on an original rigorous dynamic model of a slurry bubble column reactor (diameter 10 Cm, height 2.5 m) for the FT process under variable loads of synthesis gas (3.5, 5, 7.5 m^3/h) in Winddiesel technology. In fact, the reactor model has the capability of coupling a set of PDEs in the form of mass transfer and chemical reaction to appropriate hydrodynamic features. This methodology was developed in MATLAB code reflecting the concentration behavior of all key components of Fischer Tropsch over the reactor, and is validated with experimental data. In fact, this transient analysis not only proposes the effect of variable syngas load on selectivity, CO conversion and α-value as well as information about the inside of reactor; its results also address a complete Fischer Tropsch framework thanks to this mathematical modeling.

Furthermore, the results of the modeling are in good agreement with the experimental data. The experimental data is adopted from a Master of Science thesis which was conducted using the Fischer–Tropsch research plant. The plant is located in town of Güssing in Austria [27, 28]. Appendix reflects the experimental setup and its measurements for both base load (syngas flow rate of 5 m^3/h) and change load conditions (syngas flow rate of 3.5 m^3/h and 7.5 m^3/h) in one specific run [28].

Based on what has been mentioned so far, the present dissertation is structured as the follows:

A. In Chapter 2, Power to Gas technology i.e. Methanation and different types of Electrolysis (Alkaline, PEM and SOEC) is analyzed. Furthermore,

SOEC coupling with Methanation is simulated with two stages of isotherm and adiabatic reactor in commercial simulator Aspen plus.

B. In Chapter 3, Power to Liquid technology based on Low Temperature Fischer-Tropsch (LTFT) process and the Dimethyl Ether (DME) synthesis (direct one-step process) are discussed. Moreover, mathematical modeling of low temperature Fischer Tropsch (LTFT) process and the DME process are developed. Also, the performance and sensitivity analysis for the DME process in order to realize optimum operating conditions is analyzed.
C. In Chapter 4, the Fischer Tropsch Slurry reactor is introduced as the best option in our application. The challenges, hurdles and all hydrodynamic features are studied in more details. Also, a computer model of FT slurry reactor pilot plant in MATLAB Code under specific assumptions is developed.

Chapter 2

Power to Gas Technology

2.1 Introduction

The chemical conversion of electrical power into Hydrogen or Substitute Natural gas is defined as the concept of "Power to Gas ". The widespread applications of PtG and its advantages make this technology particularly attractive amongst Electric Energy Storage (EES) systems [29]. The multi-functional capabilities of a typical PtG plant encompass the exploitation of surplus energies in renewable power sources, injecting produced fuels in the existing natural gas network, plus long term carrier energy storage and fuel transportation production as a result of conversion renewable power. Furthermore, the principal advantages of PtG compared to other EES systems include the significant volume energy density of the fuel precursor and the capability of linking the electric grid to other existing infrastructures in energy transport and storage (see figure 5). [7, 10]

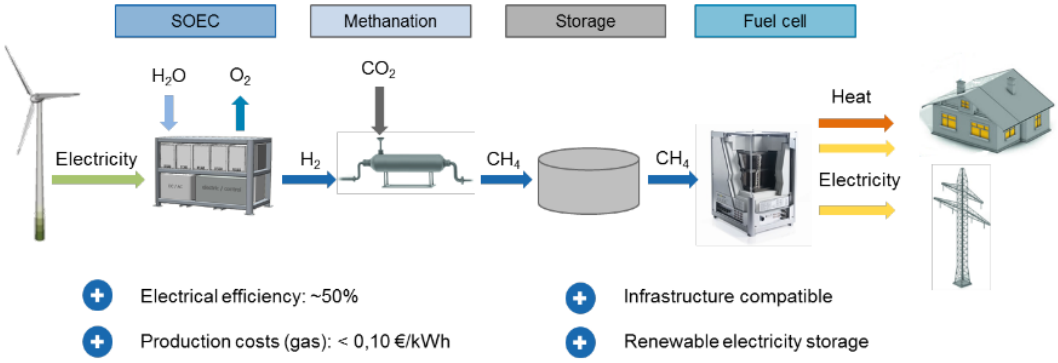

Figure 5: Power to Gas based on methanation process and electricity storage in natural gas grid [30].

In general, within the Power-to-gas process chain there are two possible end-products: 1) Hydrogen 2) Synthetic or Substitute Natural Gas (SNG)

Hydrogen which is considered as the primary usable product in the PtG process, plays an important role in the chemical and petrochemical industry, such as in the Dimethyl Ether and Fischer-Tropsch processes, which require significant volumes of hydrogen. However, its exploitation is constrained due to far-off locations of consumers from electrolysis plants or poorly designed transport and storage facilities. The storage option is also hindered because of buffering issues from demand sections. For instance, the maximum allowable hydrogen content is a limited value (0-12%) in the natural grid with respect to country standards and regulations [10]. These challenges bring about the conversion of H_2 into other valuable and more attractive energy carriers. Notwithstanding, from the electricity storage point of view, H_2 is considered as the most effective and efficient fuel precursor for reducing the costs and complexity through a one-step process. In addition, hydrogen production does not need a CO_2 source [29].

The second PtG process is SNG through Methanation process, which consists of two main processes: Hydrogen or syngas generation can be performed by steam electrolysis or co-electrolysis of H_2O and CO_2 respectively, and Methanation occurs through chemically or biologically catalyzed reactions. In hydrogen and syngas generation, in the case of steam electrolysis, the technologies of Alkaline Electrolysis (AEL), Polymer Electrolyte Membrane (PEM) electrolysis or SOEC can be employed whereas for the case of co-electrolysis, the only option is SOECs.

In methanation, the catalytic hydrogenation of CO_2/CO produces methane through the Sabatier reaction. The CO_2 required for the process could be provided from several potential CO_2 sources, such as biogas plants, fossil power plants, the atmosphere and process or exhaust gases from petrochemical complexes or from sea water. The latter source can be quite energy-intensive. The SNG produced includes considerable amounts of steam as a by-product and has to be upgraded to meet the specific requirements of Natural Gas grids. In the stage of SNG production, the reshifting to electricity can be conducted in power plants connected to the Natural Gas grid or in Solid Oxide Fuel Cells (SOFCs), which tend to achieve higher conversion efficiencies.

2.2 Electrolysis Systems

The intermittency nature of renewable sources (such as wind and solar power) makes this energy system difficult to integrate in the energy transformation process. This trend brings about several challenges, such as the utilization and storing of excess energy, distributed generation management and load leveling. In this respect, water electrolysis can overcome these difficulties by producing hydrogen, as it proposes the possibility of storing and transporting electrical energy. This hydrogen production can be employed either in its basic form or as a precursor in subsequent chemical processes. [9, 10]

Electrolysis technologies play a pivotal role in Power to Gas systems, as they establish the connection between electrical and chemical energy. In fact, a water electrolyzer utilizes electricity to disassociate water (or carbon dioxide) molecules into hydrogen and oxygen (or carbon monoxide and oxygen). In general, the electrolysis system contains a single cell, stack (consists of a set of cells) and all the auxiliary attachments which are required to run the system.

The thermodynamics and efficiency of an electrolysis system will be mentioned in the section of SOEC type. At present, there are three principal types of water electrolysis in terms of operating temperature. For low temperature applications, Alkaline electrolysis (AEC) on a large scale and Proton-Exchange Membrane electrolysis (PEMEC) on a smaller scale are available. On the other hand, for high temperature usage, a Solid Oxide Electrolysis Cell (SOEC) was proposed as a promising technology [9].

2.1.1 Alkaline Electrolysis

Alkaline Electrolysis is a standard highly developed electrolysis which is broadly applicable for industrial hydrogen production at large scales. As illustrated in Figure 7, an AEC is principally consisted of two electrodes completely immersed in an aqueous electrolyte such as sodium hydroxide (NaOH) or potassium hydroxide (KOH) electrolyte. The application of KOH is more common over NaOH due to its higher conductivity. The operating conditions are normally set at 70-90 $^{\circ}$C and pressure ranges 30 bars with current densities in the range of 300-500 mA/cm^2 and cell voltages in the range of 1.9-2.4 V. The ionic reaction scheme in result of water consumption at the electrodes is as follow [10, 29]:

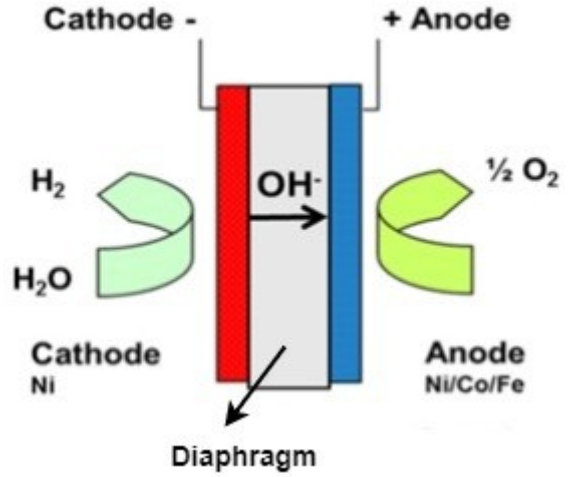

Figure 6: A schematic view of Alkaline Electrolysis Cell [32].

$$\text{Cathode:} \quad 2H_2O + 2e^- \longrightarrow H_2 + 2OH^- \qquad (1)$$

$$\text{Anode :} \quad 2OH^- \longrightarrow 1/2O_2 + H_2O + 2e^- \qquad (2)$$

The two electrodes are separated by a polymeric micro-porous diaphragm in order to prevent mixing of released H_2 and O_2. One important design factor in AEC is the space between the separator and the electrodes. The lower ohmic cell resistance is achieved by making this gap smaller. Therefore, the zero-gap systems (the gap size approach zero) can be beneficiary for AEC due to preventing bubbles formation around electrode zone. An attractive method to achieve zero-gap approach is to apply anion exchange membranes instead of using conventional separators or liquid electrodes [31].

There are several advantages and disadvantages in employing AEC. The advantages of AEC are endurance, maturation, availability and low investment cost. Whilst, the low operating pressures and low current densities can be considered as major hurdles and disadvantages.

2.2.2 Proton Exchange Membrane Electrolysis (PEME)

PEME is regarded as the second significant water electrolysis technology with less developed compared to Alkaline electrolysis. Figure 7 is depicted a schematic view of a typical PEME. The cells of PEME are housed in a Solid Polymer Electrolyte (SPE) which is in charge of proton conductions, separation of released gaseous (H_2 and O_2) and electrical insulation of the electrodes. The most common

used electrolyte for PEME is Nafion which acts as a thin conducting membrane normally based on a perfluorosulfonic acid. This membrane is in contact with both electrodes where the following ionic reactions tend to initiate:

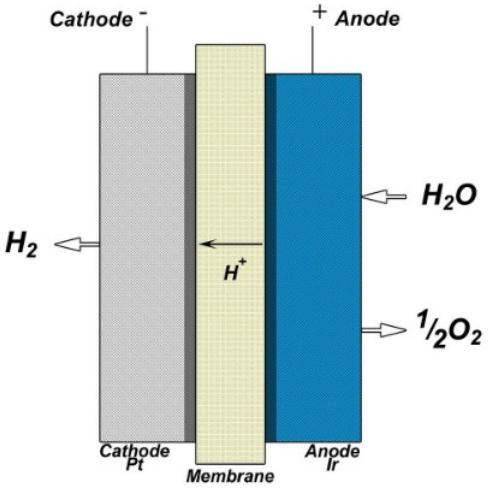

Figure 7: A schematic view of PEM electrolysis [32].

$$\text{Cathode:} \quad 2H^+ + 2e^- \longrightarrow H_2 \qquad (3)$$

$$\text{Anode:} \quad H_2O \longrightarrow 1/2O_2 + 2H^+ + 2e^- \qquad (4)$$

The operating temperature for PEM electrolysis is usually kept below 80 $^{\circ}$C because of using liquid water to enable enough proton conductivity. This system can operate at high pressures (30-60 bar) without extra compression sections. The current densities and cell voltages in the lab are set at 5-10 A/cm^2 and 2.5 voltages, respectively. The system efficiencies with respect to the HHV of H_2 are in the range of 60-70 %.

There are plenty of strength points in employing PEM electrolysis. First of all, considerable flexible mode of operation in start up and shutdown time makes this electrolysis more compatible with PtG requirements. Then high current densities and cell efficiencies at low voltages as well as ability to produce highly compressed hydrogen can be other advantages of PEM electrolysis. On the contrary, the weaknesses of that are the difficulties surrounding scale up issues, expensive materials and low level of durability [32].

2.2.3 Solid Oxide Electrolysis Cells (SOEC)

Solid Oxide Electrolysis Cells (SOEC) is considered as the only electrolysis operating at high temperature. It is established based on a dense, thin solid ceramic electrolyte which is capable of ions conductions at elevated temperature (650-1000 $^{\circ}$C). In this range of temperature, steam water is fed at the cathode electrode where the reduction occurs and produced oxygen ions transfer to the anode side where oxygen molecule evolves. These electrochemical reactions take place according to the following reactions:

$$\text{Cathode: } H_2O + 2e^- \longrightarrow H_2 + O^{2-} \qquad (5)$$

$$\text{Anode: } O^{2-} \longrightarrow 1/2O_2 + 2e^- \qquad (6)$$

The overall schematic of a SOEC cell is illustrated in Figure 8. The operating pressure is set as atmospheric. However, some SOEC system was designed to pressure up to 10 and 25 bar [33, 34]. The current densities need to be maintained at the level of 300-600 mA/Cm^2 (around AEC range) due to potential strong degradation. The equivalent cell voltages is around 1.2-1.3 V.

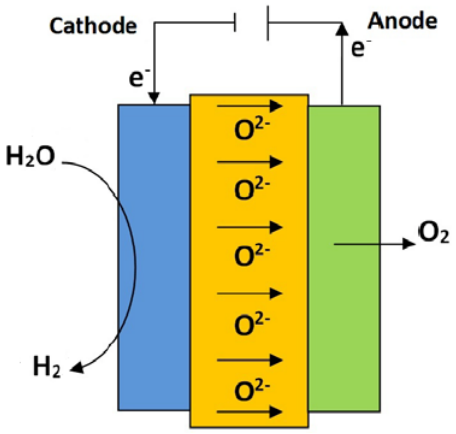

Figure 8: A schematic view of Solid Oxide Electrolysis Cell (SOEC) [9].

The single cells in SOEC are delivered in different geometries on market. They are performed in two arrangements: 1) Tubular 2) Planar. Tubular based systems create longer current paths leading to lower power density. It also has shorter start up and higher mechanical strength. On the other hands, planar configuration posses more effective manufacturability with higher electrochemical performance.

The main benefits of SOEC systems includes its capability of operating in high temperature leading to lower required electricity (Thermodynamic advantage) and lower overvoltage without using precious metallic elements in employed catalysts (Kinetic advantage). On the contrary, the degradation of sets of cell (stack components) at high operating temperatures is considered as the downside of SOEC systems. Meanwhile, the technical data of the SOEC studied in this dissertation, which was designed by the Sunfire company, is as follows: 1) the electrolysis system generates 40 Nm^3/h of H_2 with an input power of 150 kW; 2) the ability of reversing into fuel cell mode with an output power of 30 kW; 3) max temperature of 850 ºC; 4) max pressure of 30 bar; 5) dimensions (H×W×D):116×168×182 mm^3.

Since in this dissertation the simulation of PtG and PtL are conducted based on the SOEC, the study of this type of electrolysis is described in more detail. Therefore, other important features of SOECs including Co-electrolysis and SOECs' thermodynamic are focused in the following subsections [9].

2.2.4 Co-electrolysis of H_2O and CO_2 in SOECs system

The bi-functional feature of SOECs which relates to simultaneous dissociation of water and carbon dioxide referred as Co-electrolysis system. It becomes more attractive when the energy required for electrolysis is provided from renewable energy sources instead of consuming fossil fuels. Therefore, SOEC system proposes not only hydrogen generation but also producing wide variety of fuels, solvents, fertilizers and other synthetic products with minimum emitting GHGs. [10, 34]. In Co-electrolysis process, the Oxygen is represented at the anode electrode, while carbon monoxide, hydrogen and other unreacted components are produced at the cathode side according to equation (7). Besides, within catalyst Ni/YSZ electrode several side reactions such as water gas shift and methanation may promote. Water gas shift reaction (Eq. 8) tends to initiate above 650 $^{\circ}C$ and to reach equilibrium quite fast. In addition, Methanation is favored at high concentrations of CO and H_2 plus low temperature and high pressure reflected in Eq. (9).

$$H_2O + CO_2 \longrightarrow H_2 + CO + O_2 \qquad (7)$$

$$H_2O + CO \longrightarrow H_2 + CO_2 \qquad (8)$$

$$CO + 3H_2 \longrightarrow CH_4 + H_2O \qquad (9)$$

On the other hand, catalyst Nickel also stimulates some side-reactions i.e. Boudouard reactions (coke formation) which is detrimental for SOEC system. In

case of high voltage operation accompanied high concentration CO, side-reaction (Eqs. (10) (11)) tend to increase to larger extent [35].

$$2CO \longrightarrow C(s) + 0.5O_2 \qquad (10)$$

$$CO \longrightarrow C(s) + 0.5O_2 \qquad (11)$$

The integration of Methanation in Co-electrolysis system causes mutual thermal synergies between exothermic methanation and endothermic electrolysis and it reaches the round trip efficiency of the system to more than 70 % [29].

2.2.5 Thermodynamic analysis of SOECs system

The thermodynamic parameters of a water electrolyzer are identified by making energy balance over the SOEC system. In principle, total energy demand for splitting water molecule in electrolysis cell is denoted by ΔH (T) based on Eq. 12. This amount is supplied by "electrical energy" which represents the Gibbs free energy ΔG (T) plus "heat energy" which corresponds to the amount of T ΔS (T):

$$\Delta H\,(T) = \Delta G\,(T) + T\,\Delta S\,(T) \qquad (12)$$

When this equation is defined in terms of voltage, new parameters turn out to be defined as below:

Reversible voltage:

The minimum voltage for splitting reaction water into its constituents is referred as Reversible voltage or Gibbs voltage which is calculated when we assume input energy to drive electrolyzer is supplied by electrical component of required energy:

$$V_{rev} = \frac{\Delta G}{n\,F} = 1.23\ V \qquad (13)$$

Considering ΔG equals 237.22 kJ/mol at standard conditions of 298 K and 1 bar, n denotes the number of transferred electrons in Eqs. 13 and 14 and F which is the Faraday constant equals 96487 C/mol. By assuming these values in Eq. (13) the Gibbs voltage calculates as 1.23 V [10].

Thermo-neutral voltage:

Thermo-neutral voltage is attributed to the enthalpy change related to water splitting reaction. And it is calculated when we assume the operating voltage (Electrical input) is equal to total energy demand for electrolysis:

$$V_{th} = \frac{\Delta H}{nF} = \frac{\Delta G}{nF} + \frac{T\Delta S}{nF} = 1.48\ V \qquad (14)$$

Considering ΔH equals 28584 kJ/mol at standard conditions, plus above assumptions the thermo-neutral voltage is achieved at 1.48 V. In fact, in thermo-neutral state the heat generated by system irreversibility exactly equals the heat captivated by the electrolysis reaction in a specific value of cell voltage. This is the desired mode at which electrolysis system operates [10, 29].

In terms of operating voltage, there are three different operating modes: If the operating voltage U_B (Electrical input which is employed for electrolysis cell) is lower than V_{th} heat must be absorbed as thermal energy for water splitting (Endothermic operation). In this case, minimum degradation occurs since electrolysis operates at lowest power densities. If $U_B = V_{th}$, as already mentioned no thermal energy is required or released (Authothermal operation). If $U_B > V_{th}$, the difference (U_B-V_{th}) has to be properly removed as surplus heat to decrease degradation of the system (Exothermic operation) [9, 10, 29].

These aforementioned thermodynamic parameters are strongly dependent on operating temperature and pressure in electrolysis system which has to be carefully selected [10]. As shown in figure 9, the required electrical energy (ΔG corresponding voltage V_{rev}) continually decreases with rising temperature leading to 30 % reduction by changing from 273 to 1273 K (see figure 9).

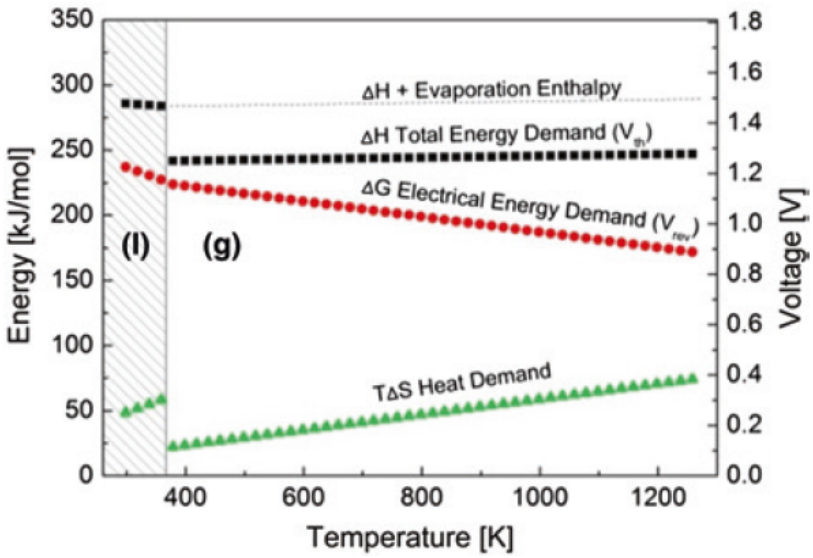

Figure 9: Reaction Enthalpy and Gibbs energy with equivalent voltage as function of temperature [10].

On the other hand, total energy demand (ΔH, equivalent voltage Vth) remains more or less constant with increasing temperature. This trend illustrates that in case of employing steam electrolysis lower energy requires compared to water electrolysis [10]. In addition, from this figure the ratio of ΔG electrical energy demand (ΔG) to total energy (ΔH) is about 93% at 100°C and about 70% at 1000°C, which illustrates that in elevated temperature electrolysis about 30% of the required energy can be provided as heat. Thermal required energy of the cell can be supplied either externally using a thermal source or internally through Ohmic heating depending on whether the process function is autothermal or allothermal. The requirements of decreased electrical energy facilitates the Solid Oxide Electrolysis cells to work at lower voltages (around 0.95 to 1.33 V) than those involved for other typical electrolyzers [36].

2.2.6 Electrolyzer Efficiency

The theoretical conversion efficiency of an electrolyzer system is typically defined as the storable energy unit (heating value of hydrogen) per unit of electrical energy input for electrolysis:

$$\eta_{sys} = \frac{\text{Energy Output}}{\text{Energy input}} \rightarrow \frac{\text{Heating value } H_2}{\text{Electrical Energy input}} \qquad (15)$$

The energy output is regarded as heating value of hydrogen. It is identified by HHV (higher heating value) or LHV (lower heating value) of H_2. Their values for hydrogen equals to HHV=3.54 kWh/m^3, LHV=3 kWh/m^3. Since liquid water is usually employed as feedstock, the energy needed for vaporizing of water has to be considered. Thus, HHV of hydrogen is used for calculating the efficiency of electrolysis system. In typical water electrolysis, the energy input is generally constrained to electrical energy (apart from when the $U_B < V_{th}$). In efficiency calculation, it is significant to notice in which level of element utilization (system or cell) the electrolyzer is considered to operate. Subsequently, there are three types of efficiencies i.e. current efficiency, energy efficiency and voltage efficiency according to system-level, cell-level or stack-level, respectively. Declining the electrolyzer utilization below 50 % of input power brings about 10-30 % reduction of energy efficiency [10].

The electrical efficiency at cell or stack level is defined as a product of a faradaic (current) efficiency (η_F) multiple a voltage efficiency (η_V) which the latter is referred as the ratio of thermo-neutral voltage (V_{th}) and the applied voltage (V_{app}). Whilst, the former (η_F) is referred as the ratio of the amount of

produced hydrogen by measurement and the theoretical amount of that. Given these definitions, the electrical efficiency equals as below:

$$\eta_{el} = \eta_V * \eta_F = \frac{V_{th}}{V_{app}} * \frac{n_{meas}}{n_{th}} \longrightarrow \eta_V \qquad (16)$$

Since the electrical efficiency of typical electrolyzer is considerably lower than 1 the operating voltage of electrolyzer surpass 1.48 because of irreversible losses such as overvoltages and internal resistances.

In practice, the operating voltage can be described as the summation of the reversible voltage, the concentration overvoltage due to mass transfer limitations plus activation overvoltage which includes cathodic and anodic overpotentials attributed to the reaction kinetics (effects of electrode polarization) and also the addition of ohmic overvoltages due to ohmic resistances [10, 29, 37]:

$$V_{cel} = V_{rev} + V_{act} + V_{ohm} + V_{conc} \qquad (17)$$

For a specific electrolyzer setup with a determined current density, by increasing temperature total overvoltage basically decreases because of elevated overall kinetics. Elevating the operation temperature also has a beneficial thermodynamic influence on ΔG, hence on the reversible voltage, as already explained in the previous section. Due to these variety reasons the delivered operating voltage can be considerably decreased by increasing temperature. The operating pressure barely affects kinetics or thermodynamics of the electrolysis process. As a result it is less put forward in the electrolyzer's efficiency at the cell level. [10].

2.3 Methanation

The main conversion of H_2 and CO_2/CO through two routes i.e. catalytic or biological is referred as Methanation process. These pathways depend on catalyst used (inorganic or bio-catalysts) and CO_2 sources (biogas or other sources) [29]. The main process of catalytic conversion of methane out of hydrogen and carbon monoxide was discovered by Sabatier and Senderens in 1902 [38].

The reaction scheme in chemical reactors includes CO and CO_2 methanation plus other reactions such as water gas shift and Boudouard:

$$CO + 3H_2 \longleftrightarrow CH_4 + H_2O \qquad \Delta H_R^0 = -206.2 \text{ kJ/mol} \qquad (18)$$

$$CO_2 + 4H_2 \longleftrightarrow CH_4 + 2H_2O \qquad \Delta H_R^0 = -165 \text{ kJ/mol} \qquad (19)$$

$$CO_2 + H_2 \longleftrightarrow CO + H_2O \qquad \Delta H_R^0 = +41.2 \text{ kJ/mol} \qquad (20)$$

$$CO_2 + C \longleftrightarrow 2\,CO \qquad \Delta H_R^0 = +17245 \text{ kJ/mol} \qquad (21)$$

All reaction enthalpies are calculated at temperature of 25 °C. From experimental data it can be concluded that CO methanation (80-100%, 200 °C) has higher conversion rates compared to CO_2 methanation (40-90%, 250 °C). This is due to higher stability of molecule CO_2 than CO from thermodynamic point of view. Moreover, CO_2 methanation can be interpreted as the combination of CO-methanation and water gas shift reaction whereby the entire reaction promotes more slowly [9]. Since the whole reaction is strongly exothermic and mole-reducing towards the products the reaction are favored by low temperature and high pressure. Considering Boudouard reaction, low temperature prevents coke formation and catalyst deactivation [10]. However, if the temperature is lower than minimum allowable temperature for reactants which is called "Catalyst Light-off temperature[1]" dampens the reaction rate for CO_2 methanation [30]. Therefore, the appropriate catalysts are required to elevate the reaction rate and to reach the CO_2 conversion at reasonable amount even at moderate temperatures.

In general, wide-ranging metal catalytic systems, such as Ni, Co, Fe and Ru for methanation based on different oxide supports (SiO_2, Al_2O_3, TiO_2 and ZrO_2) have been proposed. Among these catalysts, the most stable catalyst which can reach the reaction rate at a suitable level is the Ni-based catalyst. This is due to its high selectivity and activity for methane formation and its low cost [8, 9].

[1] The minimum temperature at which catalyst is able to convert reactants to products.

In addition, the high pressure condition for reaction is due to volume reduction of chemical reaction according to the le Chatelier's principle (Eq. 19) which promotes the reaction towards products [29].

2.3.1 Methanation in Power to Gas application

Methanation is considered as the subsequent unit adjacent to the electrolysis system within Power to gas concept [10]. When the methantion is integrated with electrolysis system, we need to cope with unsteady intermittency of input renewable power. This fluctuating nature following load changes which substantially depends on the reactor concept. The catalytic multi-tublar fixed bed reactors are the most applicable type of reactors in CO_2 hydrogenation to gaseous hydrocarbons processes (e.g. methanation). Their advantages include great potential to scaling up, minimum maintenance and low cost, operating at elevated pressure as well as simplicity. As a result, a catalytic fixed bed reactor was proposed to conduct the CO/CO_2 methantion under flexible load conditions in large-scale. In this respect, the main challenge is considered as heat management and its utilization within the Power-to Gas process chain [24]. Furthermore, the selection of appropriate catalyst in order to possess more selectivity for CO_2 and less sensitivity to catalyst poisons is indispensable. This trend minimizes the efforts and costs for off-gas purification (upgrade downstream). Given these measurements, the economic viability of methantion tends to improve within the power to gas concept [10, 30].

In plant-wise study of Power-to-Gas system, the boundary conditions get larger. The availability of renewable energy with respect to plant size, temporal profile and quantity of renewable power, size of hydrogen storage and carbon dioxide source have to be carefully analyzed. Thus, the methanation unit is evaluated based on its boundary condition and its application in the PtG system with respect to the capacity of natural gas grid [10].

2.3.2 The stage of development and process concepts

In recent decades, wide variety of methanation processes based on feedstock and reactor type in different stage of development (scale) has been developed by several companies [39, 40, and 41]. Fossil coal and biomass are considered as the feedstock within the process chain of coal to gas (CtG) and biomass to gas (BtG). These routes deliver one process step of methanation.

In the stage of development, the reactor types for methanation include Fixed bed Reactor, Fluidized bed, structure reactor (coated honeycombs) and Bubble

column slurry reactor, each of which developed within particular process under specific operating condition. For instance, Fixed bed reactor belongs to the Lurgi, TREMP, Linde, HICOM and RMP process. In this dissertation, as a case in point, two methanation processes i.e. TREMP and Lurgi processes are explained depending on their reactors' arrangement. Firstly, the flow diagram of the TREMP[1] process is illustrated in figure 10. This process was designed in 1980 at semi-commercial scale with three fixed bed reactors in series operated at temperature range 300-700 °C and pressure 30 bar [10]. As shown in figure 10, this process consists of a series of adiabatic fixed bed reactors with intermediate cooling preceding each reactor. The positive points of this system are simple construction, not complicated control system and low soot formation in the second and third stage because of water formation in the first stage.

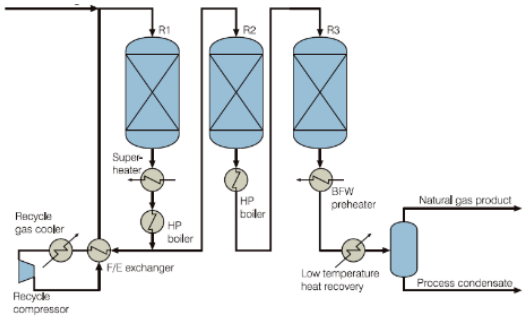

Figure 10: Simplified process flow diagram of TREMP technology [30].

However, this process suffers from several downsides such as possibility of soot formation in the first stage and low converted methane at the outlet (about 70 %) which makes it inconsistent to the quality of the natural gas grid. Furthermore, the current challenge of this technology is to create isothermal operation of the reactors by the efficient cooling system. One possible solution could be the use of specific cooling medium named molten salts by having capability of operating in atmospheric pressure as well as elevated pressures [30]. The second methanation scheme which is related to Lurgi process was developed at pilot plant. As illustrated in figure 11, it consists of two adiabatic fixed bed reactors in series with internal recycling stream. The technology was delivered in two modes. In the first design, the syngas was generated in a coal gasification plant at commercial scale. A part of syngas was fed from a side-stream of the Fischer-Tropsch plant. In the second design, naphtha is converted to methane at pilot plant [39].

[1] Topsoe's Recycle Energy Efficient Methanation Process; trademark of Halder Topse, Denmark [22].

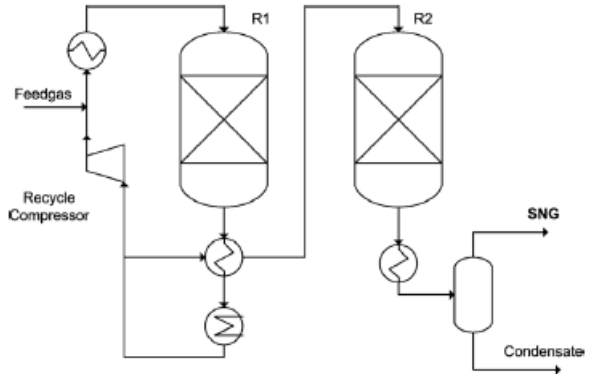

Figure 11: Lurgi methanation process through two adiabatic reactors [39].

For other methanation technologies with different types of reactor references [39-41] are suggested.

2.3.3 The latest developments of methanation

The process development of methanation within Power to Gas system aims to improve methanation technologies. This is achieved by revamping the reactors' design in order to eliminate the challenges of previous schemes. Having proposed those aforementioned methanation processes, a collaborative project named "HELMETH[1]" has been initiated in 2015 by a European research program. The main objective of this project is to reach a highly effective and efficient Power to Gas concept through methane as chemical storage. The highlight of this project is the thermal integration between exothermic methanation and endothermic high temperature electrolysis. This scheme by utilization of renewable energy for high temperature electrolysis makes the chemical storage quite energy efficient. The product (Substitute Natural Gas) is completely in line with the requirements of storage infrastructure and the existing pipeline network.

To achieve the requirements of HELMETH project, a particular configuration of methanation was prepared as illustrated in figure 12. This plan is based on one adiabatic and one near-isothermal reactor with an interstage cooling. Besides, an evaporation cooling was employed to maintain the second reactor in the isothemal mode. Moreover, this evaporation provides high pressure steam up to 165 bar for the high temperature electrolysis. The specification of gas product is acceptable for injection in the natural gas grid.

[1] Integrated High-Temperature Electrolysis and Methanation for Effective Power to Gas Conversion

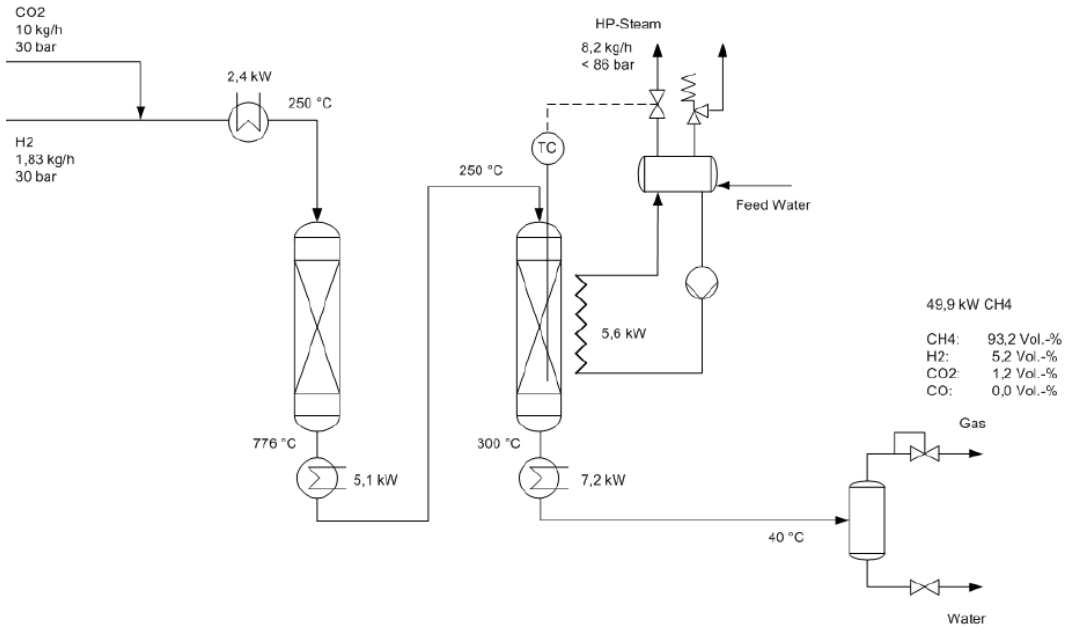

Figure 12: Proposed flow diagram of methanation reactors in HELMETH project [30].

This layout can be improved by water removal and steam circulation leading to increase the efficiency of the process [30]. In this dissertation, the improved two-stage process was simulated by software "ASPEN plus "as a state of the art process in methanation.

2.3.4 Simulation of a state of art Methanation process

The improved configuration of so-called methanation process can be achieved by two sets of modifications: 1) Steam circulation 2) Water removal.

By recycling of high pressure steam to the first stage, the soot formation is avoided in adiabatic reactor.

Water removal between stages promotes methanation reaction in a beneficial way from thermodynamic equilibrium point of view.

These two process changes are considered in the simulation of modified two-stage adiabatic/isothermal scheme by software "Aspen plus" as illustrated in figure 13. For the simulating reactors, the RGIBBS type is selected as it predicts product composition by minimizing Gibbs free energy.

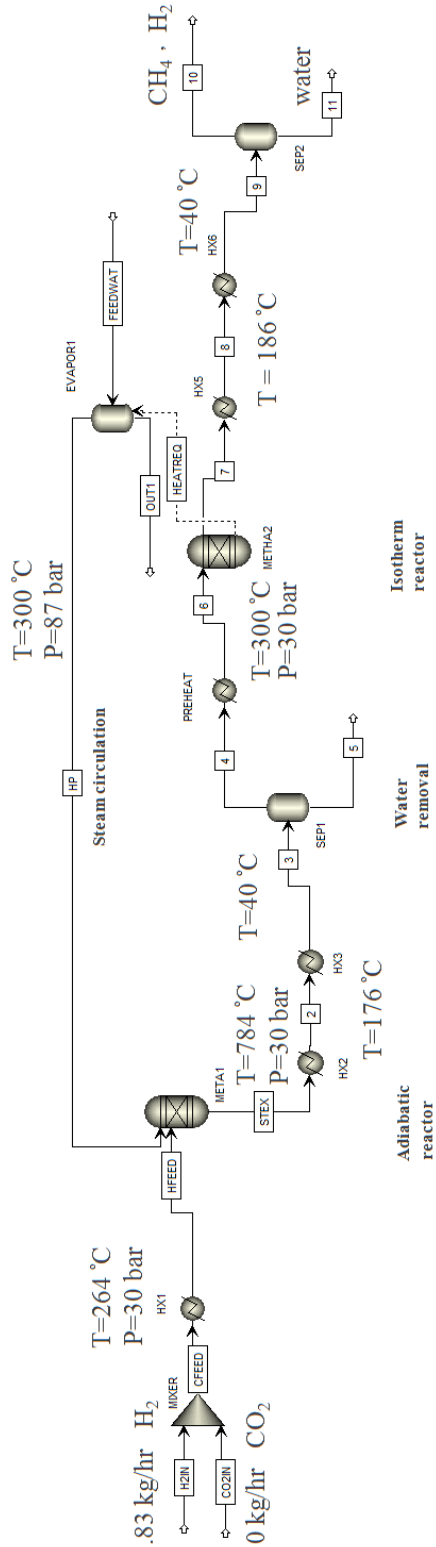

Figure 13: Simulation of Methanation based on two stages adiabatic / isothermal; configuration flow sheet in Aspen plus.

The results of simulation show the methane fraction is achieved at 95 %. This value is fully compatible with quality requirements of the natural gas grid. The other important components such as H_2, CO_2, CO are calculated as 4.1%, 0.75%, and 0.0%, respectively.

In this process, the conversion efficiency of the system is equal to the energy content of the product fuel to the whole heat required of the system plus energy content of the syngas fuel based on lower heating value (LHV) [42]:

$$\eta_{sys} = \frac{Q_{PF}}{Q_{Syngas} + \Delta Q} = \frac{m_{PF}\, LHV_{PF}}{m_{Fuel} LHV_{PF} + \Delta Q}$$

And the efficiency of the electrolysis is calculated as the energy content of syngas to the energy required for splitting of water which includes electric power (P_{el}) plus reintegrated heat needed in the power cycle ($\Delta P = \Delta Q\, \eta$) [42]:

$$\eta_{el} = \frac{Q_{PF}}{P_{el} + \Delta P} = \frac{m_{PF}\, LHV_{PF}}{P_{el} + \Delta P}$$

In this simulation, the system and electrolysis efficiencies are calculated as 87 % and 60 %, respectively.

The downside of this design is the necessity of advanced control strategy resulting in elevated investment costs. To improve an efficient methanation system that can be integrated with the high temperature electrolysis, several measurements need to be taken into account as follow:

1) The dynamic of this methanation system has to be optimized to reach the required load variation rate of 20 to 100% by maintaining the product quality constant.
2) More conductive research on a number of catalyst options for low and high temperature reaction steps.
3) To examine the condition of stand-by operation in case of low renewable energy generation.
4) To investigate more on kinetic reaction of methanation under unusual conditions (high pressure, 30 bar and very high concentration of CO_2)
5) To provide a stabilized and highly pressurized steam for electrolysis system by an appropriate cooling system.

By considering above measurements, a cost optimized multi-step methanation process with high performance will be designed.

2.4 The economics of Power to Gas technology

The economic analysis of Power to Gas concept encompasses quite comprehensive parameters‘evaluations. In general, these economic dimensions include macroeconomic and microeconomic assessments. The macro-scale of economic studies revolves around fiscal systemic approach from storage options and energy transport to the heating sectors and the infrastructure of a power itself. This trend leads to investigate a defined business model which can be achieved through several process of Power to Gas technology. On the contrary, microeconomic analysis is mainly focused on capital expenditures (CAPEX) of electrolysis, Hydrogen storage and catalytic methanation as well as operational expenditure (OPEX) including the electricity price, purchasing raw materials, overhead costs, SNG costs and potential CO_2 costs [10, 43].

2.4.1 The macroeconomic of PtG: Energy storage

In recent years, the contribution of electricity from renewable power sources has dramatically increased in the sector of energy consumption of European countries. As a consequence, photovoltaic power plants and wind turbines are substantially constructed. This increased growth of renewable power to the present providing energy section initiates security challenge to this section’s economies. This challenge arises from severe fluctuation of renewable energy from unpredictable sources such as solar and wind power.

In this respect, “Energy storage system” plays a vitally important role for coupling of surplus renewable energy with intermittent production structures. This leads to achieve a balance between excess power in time of high generations and low values in periods of shortfalls (Optimized power management). The central issue is whether the implementation of Power to Gas system is profitable with regards to region and its infrastructure. For instance, for regions of Burgenland and Vorpommern located in Austria and Germany, the usage of wind through PtG (energy storage) turned out to be cost-effective. In Burgenland, the power input covers only about 20 % of the energy consumption. The rest as an energy storage is corresponding to 2.4 TWh_{el}. On the other hand, it is assumed that 40 % of the generated energy of all plants is supplied from unstable surplus wind power. Under such conditions, a hydrogen generation of 43000 ton/year can be expected which tends to provide about 300000 hydrogen powered cars. This example illustrates the importance of energy storage through PtG system which can be profitable in Burgenland region.

2.4.2 The macroeconomic of PtG: Energy transport

An advanced dimension of electrical energy storage through Power to Gas plant is the possible conversion of energy transport from the electrical grid network to the gas distribution network. The expansion of power line strongly affects the urban planning and its topology leading to local resistance in the society. Furthermore, the serious challenges in distributed power generation can occur as following:

1) Strong potential in Line overloads due to congestion and aging of Network Service Provider (NSP) Cable.
2) Surplus Transformers are required because of Transformer overloads.
3) Strong potential in voltage instability leading to voltage band violations and thereby increasing damage of equipment.

In the context of Power to Gas installations, generated energy in the form of Hydrogen or Methane with high energy density can be transported within existing gas networks to the consumers. The level of acceptance of Power to Gas system gets hindered due to the level of research and stage of development. However, high acceptance of Hydrogen mobility in the Germany has observed.

In summary, the energy transport from electrical to the gas network can be cost effective due to two reasons. First of all, the current structure of natural gas network with higher energy density enables no extra supply of considerable capacity without spreading out of pipeline networks in large scale. This benefit results in saving investment cost surrounding infrastructure. Second, despite an expansion of gas network is in connection with the extension with the power network still there would be much lower impact in the topological structure. This advantage leads to increasing higher acceptance of population and decreasing land expenditures to a large extent. Therefore, the expansion of gas pipelines bring about lowest intervention in the settlements or the landscape with less space requirement compared to power line at the same volume of energy transport.

2.4.3 The macroeconomic of PtG: Hybrid Networks

One of the attractive features of PtG system is to have a great potential for the development of hybrid grids. In fact, the hybrid network consists of different potentially energy system in future such as gas systems, electricity, water supply, heat power and transport network, which optimally integrated to the existing infrastructure in an efficient and effective approach.

This implementation follows two beneficiary effects including security of supply and economic perspective. In the contribution of supply security, the

hybrid grids are able to offer efficient load management and to provide energy cross-storages of production from other grids. From economic point of view, it helps increasing the efficiency of resources by decreasing the expansion of different grids such as heat, gas and electricity network. This trend leads to optimize the overall performance which generally runs in parallel. The linkage between heat and electricity forms in the technology of combined heat and Power (CHP). The connection between power to the heat network is performed by heat pumps and the linkage between gas to the power network and defined heating supply is conducted via power plants and fuel cells. As a result, these links between grids not only affect the energy transport sources but also, facilitate new version of storages [10].

The hybrid networks are broadly applicable in European countries particularly the Central European Energy system. For instance, in Austria 60 % of required electrical energy is provided by hydropower. However, the complete coverage demand more renewable energy sources and also extensive of energy storage because of volatile production capacities from wind and solar energy [44].

2.4.4 The microeconomic PtG: Electrolysis

As mentioned earlier, microeconomic analysis of PtG is focused on total capital investment cost of different parts of a PtG plant including: electrolysis, hydrogen storage and methanation. The most dominant contributor to total capital cost (CAPEX) belongs to the electrolysis. According to the previous lectures [10, 43] AEL has the lowest investment cost corresponding of 1000 €/kW. This investment value is at least half that of PEM systems. In general, CAPEX in electrolysis systems depend on defined conditions such as pressure and size. Mougin et al. [45] was estimated the price of SOEC system for generation of 100 kg/day (46.4 m^3/hr) of hydrogen. Its selling price was calculated at 11200 € h/(m^3 H2). Besides, Steinmuller et al. predicted the investment cost for both AEL and PEM systems including all auxiliary equipment by the year 2030 less than 1000 €/k We. The investment cost for SOEC by the year 2030 was predicted to the defined costs of 1000 €/k We for complete utilization of electrical efficiency (corresponding to 3540 € h/(m^3 H_2) [43].

2.4.5 The microeconomic PtG: H_2 storage

Hydrogen storage plays an important role in dynamic analysis of catalytic methanation reactor within power to gas technology. The storage enables the reactor to operate as continuous as possible to obtain optimum yield for the methane product. This situation reflects on the transient behavior of the H_2 storage

to buffer all the intermittency from H_2 generation due to renewable energies. Figure 14 shows the scheme flow of methane production from renewable energy which H_2 storage acts as an intermediate between electrolysis and catalytic reactor.

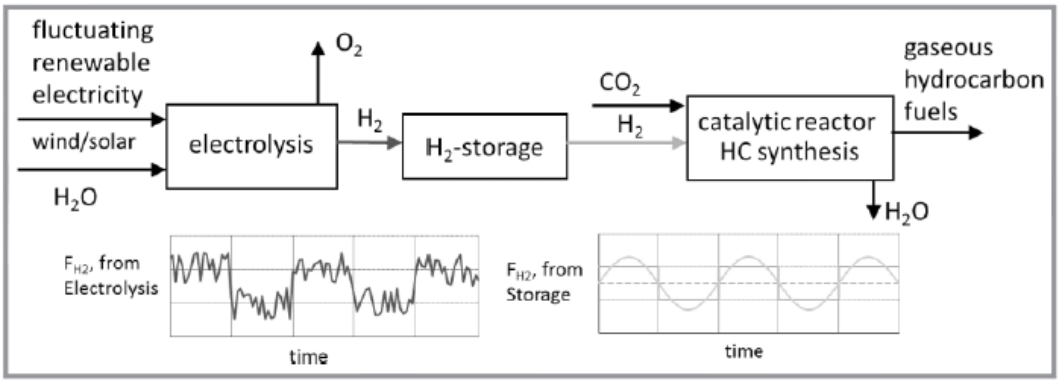

Figure 14: The scheme flow of gaseous hydrocarbon fuels from renewable energy with respect to the range of load and function of H_2 production pattern [45].

Further investigations on control strategy of H_2 storage, optimizing storage volume as well as maximum and minimum rate of load change (reactor flexibility) are all available in ref. [24, 45]. However, those parameters which associate to the investment cost of reactor and H_2 storage are introduced as follows:

Reactor Flexibility (L_m):

It refers to the operating of fixed bed reactor at different rates of load change. It is defined as the ratio of minimum volumetric H_2 flow to the reactor to maximum volumetric H_2 flow to the reactor. The lower L_m results in higher flexibility:

$$L_m = \frac{Fv_{,H2,in,reactor,min}}{Fv_{,H2,in,reactor,max}} \quad (22)$$

Proportional Constant (K_c):

The stochastic renewable energy brings about variations in the inlet flow of H_2 storage which could generate pressure fluctuations outside the desired ranges. Therefore, a control system is required to keep the storage pressure within the designed range. Based on a process control philosophy, the H_2 inlet flow is chosen as a disturbance, the H_2 outlet flow is identified as a manipulated variable and the storage pressure works as a controlled variable. In this regards, a proportional constant (K_c) as a closed control loop is defined for calculating the outlet H_2 flow as below:

$$K_c = \frac{(L_{max} - L_{min}) \cdot F_{v,H_2,in,reactor,max}}{P^*_{max} - P^*_{min}} \quad (23)$$

A proper control strategy facilitates us to optimize the storage volume with respect to the constraints imposed by synthesis in the process such as maximum allowable load. Thereby, the size of storage is estimated within this load range. In case that storage tends to operate around P_{max} , the small storage is identified. Instead, if the storage works in the region of P_{min} the oversized storage is derived.

Figure 15 illustrates that the storage volume considerably decreased with raising the reactor flexibility. The K_c value (proportional constant) also affects the storage volume. It shows by increasing K_c for each constant L_{min}, a smaller volume of hydrogen is required. Furthermore, the K_c value tends to have higher effects at small values of L_{min}. Even though, at higher K_c value no influence on the storage size is detected [24].

According to ref. [45] the investment cost of H_2 storage is calculated as a function of storage volume as below:

$$I_{storage} = 8.7 \left(\frac{V_{storage}}{1800}\right)^{0.8} \quad (24)$$

In practice, if the H_2 storage size tends to be larger, the investment cost gets higher and it is better to operate the methanation process under part load in order to decrease the size of H_2 storage.

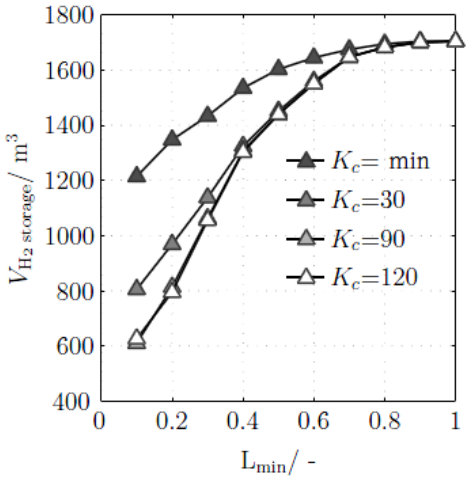

Figure 15: The influence of reactor flexibility (L_{min}) and proportional constant on Volume storage of hydrogen [24].

Figure 16 shows the relationship of relative size of H_2 storage and reactor which is corresponding to the relative investment (based on eq. 24) with reactor flexibility (L_{min}). As seen in figure 17, the relative investment for H_2 storage decreases as the load range of operation becomes wider (lower L_{min}, higher flexibility). For the case of reactor investment opposite trend is followed.

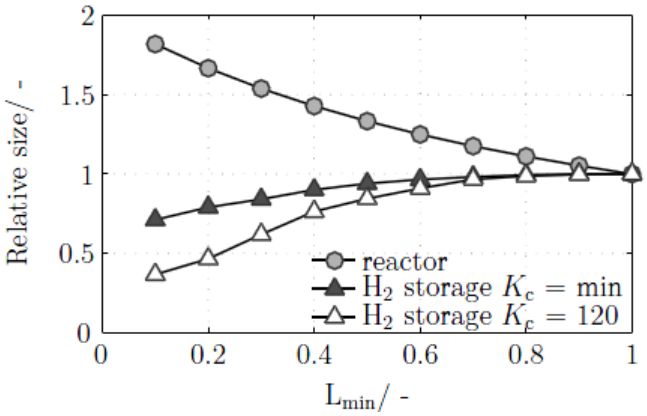

Figure 16: The influence of H_2 storage size or storage investment on reactor flexibility (L_{min}) [24].

In this section, it can be concluded that the methanation reactor under flexible load operation proposes to reduce the H_2 storage size and consequently its investment cost. However, the higher expenses related to part load operation such as larger attached equipment to reactor (separation unit), advanced control strategy and compression of recycling stream need to be also taken into account.

2.4.5 The microeconomic PtG: Methanation reactor

There is a severe uncertainty surrounding the investment costs of methanation reactor since it is strongly affected by hydrogen storage. Lower dynamic load of methanation leads to larger volume of hydrogen storage as already mentioned (figure 16). It also depends on capacity plant. For instance, In 2014, Qutotec GmbH [43] estimated the investment methanation reactor at operating pressure 20 bar for 5 MW and 110 MW plant which was calculated 400 €/kW SNG and 130 €/kW SNG, respectively. In 2009, Gassner and Marechal [46] analyzed investment costs of CO methanation from biomass gasification at operating pressure 15 bar for 14.8 MW. Costs were determined at 175 €/kW SNG which was in line with data set from Qutotec GmbH. In 2014, Aicher et al. [43] evaluated the effect of methanation dynamics on the investment cost of H_2 storage at a wind farm in Germany with an installed electrolysis capacity of 36 MW.

Table 2: A Comparison evaluation cost between two methanation plants: Methanation pressure 20 bar, H_2 storage 30-200 bar [43].

Investment in M €	Electrolysis	Compressor	H_2 Storage	Methanation	Total
Case 1	28.8	1	8.3	0.7	38.8
Case 2	28.8	1	4.8	1.2	35.8

In this analysis two cases were compared based on investment costs of different parts of a Power-to-Gas plant. Case 1 operating in steady state mode generates 311 m^3/h CH_4 with H_2 storage volume of 1700 m^3. On the contrary, Case 2 operating within a load change of 40-100 % produces 591 m^3/hr with H_2 volume storage of 850 m^3. The evaluation shows that even though the methanation cost is higher in the second case, still total cost reduced thanks to the dynamic mode of methanation reactor and significant contribution cost of H_2 storage volume.

The other aspect of cost assessment in methanation is focused on comparative analysis between biological and chemical methanation. In 2013, Grond et al. analyzed the investment costs of methanation reactor with capacity smaller than 10 MWth as illustrated in Figure 17. The data measurement shows it is a degradation cost for both methanation plants by increasing capacity production of methane with significant lower values towards biological methanation.

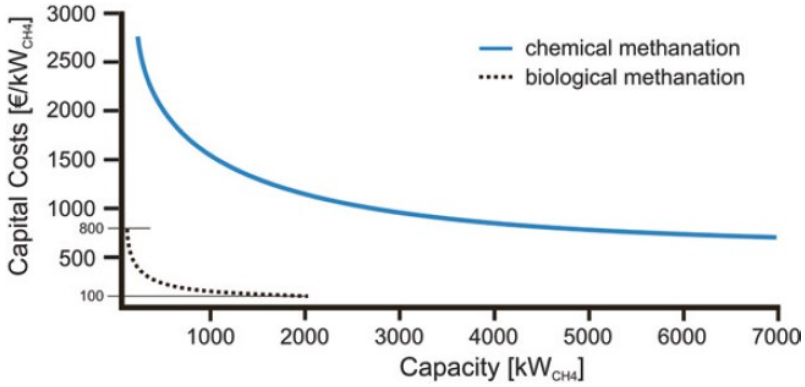

Figure 17: Cost assessments for biological and chemical methanation [10].

The lower cost of biological methanation can be attributed to the moderate operating conditions (temperature <70 °C and atmospheric pressure) leading to utilize more cost-effective materials. In addition, the absence of catalyst with no feed gas purification makes biological methanation more cheaper and simpler process.

In conclusion, the economic analysis of Power to Gas system aims to optimize the yield of plant with respect to microeconomic and macroeconomic overview. In microeconomic perspective, the cost assessment of individual component of PtG plant was evaluated. In contrast, in macroeconomic perspective, the investigation surrounding around minimization of power grid expansion and increasing contribution of renewable energies on heating and transport sections were conducted. However, in both analyses the stage of development and innovative design is essential for issuing an updated and applicable business model [24, 45].

Chapter 3

Power to Liquid Technology

3.1 Introduction

The deployment of hydrocarbon based fuels from renewable energy sources initiates from various synthesis methods, such as methanol synthesis, ammonia, dimethyl ether (DME) or Fischer-Tropsch synthesis. The proliferation of these processes not only increases the share of the renewable energy but also delivers high energy density of liquid products which can be applicable in the chemical industry and transport sectors (pipeline, truck, train, tankers) [47]. In Chapter 1, the general concepts of Power to Liquid technology and different types of FT reactor have been noted.

In this chapter, potential processes of power to liquid technology such as Dimethyl ether and Fischer-Tropsch processes, their various syntheses, simulation and efficiency are analyzed in more detail. In addition, several basic definitions, such as chain growth probability factor, catalyst types, different FT and DME kinetics are noted. First of all, the main steps of Power to Liquid Technology are put forward.

3.2 Power to Liquid Building Blocks

In general, Power to Liquids (PtL) is a production process of liquid hydrocarbons based on a CO_2 source, water and electric energy. The building blocks of Power to Liquid consist of three principal steps:

1) The H_2 production from steam electrolysis with aid of renewable energy.
2) The CO_2 provision from a potential source and its conversion
3) The process of liquid fuel production and further sub-processes regarding upgrading to desired products.

The desired products are combinations of LPG, naphtha, diesel, kerosene and wax. Figure 18 illustrates a power to liquid plant in which the required hydrogen is generated from the efficient high temperature steam electrolysis. If CO_2 is obtained from the air or biomass sources and electricity is provided by renewable sources, the GHG can be made a carbon neutral free process. After H_2 yielded from steam electrolysis step, it enters conversion reactor (RWGS) to reduce CO_2 to carbon monoxide (CO) for Fischer-Tropsch synthesis.

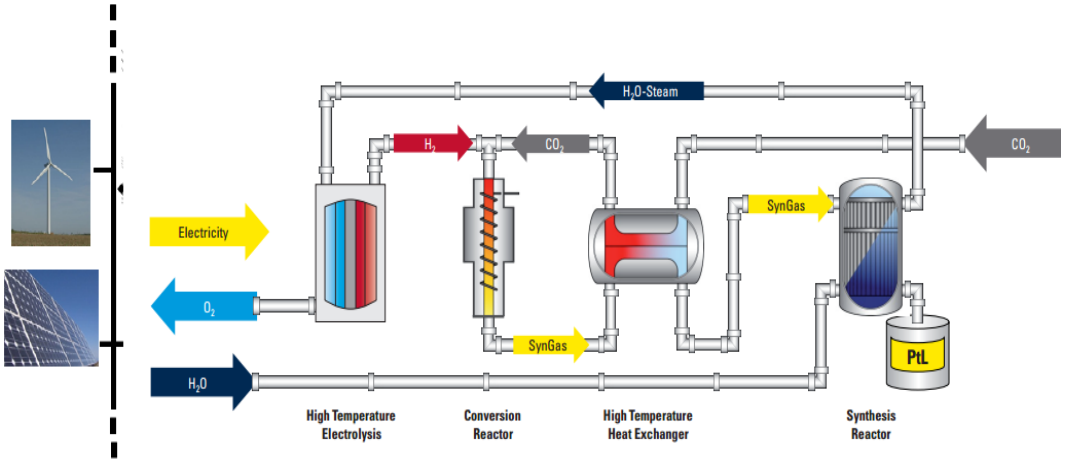

Figure 18: Power to Liquid process based on Fischer-Tropsch synthesis [47].

In a synthesis reactor (FT), the carbon monoxide and hydrogen are converted into petrol, diesel, kerosene and other hydrocarbon products for the chemical industry. The exploitation of heat released into the process to provide the heat required for electrolysis enables a high degree of system efficiency (70 percent). There are two states-of–the-art in this layout of the FT process: 1) a closed CO_2 cycle, which means the CO_2 emitted from the combustion of the fuel produced is exactly equal to the CO_2 extracted from the ambient air for the purpose of fuel

generation, which makes the process sustainable; 2) reversibility or dual functionality of the electrolysis, which means if the electricity prices go up making H_2 production unprofitable, the electrolysis system switches to fuel cell mode. In this mode, hydrogen, as an energy carrier accompanying other fuel gases, can be converted into electricity within the power & heat cycle for the public grid. Thus, this technology has the great potential to make a significant contribution towards grid stabilization.

3.3 Fischer-Tropsch Synthesis

The set of a Fischer-Tropsch reaction may occur as a result of syngas (mixture of H_2 and CO) absorption on the catalyst surface of Cobalt or Iron and consequently this conversion results in a wide variety of varying chain length products, such as paraffin and olefins i.e. wax, diesel, naphtha, gasoline and by-products, such as alcohols, light gases (unconverted syngas and methane). Therefore, the primary FT reactions are described as in the following equations [14, 16]:

$$n\mathrm{CO} + (2n+1)\mathrm{H_2} \longleftrightarrow \mathrm{C_nH_{2n+2}} + n\ \mathrm{H_2O} \qquad (25)$$

$$n\mathrm{CO} + 2n\mathrm{H_2} \longleftrightarrow \mathrm{C_nH_{2n}} + n\ \mathrm{H_2O} \qquad (26)$$

$$\mathrm{CO} + \mathrm{H_2O} \longleftrightarrow \mathrm{CO_2} + \mathrm{H_2} \qquad (27)$$

Besides, there are also several side reactions tend to occur in FT reactor such as alcohols production:

$$\mathrm{nCO} + 2\mathrm{nH_2} \longleftrightarrow \mathrm{C_nH_{2n+2}O} + (\mathrm{n\text{-}1})\ \mathrm{H_2O} \qquad (28)$$

Also, Boudouard can occur in extreme high temperatures leading to catalyst deactivation due to sintering, coking and carbon disposition as following [14]:

$$2\mathrm{CO} \longrightarrow \mathrm{C} + \mathrm{CO_2} \qquad (29)$$

3.3.1 Chain growth probability factor (α-value)

The selectivity of FT products which reflects the weight distribution of hydrocarbons based on their carbon numbers is identified by a parameter named α-value which is called chain growth probability factor. This predefined selectivity depends on operating temperature, pressure, syngas composition (H_2/CO ratio) and the type of catalysts and promoters used in the process.

Technically, α-value is defined as a ratio of the propagation of the chain growth (R_p) divided by summation of propagation and termination rate (R_t) of that as the following equation [48]:

$$\alpha = \frac{R_p}{R_p + R_t} \qquad (30)$$

The first kinetic model based on the product distribution of the hydrocarbon was proposed by Anderson within Anderson-Schulz-Flory (ASF) equation. The molar and mass fraction of a hydrocarbon was introduced as below:

$$M_n = \alpha^{n-1}(1-\alpha) \qquad (35)$$

$$W_n = \alpha^{n-1}(1-\alpha)^2\, n \qquad (36)$$

In fact, α-value identifies the distribution of Fischer-Tropsch products in terms of total carbon number of hydrocarbons according to eq. 36. (See figure 19) [49].

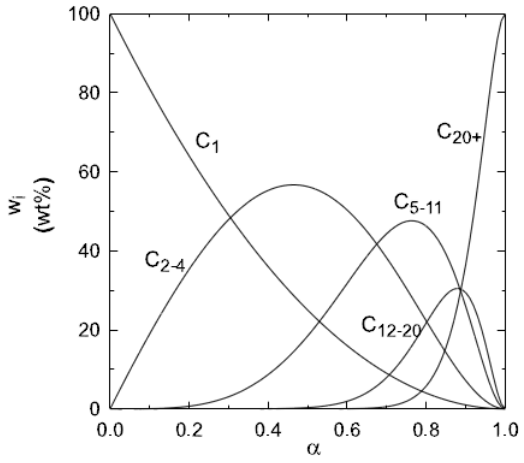

Figure 19: Fischer-Tropsch selectivity as a function of the chain growth probability based on eq. 36 [49].

Several empirical correlations for alpha value based on various experiments and tested equations were proposed. However, Song et al. (2004) [50] proposed the most developed correlation which was developed based on cobalt catalyst and was dependent on the temperature and H_2 and CO composition in the syngas:

$$\alpha = \left(A\frac{y_{co}}{y_{H_2}+y_{co}} + B\right)[1 - 0.0039(T - 533)] \quad (31)$$

Which constants are equals:

$$A= 0.2332 \quad B= 0.633 \quad (32)$$

$$y_{co} = 0.2 \qquad y_{H_2} = 0.4$$

And operating temperature (T) should be replaced in terms of Kelvin.

Hamelinck et al. (2004) [51] took further step to propose a correlation which was not only dependent on above parameters but also had a dependency of the pressure as below:

$$\alpha = 0.75 - 0.373\sqrt{-\log(S_{C_{5+}})} + 0.25S_{C_{5+}} \quad (33)$$

$$S_{C_{5+}} = 1.7 - 0.0024 - 0.088^{y_{H_2}}/_{y_{CO}} + 0.18(y_{H_2} + y_{CO}) + 0.0078 * P_t \quad (34)$$

The temperature level is quite important to find which reactor is the most suitable for producing a required product. Hence, in terms of temperature and thereby specific product two modes of Fischer-Tropsch operation exist:

Low Temperature Fischer-Tropsch (LTFT):

This mode is used in case the long chain liquid hydrocarbon (wax or diesel) is required. The temperature range of 200 – 250 °C referenced as LTFT. Based on Song correlation (Eq. 31) by increasing the temperature, the product distribution (α-value) tends to shift lower values leading to higher selectivity of light gases (C_1-C_4). The preferable reactor is slurry bubble column reactor or multitubular fixed bed. The ideal syngas ratio (H_2/CO) is equal two.

High Temperature Fischer-Tropsch (HTFT):

High temperature mode is used when specifically gases products (C_1-C_4) are required. The FT process occurs in temperature range of 300 – 360 °C. In this case, the most suitable reactor is the gas fluidized bed reactor. Also, HTFT is more favored at hydrogenation of CO_2 (CO_2 shift) and when higher H_2/CO_2 feed ratio is available (H_2/CO_2 > 4). The light hydrocarbons generated from HTFT

synthesis can be employed for increasing the heating value of SNG [52]. Furthermore, water production is higher and the reaction heat released is lowered because of being endothermic of CO_2-shift reaction [45].

.

3.3.2 Fischer-Tropsch Mechanism

The study of FT kinetics in a more realistic approach requires understanding the reaction mechanism and catalyst function. It has been many proposed mechanism to describe the product distribution FT synthesis in literature. All mechanisms initiate with chain building process within polymerization reaction as following [21]:

1) Reactant (syngas) adsorption over catalyst surface.
2) Chain initiation (formation of alkyl-group)
3) Chain growth (the joining of alkyl-group to C_nH_{2n+1}, for n=1 to N-1)
4) Chain termination (dehydrogenation of adsorbed alkyl group)
5) Product desorption (forming C_nH_{2n} as a function of carbon number)
6) Re-adsorption and additional reactions (as a result of increasing physisorption)

FT mechanism under catalyst iron initiates with monomer formation species which cause the rate determining step in syngas consumption. In this respect, three reaction mechanisms are categorized: 1) surface Carbide Mechanism; 2) enol Mechanism; 3) CO insertion Mechanism:

3.3.2.1 Enol Mechanism

In Enol mechanism the adsorbed CO reacts with hydrogen molecule to release the complex enolic species (HCOH). The chain growth occurs through bonding of the metal-enol species as shown in figure 20. Then, chain termination delivers alcohols, aldehydes and olefins where the latter can react further with hydrogen to form n-paraffin.

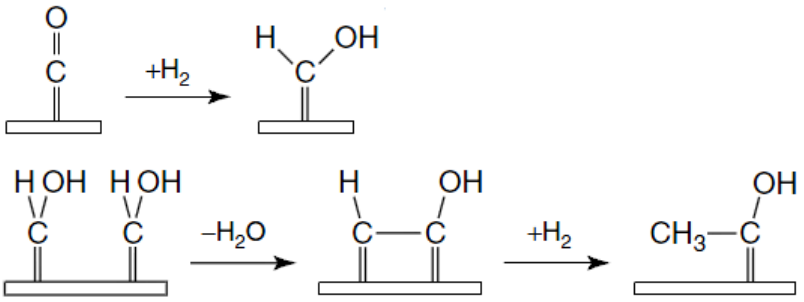

Figure 20: Fischer Tropsch synthesis in surface enol mechanism [53].

3.3.2.2 Surface Carbide Mechanism

In carbide mechanism the metal surface is carbided by molecule CO. In adsorption step, the reactants CO and H_2 are absorbed dissociatively within the first step as illustrated in figure 21. Then the carbon of metal carbide separately hydrogenated to form CH_2 species (step 2) which can grow and combine to higher alkyl species (step 3). Eventually, the chain termination is achieved either by elimination of hydrogen yielding olefin groups or by hydrogenation forming paraffin product (step 4) [21, 53].

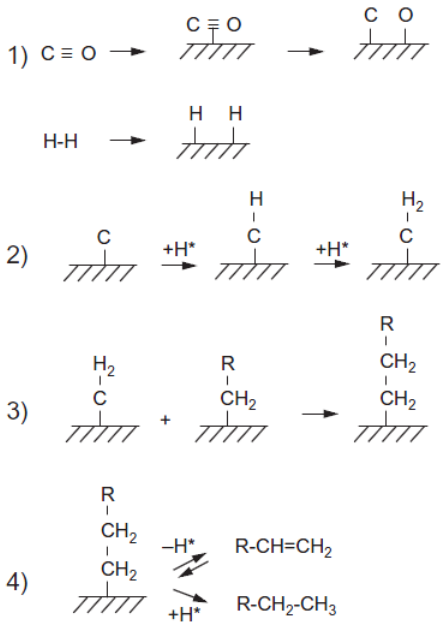

Figure 21: Fischer-Tropsch synthesis in surface carbide mechanism [21].

3.3.2.3 CO insertion mechanism

The third mechanism relates to the CO insertion to the methyl-alkyl group. The yielding alkyl species can be converted into hydrocarbons or oxygenates by hydrogenation as depicted in figure 22. In this mechanism, the same as the surface carbide mechanism, chain termination takes place by elimination or addition of hydrogen leading to an olefin or a paraffin formation. It should be noted that in this mechanism little experimental data is available in literature for hydrocarbon formation [53].

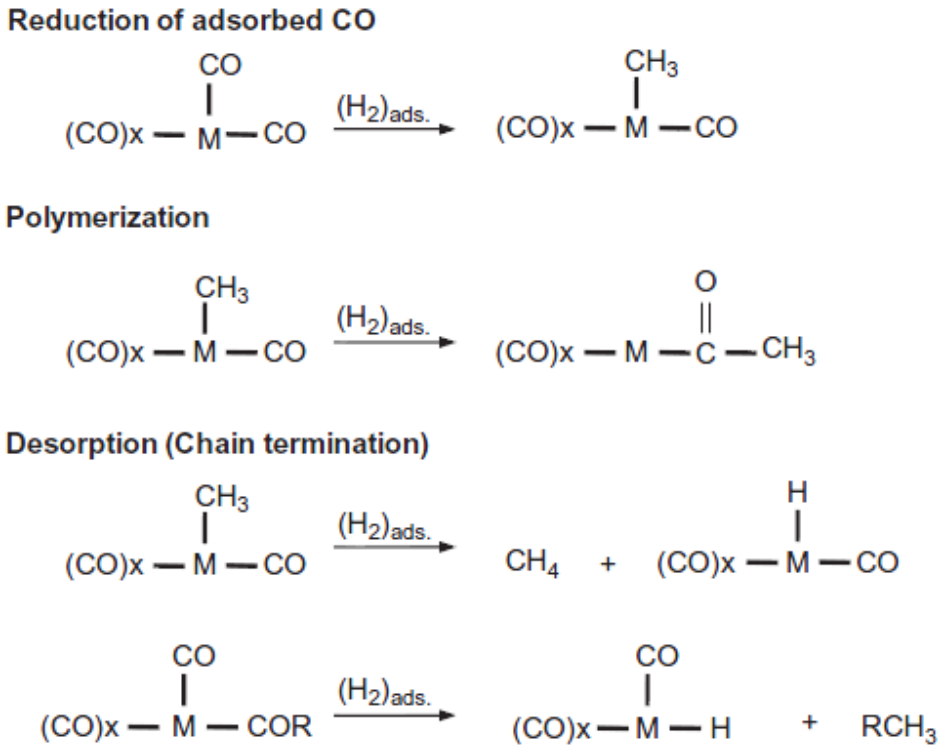

Figure 22: Fischer-Tropsch synthesis in CO insertion mechanism [53].

3.3.3 Fischer-Tropsch kinetics based on Iron catalyst

The basic kinetic equation of Fischer-Tropsch synthesis in the form of ASF distribution was mentioned in the previous section. However, the kinetic expression under catalyst cobalt and iron is different since water gas shift reaction plays an important role under iron catalyst. Furthermore, there is a major competition between water and carbon monoxide for the adsorption to the active sites of the catalyst [54]. Therefore, inhibition terms of water on iron catalysts

appears in FT kinetic expression under iron catalyst. Hence, reaction rate reduces with partial pressure of water and increases with partial pressure of hydrogen [21].

The most studies on FT kinetics over iron catalyst were conducted in Slurry Bubble Column or Fixed Bed reactors. Different forms of FT kinetics expression on iron catalyst are listed in table 3. The discrepancy amongst the rate equations illustrated in Table 3 arises from different reactors, supported catalyst and operating conditions in the process.

Table 3: Fischer-Tropsch kinetics expression on Iron Catalyst.

Catalyst	Reactor	Operating conditions			Equations	Reference
		T, °C	H_2/CO	P, MPa		
Fe	Fi*	225-265	1.0-1.8	1.2-7.2	$r_{FT} = k_{FT} P_{H_2}$	[55]
Fe	Fi	-	-	-	$r_{FT} = k_{FT} P_{H_2}^{\ 2} Pco$	[56]
Fe/Cu	Fi	220-270	1.0-1.2	-	$r_{FT} = k_{FT} \frac{P_{H_2}}{P_{CO}^{0.25}}$	[57]
Fe/MgO	Fi	200-280	10	1.0-6.0	$r_{FT} = a P_{H_2}^{\ 1.5} P_{CO}^{\ 0.2} + b P_{H_2O}^{\ 0.2} P_{CO}^{\ 0.5}$	[58]
Fe	Fi, Fl	200-340	0.5-4.0	3.12	$r_{FT} = k_{FT} \frac{P_{H_2} P_{CO}}{P_{CO} + a P_{H_2O}}$	[59]
Fe/K	SL	220-260	-	1.0-7.3	$r_{FT} = k_{FT} \frac{P_{H_2}^{\ 2} P_{CO}}{P_{CO} P_{H_2} + a P_{H_2O}}$	[60]
Fe/Cu/K	-	265	-	0.5-2.0	$r_{FT} = k_{FT} \frac{P_{H_2} P_{CO}}{P_{CO} + a P_{CO_2}}$	[61]
Fe/Plasma	Rec.	250-300	0.77-3.1	1.5-3.9	$r_{FT} = k_{FT} \frac{P_{H_2} P_{CO}}{P_{CO} + a P_{H_2O}}$	[62]

Catalyst	Reactor	Operating conditions			Equations	Reference
		T, °C	H_2/CO	P, MPa		
Fe/Cu/K	SL	250	1.2-4.0	0.25-4	$r_{FT} = k_{FT} \frac{P_{H_2}^2 P_{CO}}{(1+a P_{CO} + b P_{CO_2})^2}$	[21]
Fe/K_2O	Fi	250-315	2.4	2	$r_{FT} = k_{FT} \frac{P_{H_2} P_{CO}}{P_{CO} + a P_{H_2O}}$	[63]
Fe	Fi	220-260	0.6-2.1	1.87-2	$r_{FT}=k_{FT} C_{H_2} \frac{1}{1+ 1.6 \frac{C_{H_2O}}{C_{CO}}}$	[64]
Fe	Fi	250-350	1.5-2	3.0`-6.0	$\alpha = \frac{k_1 P_{CO}}{k_1 P_{CO} + k_5 P_{H_2} + k_6}$	[65]

* Fi: Fixed bed Reactor, SL: Slurry Bubble Column Reactor, Fl: Fluidized Bed Reactor, Rec: Recirculating Reactor.

The last kinetic expression in table 3 which is adopted from Lox and Froment (1993) [65] identified as one of comprehensive kinetics models on iron catalyst. This is able to predict not only the rate of syngas consumption but also products distribution. Therefore, the rate of olefin and paraffin are defined as follows:

$$r_{C_nH_{2n+2}} = k_5 \frac{P_{H_2}\left(\frac{k_1 P_{CO}}{k_1 P_{CO}+k_5 P_{H_2}}\right)\alpha^{n-1}}{1+\left(\frac{k_1 P_{CO}}{k_1 P_{CO}+k_5 P_{H_2}}\right)\frac{1}{1-\alpha}} \quad (n=1, 2\ldots, 10) \qquad (35)$$

$$r_{C_nH_{2n}} = k_6 \frac{P_{H_2}\left(\frac{k_1 P_{CO}}{k_1 P_{CO}+k_5 P_{H_2}}\right)\alpha^{n-1}}{1+\left(\frac{k_1 P_{CO}}{k_1 P_{CO}+k_5 P_{H_2}}\right)\frac{1}{1-\alpha}} \quad (n=2, 3\ldots, 10) \qquad (36)$$

3.3.4 Fischer-Tropsch kinetics based on Cobalt catalyst

The main difference of FT kinetics on cobalt catalyst is the absence of water gas shift due to not adsorbing water on the active site of the cobalt catalyst. Thus, water is not present in the modeling of FT kinetics using cobalt catalyst.

Driving of FT reaction rate equation starts from elementary reaction rate in the form of a power law expression as following:

$$\text{Rate} \propto f(T)\,(\text{concentration})^{n} \qquad (37)$$

where n is the reaction order. This basic form of kinetics normally fits the data because of its property and its simplicity [66]. For instance, Visconti el al. described a power law expression for the adsorption reaction of hydrogen according to their conducted experiment under catalyst Co/Al_2O_3. The reaction rate was a function of syngas surface reaction rates in terms of H_2 and CO partial pressures [67].

The other common form of FT kinetics is Langmuir-Hinshelwood-Hougen-Watson (LHHW) type expression which is based on reactants absorption on the catalyst surface and predominant surface component. This indicates rate determining step in order to estimate suitable kinetic parameters. These parameters can be used as initial values for fitting the equation. The general form of LHHW model is defined as following [54, 66]:

$$\text{rate} \propto \frac{(\text{kinetic factor})(\text{driving force})}{(\text{adsorption term})^{n}} \qquad (38)$$

In 1991, Satterfield and Yates [68] proposed FT kinetics considering CO as a predominant surface component on cobalt surface. Thus CO is replaced in adsorption term as its absorption is stronger than H_2. Having made assumptions on adsorption and desorption over the cobalt surface, the kinetic expression is simplified as following [54, 68]:

$$-R_{CO} = \frac{a\,P_{CO}\,P_{H_2}}{(1+b\,P_{CO})^{2}} \qquad (39)$$

a and b which are supposed to be temperature-dependent constants are identified as a kinetic parameter and an adsorption coefficient, respectively. For

example, Krishna and Sie (2000) [69] introduced these constants in terms of temperature with respect to properties of supported CO/MgO catalyst by assuming $\rho_L = 647$ kg/m^3:

$$a = 8.8533 \times 10^{-3} \exp [4494.41\ (1/493.15 - 1/T)]\ \frac{mol}{s\ kg_{cat} bar^2} \quad (40)$$

$$b = 2.226 \times \exp [-8236\ (1/493.15 - 1/T)]\ \frac{1}{bar} \quad (41)$$

There are numerous FT kinetics over catalyst cobalt in literature. Here as an illustration, a number of them list in Table 4.

Table 4: Fischer-Tropsch kinetics expression on the Cobalt Catalyst.

Catalyst	Reactor	Operating conditions			Equations	Reference
		T, °C	P, Mpa	H_2/CO		
Co	-	-	-	-	$r_{FT} = k_{FT} \frac{P_{H_2}^{\ 2}}{P_{CO}}$	[56]
Co	-	-	-	-	$r_{FT} = k_{FT}\ P_{H_2}\ P_{CO}^{\ 0.5}$	[70]
Co	-	-	-	-	$r_{FT} = k_{FT} \frac{P_{H_2}^{\ 0.55}}{P_{CO}^{0.33}}$	[71]
Co/Al_2O_3	Fi	250	0.015-0.1	0.25-5	$r_{FT}=k_{FT}\frac{P_{H_2}^{\ 2} P_{CO}^{\ 0.5}}{(1+P_{CO}^{0.5}+b\ P_{H_2}^{\ 1.5})}$	[72]
Co/Zr/SiO_2	SL	200-280	2.1	0.5-2	$r_{FT}=k_{FT} \frac{P_{H_2}^{\ 2}\ P_{CO}}{P_{CO}\ P_{H_2} + a\ P_{H_2O}}$	[73]
Co/MnO	Fi	210-250	0.6-2.6	1.6-4.1	$r_{FT} = k_{FT} \frac{P_{H_2}\ P_{CO}}{P_{CO}\ + a\ P_{H_2O}}$	[74]

Catalyst	Reactor	Operating conditions			Equations	Reference
		T, °C	P, Mpa	H_2/CO		
Co	-	190	0.2-1.5	0.5-8.3	$r_{FT}=k_{FT}\frac{P_{H_2}P_{CO}^{0.5}}{(1+P_{CO}^{0.5}+bP_{H_2}^{1.5})}$	[75]
Co/Al_2O_3	SL	220	2.0	1.6-3.35	$r_{FT}=k_{FT}\frac{P_{H_2}^{1.5}P_{CO}}{(P_{H_2O}+aP_{H_2}P_{CO})^2}$	[76]
Co/MgO/SiO_2	SL	220-240	1.5-3.5	1.5-3.5	$-r_{FT}=k_{FT}\frac{aP_{CO}P_{H_2}}{(1+bP_{CO})^2}$	[68]
Co/MgO/SiO_2	Fi	190-210	0.01-2.54	-	$r_{FT}=\frac{k_{FT}(P_{H_2}^{1.5}.\frac{P_{CO}}{P_{H_2O}})}{(1+a.\left(P_{H_2}.\frac{P_{CO}}{P_{H_2O}}\right))^2}$	[77]

3.4 The Simulation of Power to Liquid based on FT synthesis

In this dissertation, the simulation of Power to Liquid based on FT synthesis over a cobalt catalyst has been conducted. The simulation was performed by a commercial simulator, Aspen plus V8.0, based on high temperature electrolysis, reverse water gas shift and low temperature Fischer-Tropsch synthesis (see figure 23).

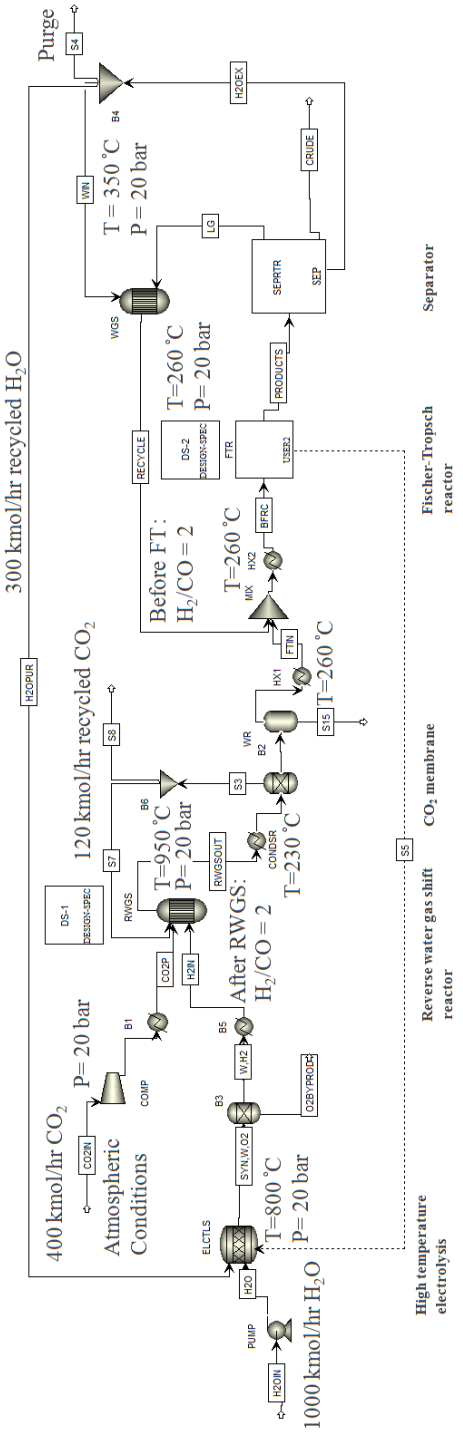

Figure 23: Simulation of Fischer-Tropsch process based on renewable energy; configuration flow sheet in Aspen plus.

In the simulation as figure 23 shows, first the steam is split by high temperature electrolysis into its constituents (H_2 & O_2) then, the oxygen is separated and hydrogen enters the RWGS reactor in order to reduce the CO_2 coming from the direct CO_2 capture equipment. The shift reaction occurs at a very high temperature and pressure and the heat required for reduction is supplied by electrical energy. The temperature of RWGS is calculated by Design Specification in Aspen plus by setting a syngas ratio equal to 2. This assumption is made to have an inlet syngas ratio of the FT reactor similar to the usage ratio (H_2/CO), which is about 2. The syngas accompanied by optimal carbon conversion in the FT reactor [6]. After decreasing the temperature to 230 $^{\circ}$C, the syngas accompanying steam and unconverted CO_2 goes to a polymeric high temperature CO_2 membrane which separates the CO_2 from the water and syngas. Then the syngas, with proper operating conditions (T=230 $^{\circ}$C, P = 20 bar and H_2/CO ~ 2), is fed into the FT reactor and delivers a wide variety of FT products. After the FT reactor, a three phase separator separates the water and off-gas from the liquid products. In the subsequent FT unit there is an external recycle stream which passes through a water gas shift reactor to the inlet of the FT reactor. The external recycling aims to provide sufficient hydrogen for the hydrogenation of the CO to maintain the syngas ratio constant before the FT reactor. Also, a majority of steam is recycled to the electrolysis to exploit the water produced. A particularly important point is the integration of heat released from the FT reactor to the steam electrolysis to provide the heat required.

To model the FT reactor in the process, an external subroutine within Excel Spreadsheet through USER2 MODEL on the simulator is implemented. This subroutine is defined based on a novel stoichiometric model in the form of FT generic reaction, which is adopted from [6]:

$$n\,CO + (n - p + 0.5\,m)\,H_2 \longrightarrow C_nH_mO_p + (n - p)\,H_2O \qquad (42)$$

where n, m and p indicate the number of carbon, hydrogen and oxygen atoms in a specific hydrocarbon product. As already mentioned, there are several by-products in FT synthesis which are represented as Oxygenated Compounds. In this approach, they are known as pseudo-components and are classified by aqueous phase (eq. 43), vapor phase (eq. 44), and organic phase (eq. 45). The carbon converted in each phase equals 1.0 %, 0.1% and 0.4%, respectively [6]. In

this modeling, the oxygenated compounds need to be excluded in order to predict the desired products in a more precise way.

Aqueous phase: $1.95CO + 3.815\ H_2 \longrightarrow C_{1.95}H5.77O_{1.02} + 1.93H_2O$ (43)

Vapor phase: $2.43CO + 4.275\ H_2 \longrightarrow C_{2.43}H_{5.69}O + 1.43H_2O$ (44)

Organic phase: $4.78CO + 9.25\ H_2 \longrightarrow C_{4.78}H_{11.14}O_{1.1} + 1.43H_2O$ (45)

According to the following equation, the effluent molar flow rate of each FT product is equal to the multiplication of the carbon monoxide molar flow rate, the CO conversion, the exclusion term of oxygenated compounds and the coefficient Cr_i:

$$F_i^{FTout} = F_{co}^{FTin} \times X_{co} \times Cr_i \times (1 - 1\% - 0.1\% - 0.4\%) \quad (46)$$

The coefficient of C_{ri} denotes the fraction of carbon at each hydrocarbon product which defines as following:

$$Cr_i = \frac{n\,W_n}{\sum_{n=1}^{60} nW_n} \quad (47)$$

$$W_n = n\,(1-\alpha)^2\,\alpha^{n-1} \quad (48)$$

The CO conversion in this calculation is assumed to be 80 % based on [6].

On the other hand, as already mentioned, the α-value depends on temperature according to Song et al. 2004 correlation [50]. The equations (43), (44) and (45) are defined based on generic reaction (42) at Excel spreadsheet for FT hydrocarbons C_1 to C_{60}. Then the spreadsheet is implemented as an external subroutine on Aspen plus and the results reflect in the form of the concentrations of C_1 to C_{60} in a lookup table (see table 5). It should be noted that this FT mathematical modeling was developed using the stoichiometry-based method (Eq. 42) (without using explicit kinetic reactions) and the syngas ratio at the inlet of the reactor is set to 2 (optimal ratio for producing long-chain hydrocarbons in LTFT synthesis). Besides this, an important property of cobalt-based catalysts is their ability to operate using syngas having a stochiometric ratio (i.e = 2) since they do not promote water gas shift reaction. As a result, in this mathematical modeling it is assumed that the FT process is operated under cobalt catalyst. Figure 24 summaries the methodology of the FT modeling in Aspen plus with aid of implementing Excel spreadsheet and related correlations.

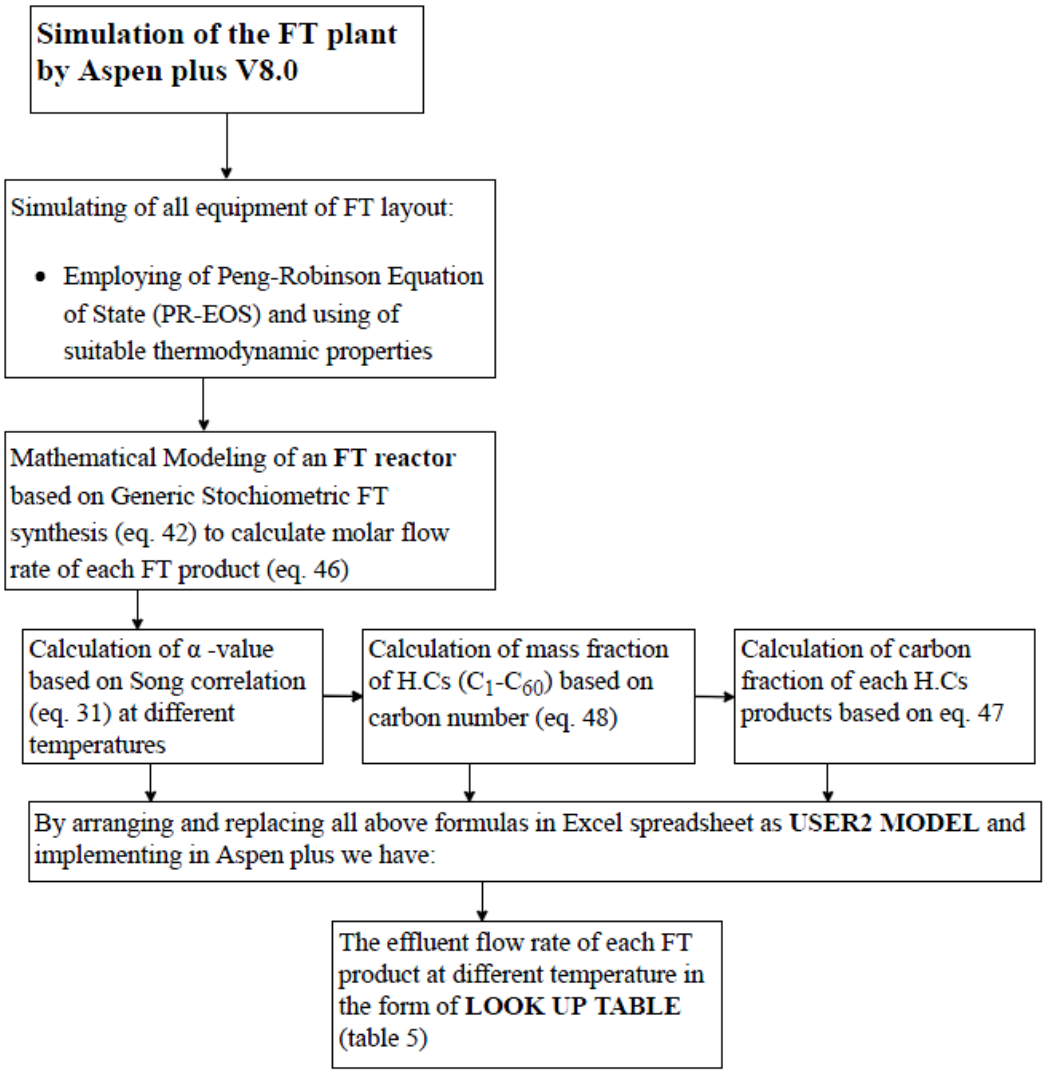

Figure 24: Methodology of the FT modeling with aid of Excel spreadsheet in Aspen plus.

Table 5: The Lookup table: FT products in different temperature

FT Products	210 °C	220 °C	230 °C	240 °C	250 °C	260 °C
CH_4	0,57811	0,89793	1,34416	1,94286	2,71995	3,70177
C_2H_6	0,19506	0,29309	0,42394	0,59138	0,79796	1,04523
C_3H_8	0,24682	0,35875	0,50141	0,67502	0,87787	1,10674
NC_4H_{10}	0,26373	1,48326	2,00315	2,60256	3,26220	3,95833
NC_5H_{12}	0,32931	0,44792	0,58451	0,73289	0,88542	1,03403
NC_6H_{14}	0,33335	0,43861	0,55305	0,66924	0,77927	0,87591
C_7H_{16}	0,43742	0,55676	0,67834	0,79220	0,88906	0,96181
C_8H_{18}	0,42170	1,21153	1,42631	1,60754	1,73884	1,81050
C_9H_{20}	0,40019	0,47666	0,54223	0,58979	0,61489	0,61620
$C_{10}H_{22}$	0,37509	0,43219	0,47505	0,49868	0,50108	0,48330
$C_{11}H_{24}$	0,34804	0,38794	0,41203	0,41742	0,40426	0,37528
$C_{12}H_{26}$	0,32028	0,34535	0,35442	0,34652	0,32345	0,28899
$C_{13}H_{28}$	0,29269	0,30529	0,30274	0,28566	0,25700	0,22100
$C_{14}H_{30}$	0,26589	0,26829	0,25707	0,23410	0,20299	0,16800
$C_{15}H_{32}$	0,24031	0,23457	0,21718	0,19086	0,15951	0,12707

FT Products	210 °C	220 °C	230 °C	240 °C	250 °C	260 °C
$C_{16}H_{34}$	0,21623	0,20417	0,18266	0,15492	0,12479	0,09567
$C_{17}H_{36}$	0,19380	0,17702	0,15303	0,12526	0,09725	0,07176
$C_{18}H_{38}$	0,17310	0,15295	0,12776	0,10092	0,07552	0,05363
$C_{19}H_{40}$	0,15413	0,13174	0,10633	0,08106	0,05846	0,03996
$C_{20}H_{42}$	0,13686	0,11316	0,08825	0,06493	0,04514	0,02969
$C_{21}OP$	0,40406	0,32321	0,24356	0,17294	0,11587	0,07337
$C_{22}OP$	0,35708	0,27630	0,20119	0,13787	0,08903	0,05425
$C_{23}OP$	0,31491	0,23572	0,16584	0,10968	0,06826	0,04004
$C_{24}OP$	0,27719	0,20071	0,13645	0,08709	0,05224	0,02949
$C_{25}OP$	0,24356	0,17061	0,11207	0,06903	0,03991	0,02169
$C_{26}OP$	0,21368	0,14479	0,09190	0,05463	0,03044	0,01592
$C_{27}OP$	0,18718	0,12270	0,07525	0,04317	0,02319	0,01167
$C_{28}OP$	0,16374	0,10383	0,06153	0,03407	0,01764	0,00854
$C_{29}OP$	0,14306	0,08775	0,05025	0,02685	0,01340	0,00625
C_{30}	0,11140	0,07014	0,03999	0,02091	0,01012	0,00455
C_{31}	0,09711	0,05914	0,03258	0,01645	0,00767	0,00332

FT Products	210 °C	220 °C	230 °C	240 °C	250 °C	260 °C
C_{32}	0,08456	0,04982	0,02652	0,01292	0,00581	0,00242
C_{33}	0,07355	0,04192	0,02156	0,01014	0,00439	0,00176
C_{34}	0,06393	0,03525	0,01752	0,00795	0,00332	0,00128
C_{35}	0,05551	0,02961	0,01422	0,00623	0,00251	0,00093
C_{36}	0,04816	0,02485	0,01153	0,00487	0,00189	0,00068
C_{37}	0,04176	0,02084	0,00934	0,00381	0,00142	0,00049
C_{38}	0,03617	0,01747	0,00757	0,00298	0,00107	0,00036
C_{39}	0,03132	0,01463	0,00612	0,00233	0,00081	0,00026
C_{40}	0,02709	0,01224	0,00495	0,00182	0,00061	0,00019
C_{41}	0,02343	0,010241	0,004003	0,001416	0,000457	0,000135
C_{42}	0,02024	0,008561	0,003233	0,001104	0,000343	9,76E-05
C_{43}	0,01748	0,007152	0,00261	0,00086	0,000258	7,05E-05
C_{44}	0,01509	0,005972	0,002106	0,00067	0,000193	5,09E-05
C_{45}	0,01302	0,004984	0,001698	0,000521	0,000145	3,68E-05
C_{46}	0,01122	0,004157	0,001369	0,000405	0,000109	2,65E-05
C_{47}	0,00967	0,003466	0,001103	0,000315	8,15E-05	1,91E-05

FT Products	210 °C	220 °C	230 °C	240 °C	250 °C	260 °C
C_{48}	0,00833	0,002889	0,000888	0,000245	6,11E-05	1,38E-05
C_{49}	0,00717	0,002406	0,000715	0,00019	4,57E-05	9,94E-06
C_{50}	0,00617	0,002004	0,000575	0,000148	3,42E-05	7,16E-06
C_{51}	0,00531	0,001668	0,000462	0,000115	2,56E-05	5,16E-06
C_{52}	0,00457	0,001388	0,000372	8,9E-05	1,91E-05	3,71E-06
C_{53}	0,00393	0,001154	0,000299	6,9E-05	1,43E-05	2,67E-06
C_{54}	0,00337	0,00096	0,00024	5,35E-05	1,07E-05	1,92E-06
C_{55}	0,00290	0,000798	0,000193	4,15E-05	7,99E-06	1,38E-06
C_{56}	0,00249	0,000663	0,000155	3,21E-05	5,96E-06	9,93E-07
C_{57}	0,00214	0,00055	0,000124	2,49E-05	4,45E-06	7,13E-07
C_{58}	0,00183	0,000457	9,97E-05	1,93E-05	3,32E-06	5,12E-07
C_{59}	0,00157	0,000379	7,99E-05	1,49E-05	2,48E-06	3,68E-07
C_{60}	0,00135	0,000315	6,41E-05	1,15E-05	1,85E-06	2,64E-07

At this stage, in order to understand the variation of each FT hydrocarbon cut with temperature, hydrocarbons are clustered into five different carbon cut, each of which represents specific FT product. These carbon cuts are lumped in the form

of C_1, C_2-C_4, C_5-C_{10}, C_{11}-C_{19}, and C_{20}-C_{60} which are attributed to methane, LPG, naphtha, diesel and wax, respectively. By doing so, figure 25 illustrates the influence of temperature on the so-called hydrocarbon cuts.

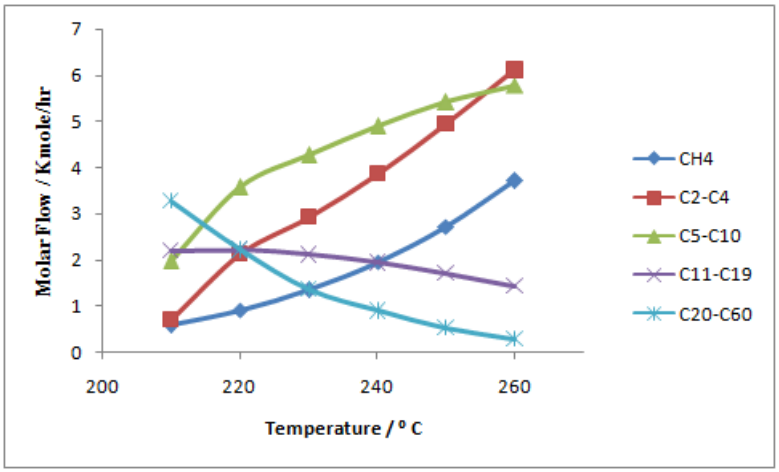

Figure 25: The influence of operating Temperature on molar flow.

As seen in Figure 25, with increasing temperature the molar flow of heavier hydrocarbons i.e. wax and diesel decrease whilst, the molar flow of methane, LPG and naphtha increase as to be expected. This is due to the temperature impact on α-value which tends to shift the products to heavier hydrocarbons at lower temperatures corresponding higher chain growth probability factor.

3.5 The Efficiency parameters in PtL:

3.5.1 The Calculation of the Efficiency of FT process:

The system efficiency for this investigated layout is described by the enthalpy flow of produced fuel divided by the enthalpy flow of syngas fed into electrolysis plus compressor's work. For FT liquid fuels the enthalpy flow is calculated based on lower heating value (LHV) of relevant chemicals [47, 78].

$$\eta_{FT} = \frac{\sum_{i=1}^{n} n_i \times LHV_i}{\sum_{j=1}^{m} E_j + W_{comp}} \qquad (49)$$

where, n denotes the number of carbons (n=60), m refers to the number of reactions involved in the process (m=4). The reactions in this layout are as following:

A) Evaporation:

$$3\ H_2O_{(L)} \longrightarrow 3\ H_2O_{(G)} \qquad E_1 = +\ 141\ KJ/mol \qquad (50)$$

B) Water Electrolysis

$$3\ H_2O_{(G)} \longrightarrow 3\ H_2 + 1.5\ O_2 \qquad E_2 = +\ 726\ KJ/mol \qquad (51)$$

C) Reverse Water Gas Shift

$$3\ H_2 + CO_2 \longrightarrow 2\ H_2 + CO + H_2O \qquad E_3 = +\ 41\ KJ/mol \qquad (52)$$

D) Fischer-Tropsch synthesis

$$2\ H_2 + H_2O + CO \longrightarrow CH_2 + 2\ H_2O \qquad E_4 = -\ 147\ KJ/mol \qquad (53)$$

The LHV or net calorific value of a fuel is referred as the energy content of a fuel which is released in the form of heat while the combustion occurs. The temperature of combustion products is returned to be 150 $^{\circ}$C and the product of water is assumed in vapor form which its vaporization latent heat is not recovered. This usable energy content can be either adopted from API technical data book or can be calculated from following empirical relations based on the amount of energy stored in paraffins and olefins [79]:

$$LHV_{paraffins} = 608.44n + 213.31 \qquad (n=60) \qquad (49)$$

$$LHV_{olefins} = 604.93n + 113.83 \qquad (n=60) \qquad (50)$$

By considering and replacing above quantities in Eq. 49 the efficiency of the Fischer-Tropsch process is calculated as 71.2 %.

3.5.2 The Calculation of H_2O-electrolysis efficiency in PtL:

The efficiency contribution of the steam electrolysis is defined as enthalpy flow of the generated syngas divided by input power which includes the electrical and thermal required energy for water electrolysis plus the energy content of the electrolyzer's reactants [78].

$$\eta_{el} = \frac{\sum_{Syngas} n_j LHV_j}{Q_{el,net} + P_{el} + \sum_{el} r_i LHV_i} \quad (51)$$

where, n_j and r_i denote moles of syngas out of electrolysis and moles of electrolyzer's reactant. Also, $Q_{el,net}$ and P_{el} represent thermal and electrical required energy for electrolysis, respectively. By considering these values, the efficiency is calculated as 82 %.

3.5.3 The Calculation of the efficiency of PtL system:

Total efficiency of PtL system which includes three aforementioned steps identifies the usable energy content (enthalpy flow) of produced fuel divided by total power consumption within the PtL process including reactants 'enthalpy feeding the electrolysis, the work of compressor and overall heat energy requirements.

$$\eta_{total} = \frac{\sum_{i=1}^{n} n_i \times LHV_i}{\sum_{el} r_i LHV_i + Q_{sys,net} + P_{el} + W_{comp}} \quad (52)$$

This total efficiency reflecting overall system performance of PtL technology is calculated as 76.6 %.

3.6 Dimethyl Ether Synthesis

The second pathway for producing clean sustainable liquid fuels based on renewable energy is emerged as Dimethyl Ether synthesis. DME is an industrially proven fuel for diesel engines because of low emission of CO and particulates in the exhaust gas and its relatively high cetane number [80, 81]. In general, DME is produced from syngas which can be derived from different energy sources such as biomass, coal, waste and natural gas. In this respect, the conversion of syngas to DME can be conducted within two approaches [82]:

1) Indirect approach (two steps process) which involves methanol synthesis and dehydration step in two separate reactors. In this method, at first syngas is converted into methanol under a specific MeOH catalyst and then methanol is dehydrated to DME in a second reactor under an acidic catalyst. This process is hindered by a relatively low conversion due to the equilibrium limitation of methanol formation. Furthermore, this method results in increasing capital cost in two-stage process which involves more required equipment for the whole process.

2) Direct approach (one step process) is the DME production as a result of synergetic reactions amongst methanol synthesis, water gas shift and methanol dehydration. These reactions all occur in one reactor under a hybrid catalyst without separating MeOH to dehydrate it.

In this dissertation, for DME process, the optimized configuration of one step DME production based on renewable energy is taken into account. At first, the kinetics used for direct one step DME process is introduced then the process is simulated by software Aspen Plus.

3.6.1 Kinetics and Reaction scheme for DME process:

The kinetics used in this study is adopted from one step DME simulation over catalyst $Cu/ZnO/Al_2O_3$ [85]. The overall DME reaction scheme is composed of three-step reactions including methanol synthesis, methanol dehydration and water gas shift. In this reaction scheme, the methanol formation includes two reactions due to presence of CO, CO_2 and H_2 as main reactants:

$$CO + 2H_2 \longrightarrow CH_3OH \qquad \text{-43.4 kcal/mol-DME} \qquad (53)$$

$$CO_2 + 3H_2 \longrightarrow CH_3OH \qquad \text{-13.5 kcal/mol-DME} \qquad (54)$$

The water gas shift reaction has an important role to promote H_2 for methanol formation and DME synthesis:

$CO + H_2O \longrightarrow CO_2 + H_2$ -9.8 kcal/mol-DME (55)

And the DME is produced through methanol dehydration through following reaction:

$2CH_3OH \longrightarrow CH_3OCH_3 + H_2O$ -5.6 kcal/mol-DME (56)

The overall reaction which is the combination of (53), (55) and (56) is as follows:

$3CO + 3H_2 \longrightarrow CH_3OCH_3 + CO_2$ -58.8 kcal/mol-DME (57)

The kinetics for above reactions' cmponents is expressed in the form of Langmuir Hineshwood Hougen Watson (LHHW) as follows [85]:

$$r_{CO} = \frac{k_1 \, f_{CO} \, f_{H_2}^2 \, (1-\beta_1)}{(1+K_{CO} f_{CO} + K_{CO_2} f_{CO_2} + K_{H_2} f_{H_2})^3} \qquad \beta_1 = \frac{f_{CH_3OH}}{K_{f_1} f_{CO} f_{H_2}^2} \qquad (58)$$

$$r_{CO_2} = \frac{k_2 \, f_{CO_2} \, f_{H_2}^3 \, (1-\beta_2)}{(1+K_{CO} f_{CO} + K_{CO_2} f_{CO_2} + K_{H_2} f_{H_2})^4} \qquad \beta_2 = \frac{f_{CH_3OH} \, f_{H_2O}}{K_{f_2} f_{CO_2} f_{H_2}^3} \qquad (59)$$

$$r_{DME} = \frac{k_3 \, f_{CH_3OH} \, (1-\beta_3)}{(1+\sqrt{K_{CH_3OH} \, f_{CH_3OH}})^2} \qquad \beta_3 = \frac{f_{DME} \, f_{H_2O}}{K_{f_3} f_{CH_3OH}^3} \qquad (60)$$

$$r_{WGS} = \frac{k_4 \, f_{H_2O} \, (1-\beta_4)}{1+K_{CO} f_{CO} + K_{CO_2} f_{CO_2} + \sqrt{K_{H_2} f_{H_2}}} \qquad \beta_4 = \frac{f_{CO_2} \, f_{H_2}}{K_{f_4} f_{CO} f_{H_2O}} \qquad (61)$$

All reaction rate constants follow power law form according to Table 6. Also, the equilibrium constants, adsorption coefficient and modified values for reaction rate constants are mentioned at Table 6.

Table 6: Reaction rate constants, adsorption coefficients and equilibrium constants for DME synthesis [80].

Parameters	Reference		Modified	
A(i)exp(B(i)/RT)	A(i)	B(i)	A'(i)	B'(i)
k_1	7380	-54307	7380	-58464
k_2	5059	-67515	5059	-67509
k_3	1062	-46473	1062	-43473
k_4	7.3976	-20436	7.3976	-10808
K_{CO}	3.934×10^{-6}	37373	3.934×10^{-6}	1.65
K_{CO_2}	1.858×10^{-6}	53795	1.858×10^{-6}	53795
K_{H_2}	0.6716	-6476	0.6716	-6476
K_{CH_3OH}	3.480×10^{-6}	54689	7.928×10^{-4}	48221

3.6.2 The Simulation of Power to Liquid based on DME synthesis

In the simulation of DME process based on renewable energy, Soave Redlich Kwong (SRK) is utilized as the governing equation of state (EOS). This equation is employed for the thermodynamic properties between mixtures and pure components as well as binary components. As figure 26 shown, at first the steam is split in high temperature electrolysis into its constituents (H_2 & O_2) then, the oxygen is separated and hydrogen enters the RWGS reactor in order to reduce CO_2 coming from the direct CO_2 capture equipment. After CO_2 reduction in the RWGS reactor, the mixture of CO, CO_2 and H_2 is fed into the one step DME

reactor. The reactor RPLUG (Shell and tube type) in terms of multitublar non-adiabatic packed bed reactor is chosen. In this simulation, DME production is led by both CO_2 and CO species within catalytic reactions over the LHHW kinetics model. The kinetics relations of (58-61) in the form of LHHW are implemented in software Aspen plus. In the section of sensitivity analysis, temperature and pressure of the reactor are defined as manipulated variables in order to find maximum yield and selectivity of DME in the specific temperature and pressure.

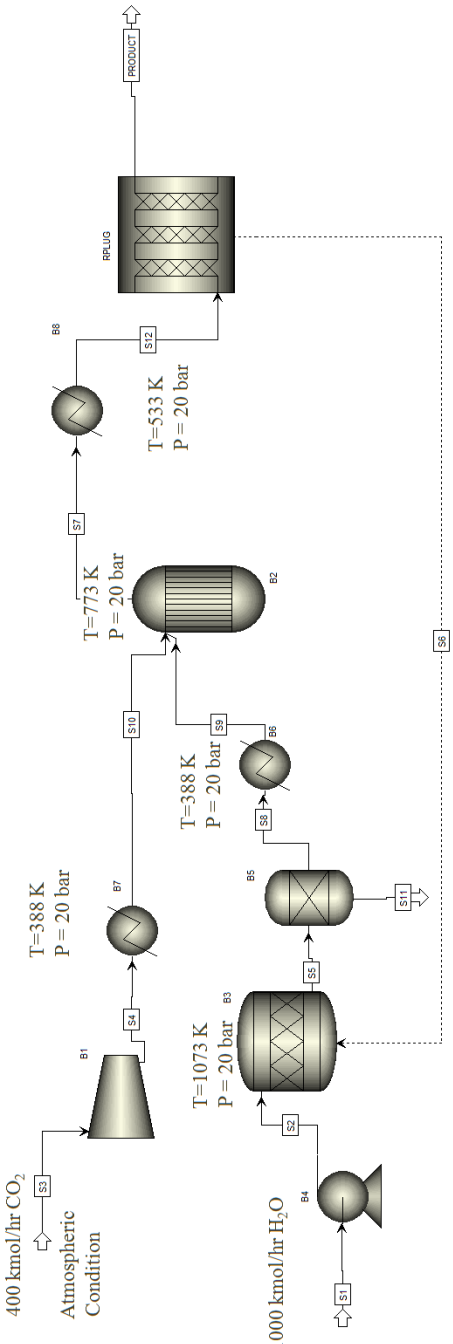

Figure 26: Simulation of DME process based on renewable energy; configuration flow sheet in Aspen plus.

The selectivity and yield of DME are defined as follows:

$$\text{Selectivity} = \frac{\text{Exit molar flow rate of desired product (DME)}}{\text{Molar flow rate of overall product}} = \frac{2\,F_{DME}}{2\,F_{DME} + F_{CH_3OH}} \quad (62)$$

$$\text{Yield} = \frac{\text{Exit molar flow rate of desired product (DME)}}{\text{Molar flow rate of initial reactants}} = \frac{2\,F_{DME}}{F_{CO} + F_{CO_2}} \quad (63)$$

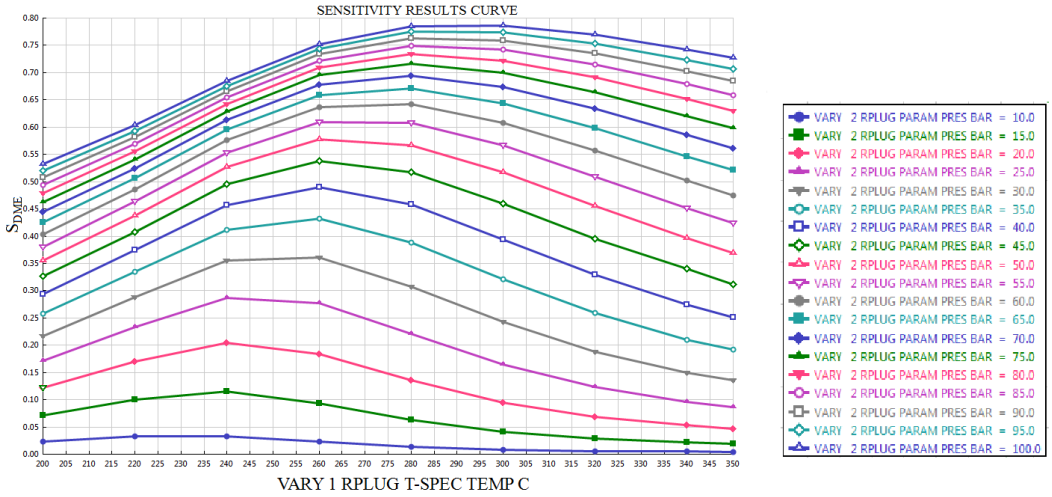

Figure 27: Maximum DME selectivity in specific feed molar flow rate and composition.

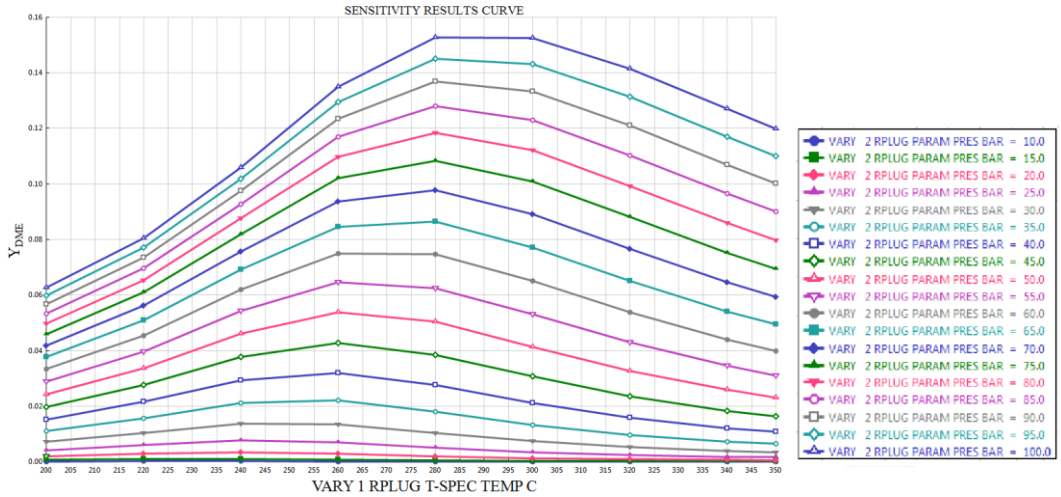

Figure 28: Maximum DME yield in specific feed molar flow rate and composition.

These two variables (S_{DME}, Y_{DME}) are tabulated in Model Analysis Tools at different operating temperatures and pressures. In fact, this analysis reflects the influence of temperature and pressure on the selectivity and yield of Dimethyl Ether. As figure 27 illustrated, by increasing the temperature, the DME selectivity increases to around 260 °C, then decreases by increasing the temperature at all operating pressures. It is found that maximum DME selectivity occurs at T=280 °C and P=100 bar equal to 78 %. Similar behavior is also observed in the variation of DME yield (see figure 28). The maximum DME yield is also achieved at T=280 °C and P=100 bar equal to 15 %.

The main challenge of renewable DME synthesis in the one-step process is the CO_2 produced as a result of unreacted syngas, which leads to low DME yield. This setback also makes the separation of CO_2 and DME in the presence of methanol more difficult [82]. One proposed separation method could be to condense water and methanol, then to absorb the gas stream of condensed reaction by water; at the end, the liquid containing DME undergoes distillation in order to obtain DME product with high purity [83]. Furthermore, One-step direct DME synthesis is not industrially justifiable because of the amount of CO_2 produced by the consumption of CO in the water gas shift reaction, which makes the syngas process energy intensive and a greenhouse gas emitting process [84]. During recent years, several methods have been proposed to make the DME process more energy efficient and environmentally friendly. For instance, the DME synthesis process can be integrated with hydrocarbon reforming units recycling CO_2 to increase the yield of the DME product. However, this leads to increased operational costs in DME process design [82]. In another approach, selective H_2O removal by the sorption-enhanced reaction concept could result in the displacement of WGS equilibrium and enhance CO_2 conversion which favors the yield and selectivity of the DME product [85]. In this respect, the ratio of CO: CO_2 in the feed composition is an important parameter. If CO content feed is gradually replaced by CO_2 as in-situ H_2O removal, a strong synergy between the water formed and methanol production brings about an enhancement in methanol productivity and DME selectivity [81, 82].

By comparing the three alternative catalytic processes for renewable power to gaseous and liquid fuels (Methanation, Direct Dimethyl Ether and Low Temperature Fischer-Tropsch) it can be concluded that the Solid Oxide Electrolysis Cell is suitable for Methanation and Dimethyl Ether, since it meets the quality requirements of the natural gas grid for methanation (95%) and process efficiency of 87%. Also, for DME, in the once-through process the

product selectivity reaches 78% and its purity can be increased by considering separation units and recycling unreacted syngas. However, the SOEC for Fischer-Tropsch synthesis delivers low value liquid products because of the low capacity of the SOEC.

Chapter 4

Dynamic Modeling of Slurry Fischer-Tropsch reactor

4.1 Introduction

In recent years, several dynamic modeling of FT slurry reactor have been performed. In 2002, J.W.A de Swart and R. Krishna [86] proposed a model to predict dynamic behavior and steady state condition of a bubble column slurry reactor for Fischer-Tropsch synthesis. Their numerical approach was based on a set of PDEs solved using Method of Lines (MOL). They investigated the effect of back-mixing of liquid phase on hydrogen conversion for two different reactors diameters (1, 7.5 m). Therefore, they concluded that the level of backmixing in the liquid phase is an important parameter in scale up issues. Furthermore, it was concluded in diameter 1 m, the axial dispersion coefficient decreased leading to increased plug flow profile in the liquid phase and the results showed that steady-state is achieved within about seven minutes from start-up [86].

In 2005, Rados et al. [87] established a mathematical model of FT slurry bubble column reactor by considering the change in gas flow rate over the reactor bed. They accounted this change for overall gaseous species transport equation due to chemical reaction. They evaluated the hydrodynamic behavior of two bubble class model by supposing linear first-order reaction kinetics. They also analyzed the effect of Axial Dispersion Model (ADM) on reactor diameter and conversion. Furthermore, they compared this influence in ideal reactors such as plug flow (PF) and completely stirred tank (CST) [87]. In 2009, Hooshyar et al. [88] simulated transient FT slurry for both single and double bubble class at

heterogeneous flow regime. They concluded that there is no difference between single and double class models in terms of temperature, concentration, and conversion profile. In conclusion, they considered single bubble class with the aim of less complexity as a reliable model to analyze the slurry bubble column reactors [88]. In 2008, Laurent Sehabiague [26] et al. developed a computer model for large scale FT slurry reactor. The simulator was employed to optimize gas flow rate and reactor geometry for producing 10,000 (barrels/day) of liquid products. Different operating conditions were also used to find maximum space time yield (STY). However the condition for maximum productivity was taken into account as optimum operating condition due to lower capital and operating cost [26].

Therefore, almost all dynamic modeling of FT slurry reactors was focused on large commercial scale of Slurry bubble column reactor (SBCR) and it has been no computer dynamic model in laboratory scale (reactor diameter < 1m) for SBCR so far. In fact, modeling of pilot scale FT slurry is more difficult task due to wealth of dynamic characteristics such as the prediction of rise velocity of small bubbles and wall effects which make hydrodynamic parameters quite sensitive to system properties and presence of impurities [89].

In this chapter, dynamic modeling of Fischer-Tropsch reactor under variable load of synthesis gas is put forwarded. The experimental data is adopted from a Master of Science thesis which was conducted using the Fischer-Tropsch research plant. The plant is located in town of Güssing in Austria [27,28]. Appendix A and B reflect the setup and the experimental measurements for both base load (syngas flow rate of 5 m^3/h) and change load conditions (syngas flow rate of 3.5 m^3/h and 7.5 m^3/h) in one specific run.

4.2 Fischer-Tropsch reaction scheme

In chapter 3, different forms of FT kinetics over iron and cobalt catalyst were described in detail. In this section the kinetic characteristics of FT synthesis which is employed for modeling of slurry reactor is described. Table 7 summarizes kinetic parameters and FT product distribution. The kinetic form of Fischer-Tropsch synthesis in terms of rate consumption of carbon monoxide over catalyst cobalt is adopted from Yates and Satterfield 1991[68] (see Table 7). In this reaction kinetics ($-R_{co}$), the parameters a and b are modified such that the CO conversion using this model matches the experimental CO conversion. Anderson-Schulz Flory model presents an expression of the distribution for n-paraffins based on their mass fraction (W_n). It can be expressed with the correlation of ASF

distribution of products as mentioned in Table 7 (W_n formula) which W_n is defined by parameter α (Chain growth probability factor). As a matter of fact, α-value gives an indication of the distribution of the weight percentage of products with respect to their carbon number [6]. Factor α has a dependency of temperature, pressure and the catalyst used in the process. Generally, in our model, alpha relation is used in terms of temperature as mentioned in the correlation of chain growth probability factor (Table 7), which is described by Song et al. (2004) [50]. In the section of model comparison, based on the ASF model, a semi-logarithmic plot of mass fraction against carbon number is taken into accounted (logarithmic relation in Table 7) which produces a straight line. The slope of the line is delivered the α-value. The calculation is conducted for different operating conditions based on both experimental and model data. Since the products of Fischer–Tropsch synthesis over catalyst cobalt are predominantly paraffins (see the generic reaction in Table 7), the rate of paraffin formation based on Anderson-Sculz-Flory (ASF) equation can be calculated from r_i equation in Table 7 [90]. In addition, Table 8 shows several labaratory parameters and operating conditions. Details of the FT reactor and experimental setup are described in appendixs and references [27, 28].

Table 7: Kinetic Characteristics of Fischer–Tropsch Slurry Bubble Column reactor (FT-SBCR): reaction parameters, product distribution.

Reaction Characteristics	**Relations**	**Constants, Parameters and Paraffin Reaction Form**
Reaction Kinetics	$-R_{co} = \frac{a\, P_{co} P_{H_2}}{(1 + bP_{co})^2}$	$a = 1.59064 \times 10^{-12}$ $b = 7.99389 \times 10^{-6}$
Chain grow probability factor (Song et al.)	$\alpha = \left(A\frac{y_{co}}{y_{H_2} + y_{co}} + B\right)[10.0039(T - 533)]$	$A = 0.2332$ $B = 0.633$ $y_{co} = 0.2$ $y_{H_2} = 0.4$
Anderson Sculz-Flory distribution of products.	$W_n = n\,(1-\alpha)^2.\alpha^{n-1}$	$\log\frac{W_n}{n} = n\log(\alpha) + \log\frac{(1-\alpha)^2}{\alpha}$
Rate of paraffin formation based on ASF distribution.	$r_i = R_{co}\alpha^{n-1}$	$n\,CO + (2n+1)H_2 \rightarrow C_nH_{2n+2} + nH_2O$

Table 8: Operating conditions and liquid properties of lab-scale Fischer–Tropsch Slurry Bubble Column.

Operating Condition	
Reactor Temperature	503 K
Reactor Pressure	20 bar
H_2/CO	2
Reactor diameter	0.1 m
Reactor height	2.5 m
Volumetric Flow Rate (loads)	3.5, 5, 7.5 m^3/h
Liquid Phase Properties	
Liquid Density	715 kg/m^3
Surface tension	0.023 N/m
Liquid Viscosity	3×10^{-3} Pa.s

4.3 Modeling Activity

4.3.1 Model Framework

A rigorous computer model for a lab-scale FT-SBCR (D = 0.1 m, H = 2.5 m) for all the key components of FT synthesis reactor was established. A set of Partial Differential Equations (PDEs) of transport species in the form of mass transfer and kinetics was successfully coupled with hydrodynamic correlations. In principle, ten diffisuion-convection equations for the gas phase (single bubble class) and ten diffisuion-convection equations with reaction term for the liquid phase ought to be solved simultaneously. The reactor model was developed with these assumptions: (1) Axial Dispersion Model (ADM) with a single class of gas bubble diameter in the form of a convection-diffusion phenomenon is considered (ADM-SBCD); (2) the gas-liquid mass transfer resistance is located on both the gas and liquid side; (3) According to the non-dimensional form of Peng-Robinson equation-of-state (PR-EOS), the compressibility factor of the gas phase corresponds to near unity ($Z \approx 1$). The PR-EOS is an appropriate fluid model for FT systems to predict vapor-liquid compositions and flow rates inside the slurry reactor [91,92]; (4) the operating pressure is assumed to be constant along the reactor height due to a low pressure drop in the slurry reactor; (5) the reactor operates under isothermal condition; (6) by supposing isobaric and isothermal conditions, the overall continuity balance occurs at the inlet and outlet of the reactor (Equation (66)); (7) liquid-solid mass transfer resistance may be ignored and consequently solid suspension in liquid is simulated as a single pseudo-homogeneous slurry phase in this work; (8) chemical reaction in the form of

Langmuir Hinshelwood Hougen Watson (LHHW) kinetics in liquid phase is taken into account.

Based on these model assumptions, the mass balances of each component in gas and liquid phases can be derived as follows:

Gas phase equations:

$$\underbrace{\frac{\partial(\varepsilon_g C_{g,i})}{\partial t}}_{\text{Accumulation}} = \underbrace{\frac{\partial}{\partial z}\left(D_g\,\varepsilon_g \frac{\partial C_{g,i}}{\partial z}\right)}_{\text{Axial Dispersion}} - \underbrace{\frac{\partial}{\partial z}\left(\varepsilon_g U_g C_{g,i}\right)}_{\text{Convection}} - \underbrace{(K_l a)_{g,i}\varepsilon_l\left(\frac{C_{g,i}}{A_i} - C_{l,i}\right)}_{\text{Mass Transfer}} \tag{64}$$

Liquid phase equations:

$$\underbrace{\frac{\partial(\varepsilon_l C_{l,i})}{\partial t}}_{\text{Accumulation}} = \underbrace{\frac{\partial}{\partial z}\left(\varepsilon_l D_{ax,l}\frac{\partial C_{l,i}}{\partial z}\right)}_{\text{Axial Dispersion}} - \underbrace{\frac{\partial}{\partial z}\left(\varepsilon_l U_l C_{l,i}\right)}_{\text{Convection}} + \underbrace{(K_l a)_{g,i}\varepsilon_l\left(\frac{C_{g,i}}{Ai} - C_{l,i}\right)}_{\text{Mass Transfer}} - \underbrace{\varepsilon_l \rho_{cat}\varepsilon_{cat} r_i}_{\text{Reaction}} \tag{65}$$

Total concentration:

$$\sum_i^n C_{g,i} = C_{tot,in} = \frac{P}{ZRT} = C_{tot,out} \tag{66}$$

In the above equations, A_i is the Henry's constant (H_i) for light hydrocarbons and syngas (C_1, C_2, CO, H_2 and H_2O). By applying Henry's law solubility factor ($P_i = x_i \times H_i^{\infty}$), the Henry's constant for each reactant gas was calculated based on the heat of solution for each component and the operating temperature [93]. Also, based on general gas law ($P_iV = n_i\,RT$) Henry's law becomes $RT\times C_{iG} = H_i \times C_{iL}$. Thus, the parameter Ai for light hydrocarbon and syngas in equations (64) and (65) becomes as follows:

$$A_i = H_i/RT \tag{67}$$

$$H_i = H_i^* \exp\left(-\frac{\Delta H_{s,i}}{RT}\right) \tag{68}$$

where, the value of parameters H_i^* and $\Delta H_{s,i}$ are listed in reference [93].

For heavier components (C_4^+), A_i was calculated using Raoult's law for the gas-liquid phase at the equilibrium. At first, in equilibrium state we have:

$$\left(\frac{C_{iG}^*}{A_i} - C_{iL}\right) = C_{iL}^* - C_{iL} \tag{69}$$

Then, based on Raoult's law, the molar concentration of light components at equilibrium becomes as follows:

$$C_{iG}^* = X_{i,L}^* \times H_i^\infty / RT \tag{70}$$

If both sides of the equation (70) are multiplied by C_{tot}^L (total concentration of liquid components), the liquid concentration at equilibrium and thereby the parameter A_i are derived as follows:

$$C_{iL}^* = \frac{C_{i,G}^*}{H_i^\infty / RT} \times C_{tot}^L \tag{71}$$

$$A_i = H_i^\infty / RT \cdot 1 / C_{tot}^L \tag{72}$$

$$C_{tot}^L = \rho_L / MW_{L,avg.} \tag{73}$$

where, ρ_L is the liquid density, $MW_{L,avg.}$ is the average molecular weight of liquid components and H_i^∞ is the Henry's constant at infinite dilution which is defined as follow:

$$H_i^\infty = \gamma_i^\infty P_{i,sat} \tag{74}$$

where γ_i^∞ is the activity coefficient for heavier components and $P_{i,sat}$ is the vapor pressure of component i which is calculated from asymptotic behavior correlations (extension of the Antoine equations). By assuming ideal behavior of FT mixture due to long-chain n-paraffins, the Henry's constant for the mixture can be expressed by:

$$\mathrm{Ln}H_{i,mix}^{\infty} = \sum_{j} x_j \mathrm{Ln}\, H_j^{\infty} \tag{75}$$

where j is the species in the solvent. Since $\mathrm{Ln}H_i^{\infty}$ and $\mathrm{Ln}\gamma_i^{\infty}$ is asymptotically linear with solute carbon number (m), the relation for deriving the infinite-dilution activity coefficient becomes as follow:

$$\mathrm{Ln}\gamma_m^{\infty} = \mathrm{Ln}\gamma_r^{\infty} \frac{(n-m)}{(n-r)} \tag{76}$$

where n denotes the carbon number of solvent (n-paraffin) and r is the carbon number of reference solute (n-C_6H_{14}) in the same solvent. They are described in more detail in references [92, 94].

As mentioned in the model assumption, since the reactor is assumed to be operated under constant pressure and temperature, the total concentration is constant. As a consequence, the gas flow rate change due to chemical reaction and mass transfer is determined by supposing the constant total concentration of components in single bubble gas diameter (Equation (66)). Therefore, the Equation (74) as a sub-model in the form of a gas state equation is incorporated into the SBCD model. This sub-model used for behavior of superficial gas velocity inside the reactor is a reliable approach since it considers the concentrations of all gaseous components [87].

$$\frac{\partial U_g}{\partial z} = -\frac{1}{C_{tot}} \sum_{i=1}^{n} K_l \times a \times \varepsilon_l \times \left(\frac{C_{g,i}}{A_i} - C_{l,i}\right) \tag{77}$$

Table 9 shows the initial and boundary conditions of Equations (64), (65) and (74). The initial values in the model are set based on pressure, temperature and concentration of components. The boundary conditions adopted from Danckwerts' type are defined for the gas and liquid at the inlet and outlet of the reactor. For the gas phase at the reactor inlet, the concentration is taken from a syngas composition under the operating conditions of the research plant, calculated based on Table 10. The inlet superficial gas velocity for single bubble gas diameter is calculated from Equation (77).

The effective gas-liquid interfacial area for mass transfer of small bubbles between two phases can be expressed as follows [95]:

$$a = 6 \times \varepsilon_g / d_B \tag{78}$$

The mass transfer coefficient (K_l) is calculated from the following empirical relation. It can be applied in a wide range of operating conditions which results in a good prediction of gas-liquid mass transfer [95]:

$$K_l a = 1.77 \times \sigma^{-0.22} \times \exp(1.65 U_l - 0.65 \mu_l) \times \varepsilon_g^{1.2} \tag{79}$$

Table 9. Initial and boundary conditions for the slurry reactor model.

Initial Condition (t = 0)	Reactor Inlet (z = 0)	Reactor Outlet (z = H)
$C_{gi} = C_{gi,in}$	$C_{gi} = C_{gi,in}$ $C_{g,i0} = \frac{P_i}{ZRT}$	$\frac{\partial C_{g,i}}{\partial z} = 0$
$C_{li} = C_{gi,in}/A_i$	$\varepsilon_l D_l \left(\frac{\partial C_{l,i}}{\partial z}\right)_{z=0} = U_l (C_{l,i} - C_{g,i0/A_i})$	$\frac{\partial C_{g,i}}{\partial z} = 0$
$U_i = U_{g,in}$	$U_{gi} = U_{g,in}$	$\frac{\partial U_g}{\partial z} = 0$

The superficial gas velocity is defined as the volumetric gas flow rate divided by the cross-sectional area of the reactor above the gas distributor [96]:

$$U_{g,in} = \frac{V_f}{A_r} \tag{80}$$

The initial bubble size depending on buoyancy forces and surface tension is derived by the theoretical Davidson and Schuler expression [97]:

$$d_B = \left[\frac{6 \sigma d_0}{g (\rho_{SL} - \rho_G)}\right]^{1/3} \tag{81}$$

The gas hold up can be defined as the volume of the gas phase divided by the reactor volume comprising of volume of catalyst used, gas volume and liquid volume and [96]:

$$\varepsilon_g = \frac{V_{gas}}{V_{gas} + V_{liquid} + V_{cat}} \tag{82}$$

This is calculated to be 0.161 ($m_G^3\ m_R^{-3}$) and the catalyst volume fraction (ε_{cat}) is calculated to be 0.34 ($m_{cat}^3\ m_L^{-3}$). It is worth noting that in the Equations (64) and (65), ε_L is the liquid holdup ($m_L^3\ m_R^{-3}$) and r_i is the reaction rate of FT species ($mol\ kg_{cat}^{-1}\ s^{-1}$). Moreover, liquid is almost stationary inside the reactor. Thus, the velocity of liquid is assumed to be 0.00089 m/s.

In the SBCRs, the gas bubble coalescence happens in a short time with an increase of the column diameter, and the large bubbles collect around the center of the column in the operation of a churn turbulent regime. This is called heterogeneous flow, which usually occurs when the superficial gas velocity is more than 0.05 m/s. When the gas-liquid mixture reaches the surface, the bubbles disengage, allowing the degassed liquid to recirculate. Therefore, the main cause of back-mixing and liquid dispersion in the pilot plant slurry FT reactor is attributed to downward velocity of the liquid in the wall region and upward direction ($V_L(r)$) in the central axis [69]. Based on Riquarts correlation [89] the magnitude of $V_L(0)$ depends on the column diameter, superficial gas velocity and kinematic viscosity of the liquid phase as described in Equation (80). The experimental data [69, 89] show that the liquid phase axial dispersion coefficient ($D_{ax,L}$) has a direct proportionality to column reactor diameter and centre-line liquid velocity as mentioned in Equation (81).

$$V_L(0) = 0.2 \times (g\ D_t)^{1/2} \times (U^3_{g,in}/g\ \nu_L)^{1/8} \tag{83}$$

$$D_{ax,L} = 0.31 \times V_L(0) \times D_t \tag{84}$$

According to reference [19,70], the two correlations given in equations (80) and (81) are the most suitable ones for the prediction of axial dispersion coefficient which was suggested in all systems (including slurry). The axial dispersion coefficient of the gas phase for the small bubbles is equal to that of the liquid phase according to the relationship which was proposed by Sehabiague et al [98].

4.3.2 Computer Solution Procedure

In this mathematical modeling, a MATLAB pdepe (Partial Differential Equations Parabolic Elliptic) solver is implemented. The solver converts a set of PDEs to ODEs (Ordinary Differential equations) using an accurate spatial discretization based on a specified grid size. The solution domain is equal to the length scale of the reactor and the optimized discretization accounts for the desired level of accuracy and the affordable CPU time [23].

For solving equations, the mass balance of 10 components of H_2, CO, H_2O, CO_2, CH_4, C_2H_6, C_4H_{10}, $C_{10}H_{22}$, $C_{18}H_{38}$, and $C_{30}H_{62}$ in two phases, gas and liquid, are considered.

4.4 Results and Discussions

The modeling of the FT slurry reactor initiates with the start-up after all heating devices are turned on and the alarm values are set. Once an operating parameter such as temperature or pressure, reaches its alarm value, the research plant is automatically switched off and this is called an alarm shut down (ASD). The alarm values are essentially important since they ensure a safe operation of the plant. Then, the FT plant is started under N_2 flow as an inert gas in the manual mode until the FT reactor attains a temperature of 453 K, at which the wax in the FT reactor is liquid. Afterwards, the plant is switched to the automatic mode and the FT reactor reaches the required operating temperature of 503 K and the plant is operated under syngas. The time needed for the start-up stage before switching the plant to automatic mode is about 2–3 h.

4.4.1 Species Distribution

4.4.1.1 The Behavior of Components H_2, CO

At first, the aforementioned hydrodynamic parameters are implemented in the computer model then the equations related to small bubbles of gas components and the liquid phase are coupled to obtain the concentration behavior of all FT key components from the beginning to the steady state conditions through the length of the reactor. As Figure 29 illustrates, at $\tau = 0$ there is no carbon monoxide and hydrogen in either of the two phases. At normal operation ($\tau > 0$), these species enter the reactor with their own inlet values (which are already calculated based on the boundary conditions in Table 3; $C_{g,in}$), initiating the reaction. At the reactor inlet a maximum value is seen and liquid is assumed to be saturated with gas phase. The CO and H_2 are consumed due to the chemical reaction and their concentration decreases across the reactor length to the equilibrium values in two phases. In this respect, “wall effects” cause small bubbles to dissolve faster into

the liquid phase before reaching steady state values. The concentration behavior of species (mol/m^3_{gas} for gaseous components and mol/ m^3_{liquid} for liquid components) shows that the steady state values are attained at 10 min, as expected from the experimental data [28]. The CO conversion in this base load condition equals 58%, which is slightly overestimated compared to the experimental data. The run is performed for T = 503 K, P = 20 bar, U_g = 0.17 m/s, ε_{cat}= 0.34.

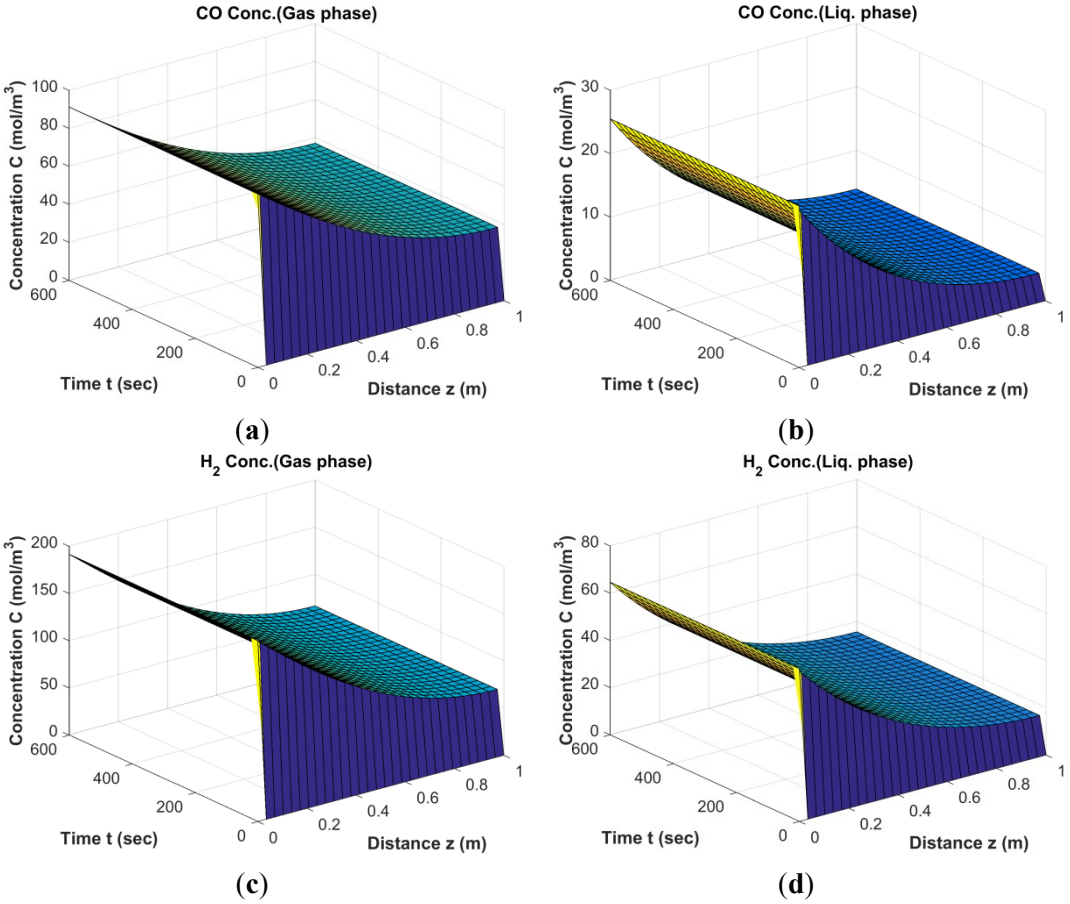

Figure 29: Results of Fischer–Tropsch (FT) Simulation; The behavior of CO, H_2 in gas phase (**a**,**c**) and liquid phase (**b**,**d**) from start-up to steady state conditions (D_t = 0.1 m, H = 2.5 m, ε_{cat} = 0.34, $U_{g,in}$ = 0.17 m/s).

4.4.1.2 The Behavior of Components H_2O, CO_2

As Figure 30 illustrates, water vapor, which is one of the products of FT synthesis, increases over the reactor height and over the time. Since the FT reaction occurs under a cobalt supported catalyst, no water gas shift reaction is promoted and the inlet CO_2 acts as an inert through the process. The CO_2

concentration increases due to the volume reduction of off-gas and syngas consumption. It is worth noting that the presence of diluents such as CO_2, CH_4 or N_2 has a beneficial influence in slurry bubble column reactors. The inert (here as carbon dioxide) facilitates supplementary mixing energy to the slurry system to maintain catalyst suspension. On the other hand, in FBRs we need to avoid diluents since they elevate the pressure drop across the reactor bed [99].

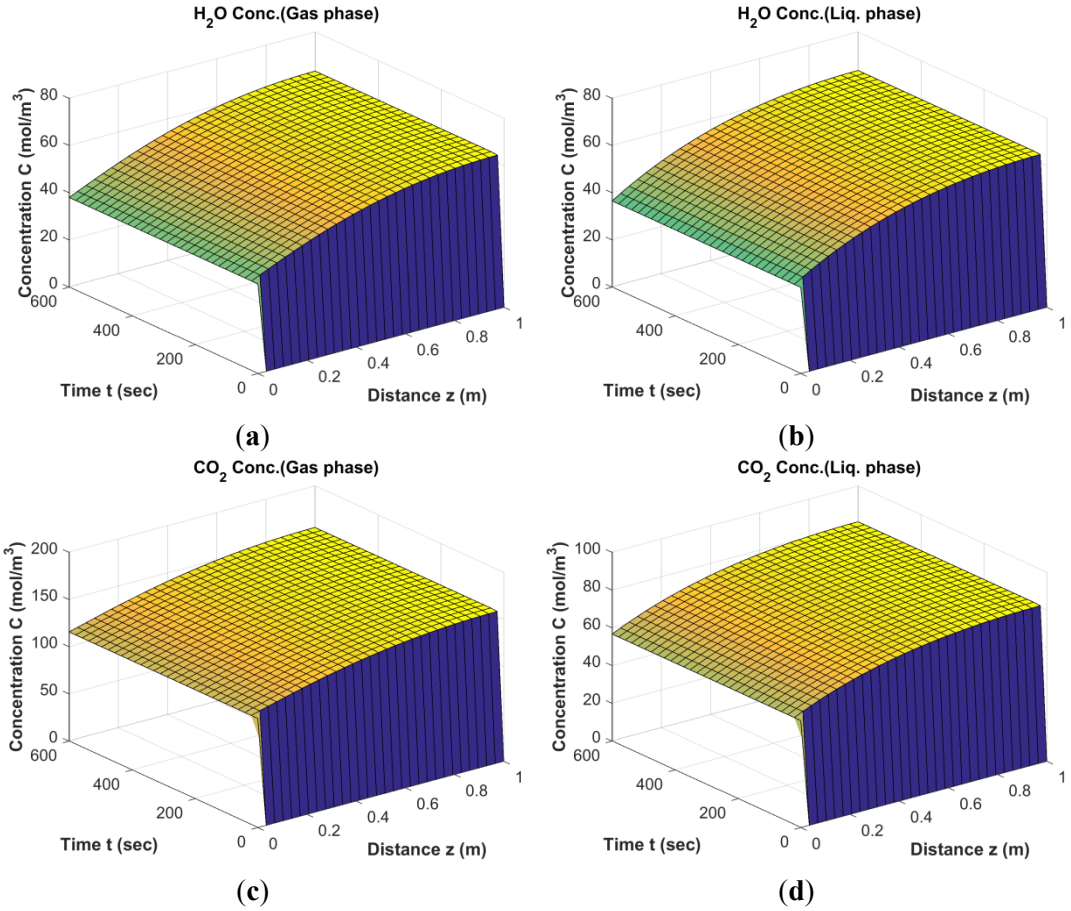

Figure 30: Results of FT Simulation; The behavior of H_2O and CO_2 in gas phase (**a**,**c**) and liquid phase (**b**,**d**) from start-up to steady state conditions (D_t = 0.1 m, H = 2.5 m, ε_{cat} = 0.34, $U_{g,in}$ = 0.17 m/s).

4.4.1.3 The Behavior of Components CH_4, C_2H_6, C_4H_{10}

Methane, ethane and butane increase over time and achieve their highest concentration at the final time in the reactor outlet. These highest values in the gas phase reach around 85, 35 and 50 mol/m^3 for CH_4, C_2H_6 and C_4H_{10}, respectively as shown in Figure 31.

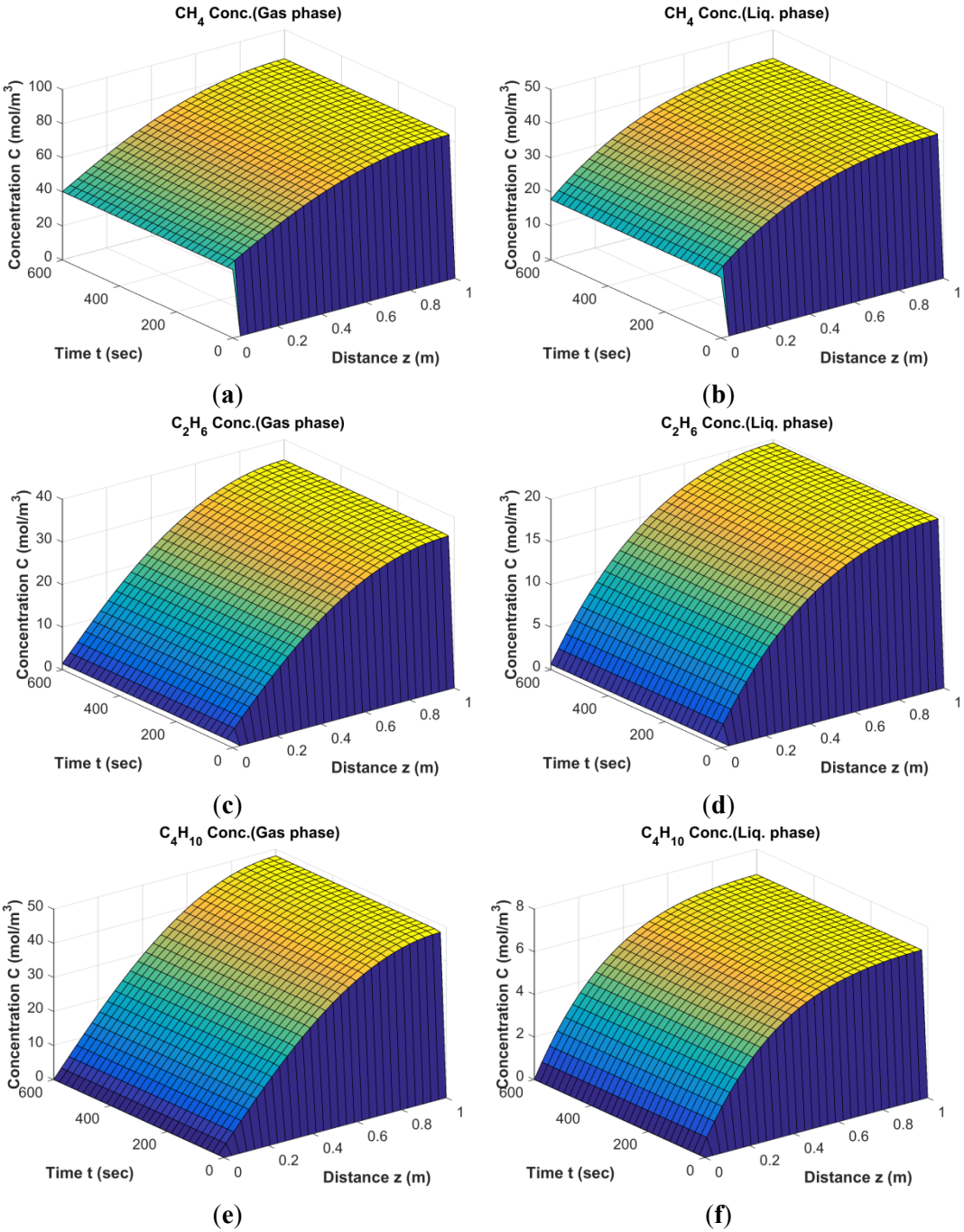

Figure 31: Results of FT Simulation; The behavior of CH_4, C_2H_6 and C_4H_{10} in gas phase (**a**,**c**,**e**) and liquid phase (**b**,**d**,**f**) from start-up to steady state conditions (D_t = 0.1 m, H = 2.5 m, ε_{cat} = 0.34, $U_{g,in}$ = 0.17 m/s).

4.4.1.4 The Behavior of Liquid Products $C_{10}H_{22}$, $C_{18}H_{38}$, $C_{30}H_{62}$

In this mathematical modeling, three components are considered as representatives of each specific carbon cut. $C_{10}H_{22}$, $C_{18}H_{38}$ and $C_{30}H_{62}$ were introduced as naphtha, diesel and wax respectively, which are derived from three condensers with reaction water in each condenser and collected in each related drum [28]. The results of modeling show that all three sets of products have a similar profile through the slurry reactor. As illustrated in Figure 32, the liquid products have an upward trend over time through the reactor height and the highest magnitude belongs to the middle distillate whereas diesel and wax stand at lower values respectively. Practically, the wax products consist of light (soft) wax ($<C_{25}$) and heavy (hard) wax (C_{25}^{+}) in LTFT synthesis. Heavier waxy products, which have lower values compared to soft ones as final products can be hydrocracked and converted into high quality liquid transportation fuels, such as gasoline, diesel and kerosene. However, gasoline production is not so profitable due to the low octane number which originates from the low degree of branch products [100, 101]. Moreover, in this work all the wax products are collected in a drum after passing the first condenser then weighted and analyzed using an off-line GC device (C_{20}-C_{60}). As a result, in this modeling C_{30} was chosen as a representative carbon cut for the wax fraction.

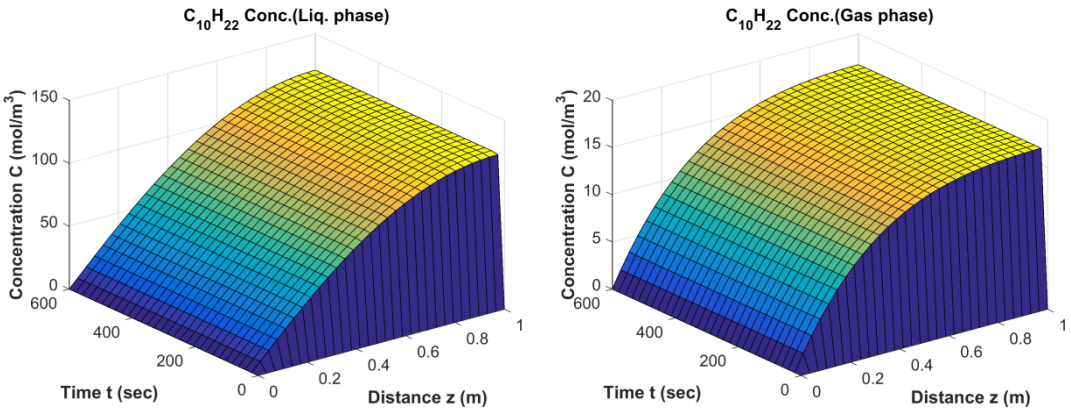

(**a**) (**b**)

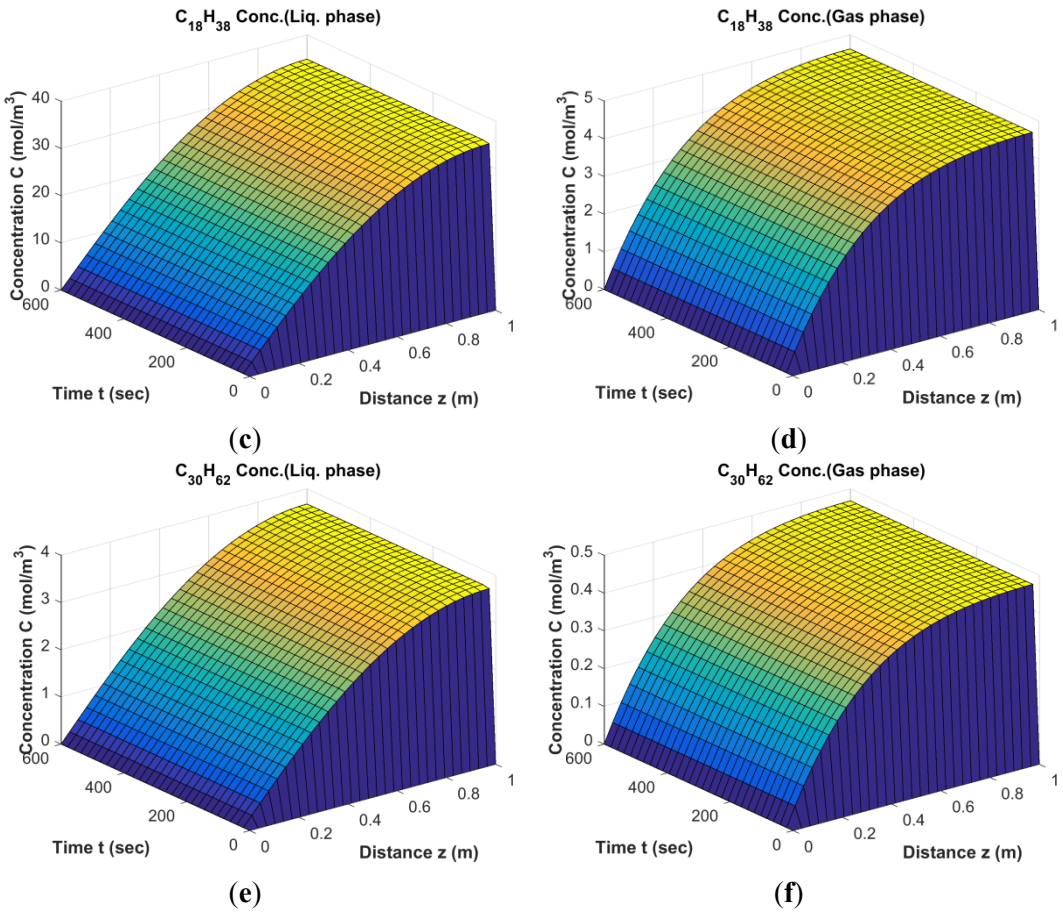

Figure 32: Results of FT simulation; The behavior of $C_{10}H_{22}$, $C_{18}H_{38}$ and $C_{30}H_{62}$ in liquid phase (**a**,**c**,**e**) and gas phase (**b**,**d**,**f**) from start-up to steady state conditions (D_t = 0.1 m, H = 2.5 m, ε_{cat} = 0.34, $U_{g,in}$ = 0.17 m/s).

These simulations results relate to base load conditions (volumetric gas flow rate 5 m^3/h). The computer model is also able to work quite well under variable loads of synthesis gas. Therefore, the flow rate in the model was changed in the range of 3.5 m^3/h–7.5 m^3/h to find maximum CO conversion and FT product selectivity.

4.4.2 Model Comparison with Experimental Data

The comparison of the model results with experimental data was conducted based on the composition (volume %) of syngas and off-gas which were measured by a GC device under base load and change load conditions. Figures 33–35 show a comparison of the predicted values by the computer model with the measured data from the conducted experiments. In general, the results show that the predicted model is in good agreement with the experimental data. When compared with FT

products only in the case of naphtha (C_8–C_{10}) is there a noticeable difference between model and laboratory data in all three operating conditions. This is due to the volatility of this carbon cut and difficulty in collecting them together. In product distribution (Figures 33c, 34c and 35c) only, two groups (C_8–C_{15}) and (C_{30}–C_{40}) show a deviation as well as discontinuities in the model prediction. The deviation is probably due to the neglect of olefin formation in the reactor modeling and the discontinuities can be attributed to the model equations which were solved for specific classes of FT species (C_1, C_2, C_4, C_{10}, C_{18} and C_{30}). As mentioned earlier, the α-value can be derived from the slope of the drawn line in all three load conditions. In the model, the α-value for volumetric flow rate of 3.5, 5 and 7.5 m^3/h is calculated to be 0.89, 0.9 and 0.88 respectively. It shows that change load conditions have almost no influence on the α-value or catalyst selectivity as predicted from the experiment.

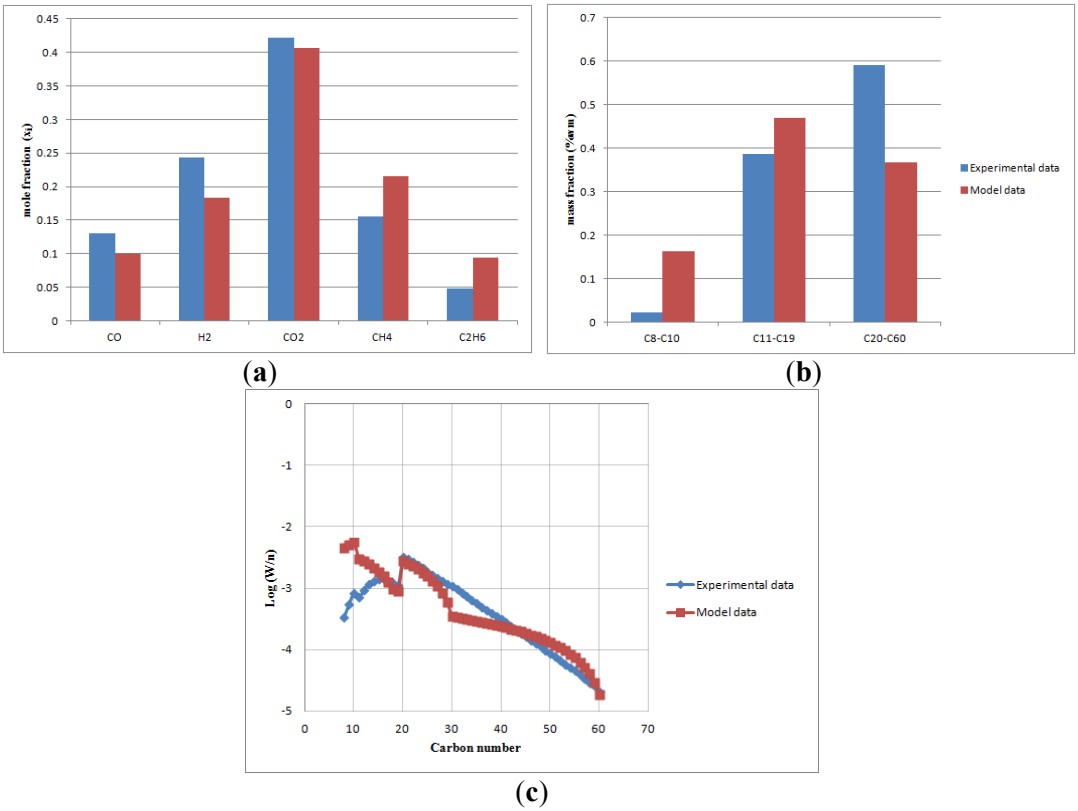

Figure 33: The comparison of the predicted model with experimental data at base load conditions (volumetric gas flow rate 5 m^3/h, T = 503 K, ε_{cat} = 0.34, P = 20 bar): (**a**) off-gas molar fractions; (**b**) FT products (naphta, diesel, wax); (**c**) ASF distribution.

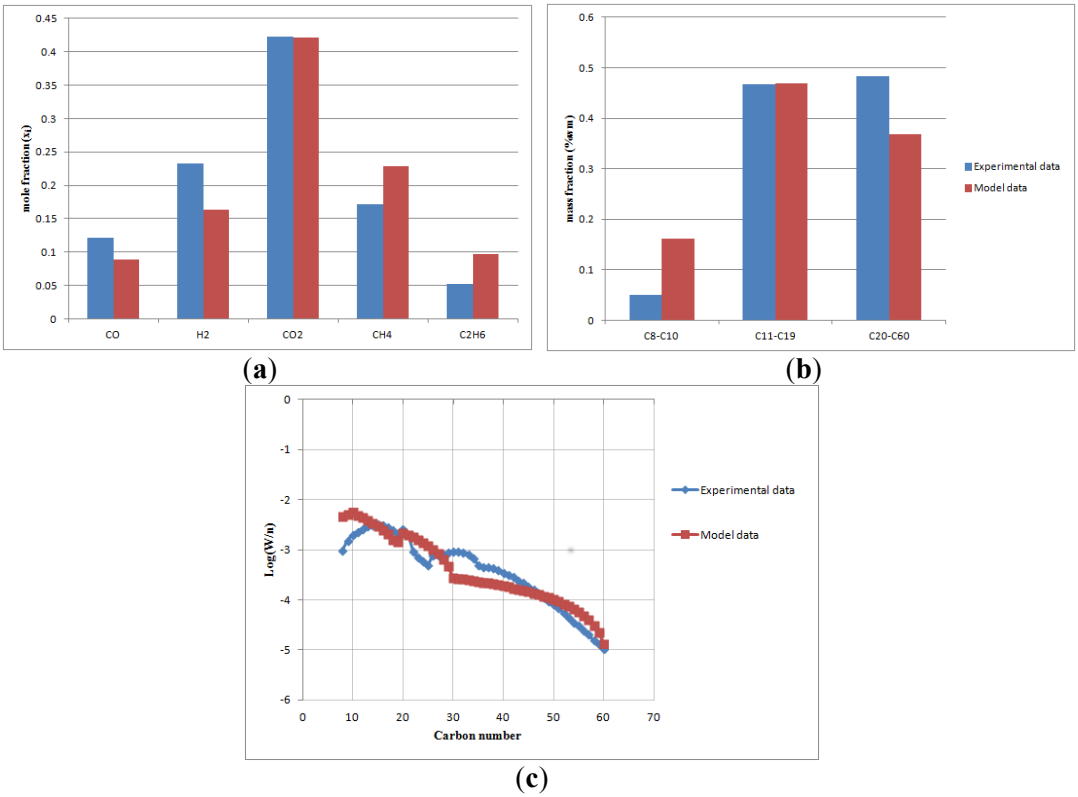

Figure 34: The comparison of the predicted model with experimental data at change load conditions (volumetric gas flow rate 3.5 m^3/h, T = 503 K, ε_{cat} = 0.34, P = 20 bar): (**a**) off-gas molar fractions; (**b**) FT products (naphta, diesel, wax); (**c**) ASF distribution.

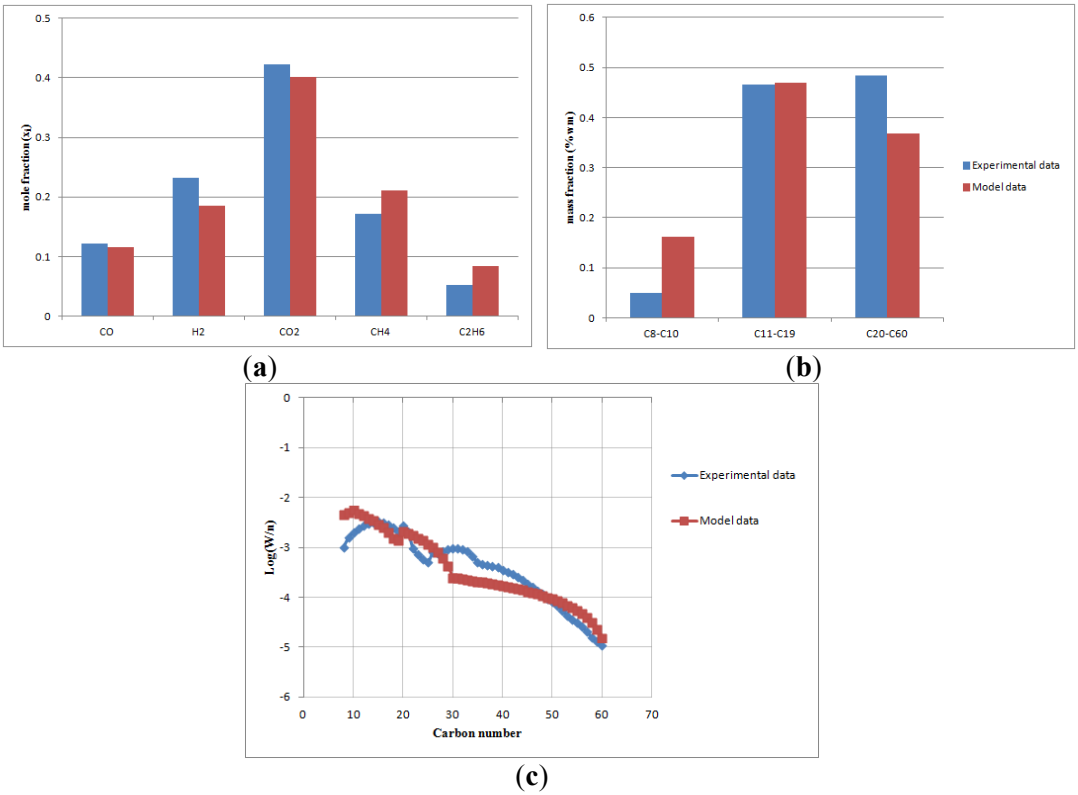

Figure 35:The comparison of the predicted model with experimental data at change load conditions (volumetric gas flow rate 7.5 m^3/h, T = 503 K, ε_{cat} = 0.34, P = 20 bar): (**a**) off-gas molar fractions; (**b**) FT products (naphtha, diesel, wax); (**c**) ASF distribution.

The results show that the CO conversion both in the model and experiments has lower values at a higher superficial velocity of syngas. This is due to the decreasing residence time of reactants at higher values of velocity. Thus, the maximum CO conversion occurs at 3.5 m^3/h which is equal to 60 %. As Figure 36 illustrates, the CO conversion also is in good agreement with the experimental data; however, the model values are slightly overestimated. This is due to larger area for gas-liquid mass transfer in the result of the assumption of the single bubble class diameter.

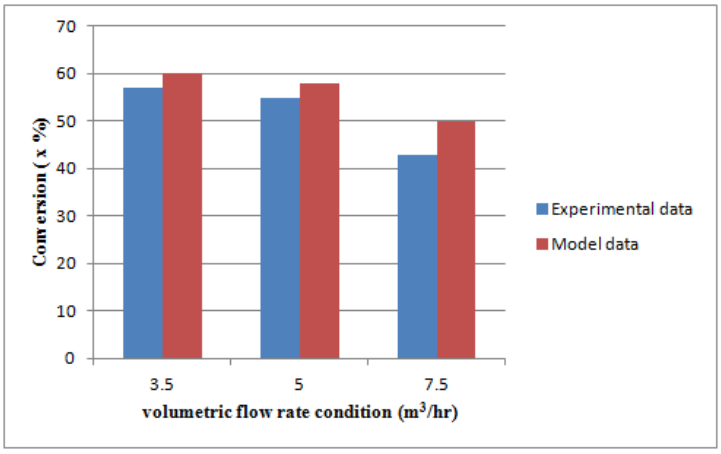

Figure 36: CO Conversion at base and change load condition based on experimental and model data.

4.5. The Effect of Temperature on Product Selectivity

One strength of FT reactor modeling is that analysis of the product selectivity with reaction temperatures can be carried out to find the desired operating conditions. Figures 37–39 illustrate the variation of product selectivity based on mass fraction with operating temperature at three loads of volumetric flow rates (3.5, 5, 7.5 m^3/h), respectively. As shown in these figures, for all three loads with increasing temperature the light gaseous (C_1–C_4), naphtha (C_5–C_{10}) and diesel increase whereas, heavier liquid fuels such as wax (C_{20}–C_{60}) tend to decrease. This trend can be expected since higher temperatures tend to shift the α-parameter to lower values thus producing more light hydrocarbons (C_1–C_4). In the design of the lab-scale SBCR for the FT process, it is advisable to operate the reactor under a narrow temperature range (483–503 K). This prevents catalyst deactivation, avoiding higher increases in methane as well as obtaining selectivity of diesel products [100]. Catalyst deactivation is of utmost importance in the FT process since it influences the product composition and the economic part of the whole process. Therefore, it is essential to investigate in depth how to prevent catalyst deactivation during the FT process. In general, catalyst deactivation mechanisms can be classified into six categories: thermal degradation, fouling, poisoning, solid-solid and/or vapor-solid reactions and attrition, vapor compound formation. Further details of deactivation mechanisms within their pathways (thermally, mechanically and chemically) are given in references [28, 102, and 103].

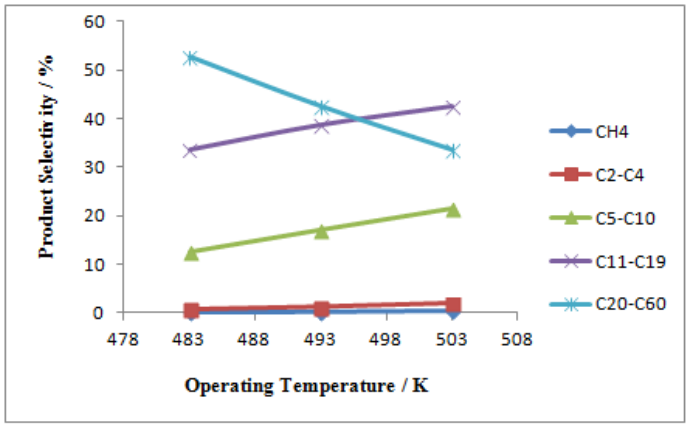

Figure 37: Influence of operating temperature on product selectivity; D_t = 0.1 m, H = 2.5 m, V_f = 3.5 m^3/h, P = 20 bar, ε_{cat} = 0.34.

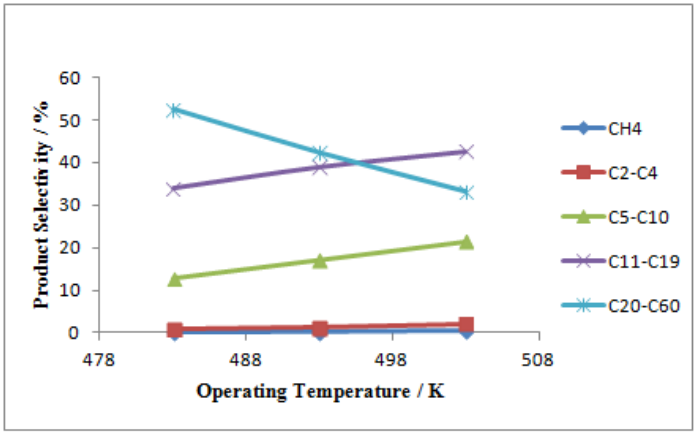

Figure 38: Influence of operating temperature on product selectivity; D_t = 0.1 m, H = 2.5 m, V_f = 5 m^3/h, P = 20 bar, ε_{cat} = 0.34.

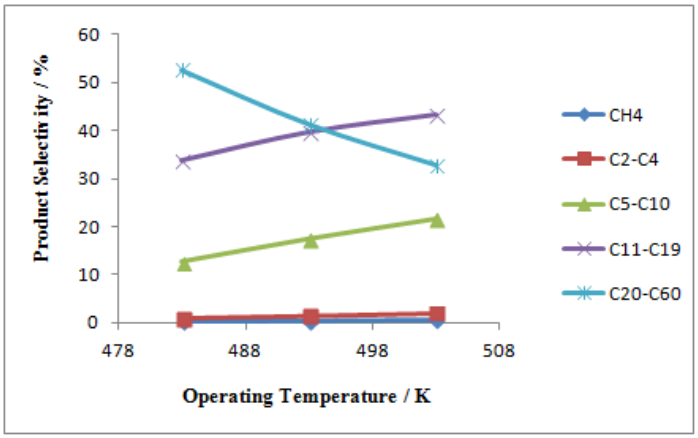

Figure 39: Influence of operating temperature on product selectivity; Dt =0.1 m, H = 2.5 m, Vf = 7.5 m3/h, P = 20 bar, ε_{cat} = 0.34.

It was concluded that by increasing the load of syngas flow rate, the selectivity of wax and diesel remain constant in each corresponding temperature. It was also concluded that there is a homogenous temperature profile within the reactor.

4.6. The Behavior of the Species inside the Reactor

The experimental data of the research FT reactor in laboratory scale is only able to reflect information about the reactor outlet. However, this mathematical modeling attempts to predict the dynamic behavior of the system through the height of the reactor which includes the concentration change of all species along the reactor length. Figure 40a,b show the molar concentration and conversion of syngas (CO and H_2) along the reactor bed at base load condition, respectively. The slightly higher values of H_2 conversion compared to CO conversion is attributed to the stochiometric ratio of H_2/CO taking the value 3 for producing methane, which then shifts to 2 in paraffin formation.

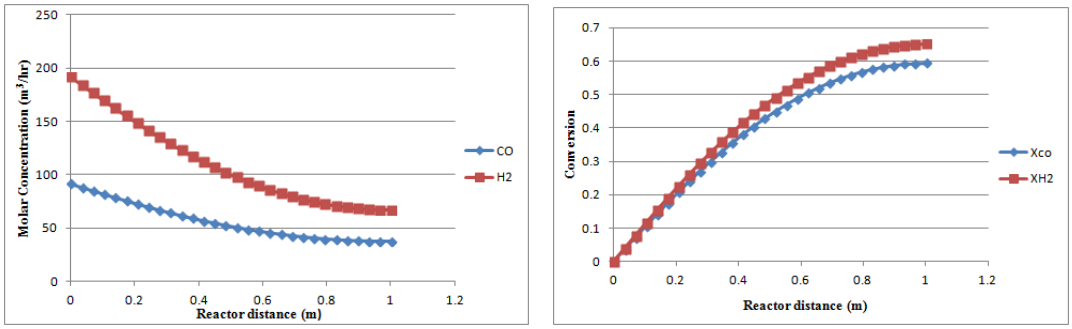

(**a**) (**b**)

Figure 40: The syngas variation on the reactor inside, (**a**) Molar concentration of CO and H_2; (**b**) CO and H_2 conversion.

The molar concentration of other FT species along the reactor height at three load conditions is also investigated as shown in Figure 41. It shows that all products increase with more or less the same intensity apart from naphtha (C_5–C_{10}) and diesel (C_{11}–C_{19}) which shift to lower values at higher syngas flow rate loads.

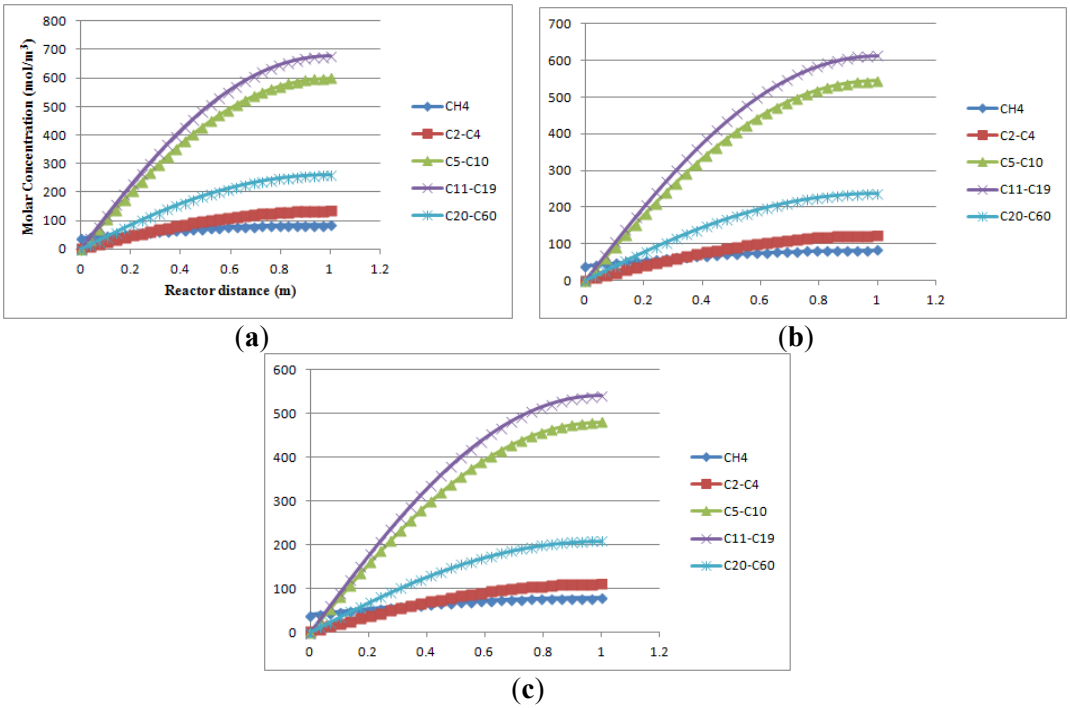

Figure 41: The molar concentration of the FT products along the reactor bed at three load conditions: (**a**) T = 503 K, P = 20 bar, V_f = 3.5 m^3/h; (**b**) T = 503 K, P = 20 bar, V_f =5 m^3/h; (**c**) T = 503 K, P = 20 bar, V_f = 7.5 m^3/h.

Furthermore, Figure 42 illustrates the reduction of superficial gas velocity at three different loads of conditions based on the overall mass balance (Equation (74)).

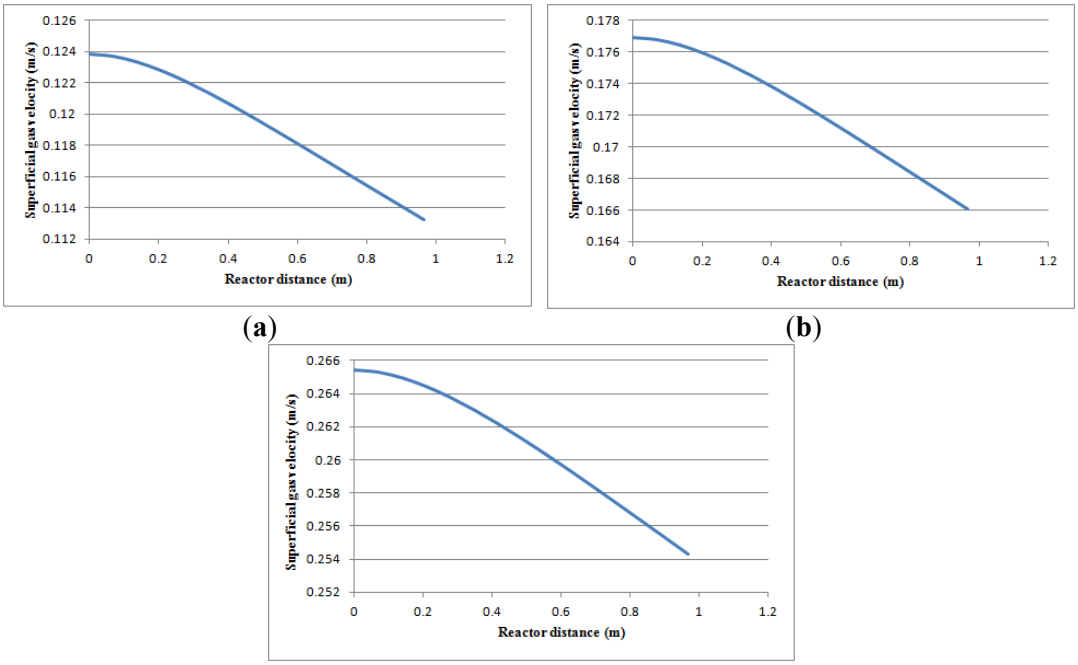

Figure 42: Reduction of superficial gas velocity as a function of reactor height at three different operating load conditions: (**a**) T = 503 K, P = 20 bar, V_f = 3.5 m^3/h; (**b**) T = 503 K, P = 20 bar, V_f = 5 m^3/h; (**c**) T = 503 K, P = 20 bar, V_f = 7.5 m^3/h.

4.7 Conclusions

In this dissertation, the conceptual design of renewable power to gaseous and liquid fuels within the three pathways of methanation, Dimethyl Ether (DME) and Low Temperature Fischer-Tropsch synthesis were analyzed using the commercial simulation software Aspen plus. In each optimized process simulation, the challenges, hurdles and limitations based on a Solid Oxide Elecrolysis Cell (SOEC) were examined. With regards to the challenges in each process, it was found that FT synthesis is more interesting to model due to the complexity of the products and the more highly developed catalyst and reactor used. As a consequence, the dissertation mainly focused on the dynamic modeling of an FT-SBCR, the reactor which is considered the best option in Fischer-Tropsch synthesis.

In the optimized configuration of methanation, a methane fraction of 95% at the outlet was achieved; which is compatible with the existing pipeline network. The main challenge of this technology is the lack of accurate and explicit kinetic data for its catalyst. Also, the heat released from methantion and its utilization for providing the heat required for electrolysis is another issue in the latest configuration of methanation. In DME synthesis, four explicit LHHW kinetics were implemented in Software Aspen plus. The main challenge in one-step direct DME synthesis (based on renewable energy) is the low value of yield and selectivity of the DME product (15% and 78% in the once-through process, respectively). However, the separation process and recycling of unreacted syngas in order to achieve high purity of the DME product is quite complex due to the presence of the the unreacted syngas and the CO_2 produced in the one-step synthesis process. Above all, it leads to higher operational costs.

In the optimized configuration of Low Temperature Fischer Tropsch (LTFT) based on renewable energy, a comprehensive simulation was conducted. To model an FT reactor, an external subroutine within an Excel spreadsheet through USER2 MODEL on the simulator was implemented. It was found that total efficiency of the system was achieved at 76.6 %. However, the main challenge of this configuration is the low value of liquid products due to the low capacity of the SOEC.

In the dynamic modeling of FT-SBCR, a comprehensive computer model was developed to investigate flexible reactor operation. This flexibility was performed by a step-change of syngas flow rate load (3.5, 5, 7.5 m^3/h) in a low-temperature Fischer–Tropsch synthesis. It was found that the dynamic simulation is not only able to predict all Fischer–Tropsch components over the reactor bed but can also

describe the behavior of superficial gas velocity as a sub-model using the overall gas mass balance. The effects of a step-change volumetric syngas flow on the performance of the FT slurry reactor, CO conversion and α-value, as well as information about the inside of reactor were investigated. The results show that the temperature distribution of the slurry reactor remains constant under base load and change load conditions. It is concluded that load change conditions do not have a negative influence on the temperature distribution inside the reactor and the dynamic model of the slurry reactor presented responds quite well to the load change conditions.

Nomenclature

A_r (m^3)	Reactor cross sectional area
a (m^2 m^{-3})	Effective gas-liquid interfacial area per unit bed volume
C_i (mol/m^3)	Concentration of component i
C_{tot} (mol/m^3)	Total concentration of gaseous components
C_{tot}^{L} (mol/m^3)	Total concentration of liquid components
C_{iG}^{*} (mol/m^3)	Concentration of gases components at equilibrium
C_{iL}^{*} (mol/m^3)	Concentration of liquid components at equilibrium
$D_{ax,L}$ (m^2/s)	Liquid phase axial dispersion coefficient
D_g (m^2/s)	Gas phase axial dispersion coefficient
D_t (m)	Reactor diameter
d_0 (m)	Gas distributor diameter
d_B (m)	Bubble diameter
g (m/s^2)	Acceleration due to gravity
H (m)	Reactor height
Hi (m_G^3 m_L^{-3})	Henry's solubility constant of gaseous component i

H_i^* (MPa. m^3/kmol)	Coefficient in Henry's law for gaseous component i
$-\Delta H_{s,i}$ (kJ/kmol)	Heat of solution for gaseous component i
Kl a (s^{-1})	Volumetric Mass transfer coefficient
$MW_{ave,L}$ (kg mol^{-1})	Average molecular weight of liquid components
P (Pa or bar)	Pressure
$P_{i,sat}$ (bar)	Vapor pressure of component i
R (J mol^{-1} K^{-1})	Gas constant
R_{co} (mol kg_{cat}^{-1} s^{-1})	Carbon monoxide consumption rate
r_i (mol kg_{cat}^{-1} s^{-1})	Chemical reaction rate of component i
T (K)	Temperature
t (s)	Time
U_g (m/s)	Superficial gas velocity
U_l (m/s)	Liquid velocity
V_{cat} (m^3)	Volume of catalyst in column
V_f (m^3/h)	Volumetric gas flow rate
V_{gas} (m^3)	Volume of gas in column
V_{liquid} (m^3)	Volume of liquid in column
$V_L(0)$ (m/s)	Center-line liquid velocity
z (m)	Axial coordinate

Z	Compressibility factor, dimensionless
Greek Letters	
α	Chain growth probability factor, dimensionless
ε_g ($m_G^3\ m_R^{-3}$)	Gas holdup, dimensionless
ε_l ($m_L^3\ m_R^{-3}$)	Liquid holdup, dimensionless
ε_{cat} ($m_{cat}^3\ m_L^{-3}$)	Catalyst volume fraction
γ_i	Activity coefficient for component i, dimensionless
ρ_{cat} (kg/m^3)	Catalyst density
ρ_{sL} (kg/m^3)	Slurry density
μl (Pa.s)	Liquid viscosity
σ (N/m)	Surface tension
ρ_G (kg/m^3)	Gas density
ν (m^2/s)	Kinematic viscosity of phase

τ	Dimensionless time coordinate

Abbreviations

ADM-SBCD	Axial Dispersion Model- Single Bubble Class Diameter
AEL	Alkaline Electrolysis
ASF	Anderson-Sculz-Flory
BtL	Biomass to Liquid
CCE	Carbon Conversion Efficiency
CCU	Carbon Capture Unit
CPU	Central Processing Unit
DME	Dimethyl Ether
EOS	Equation of State
FBR	Fixed Bed Reactor
FT	Fischer–Tropsch
GHG	Greenhouse Gas
HHV	High Heating Value

MOL	Method Of Lines
ODE	Ordinary Differential Equation
PDE	Partial Differential Equation
PEM	Polymer Electrolyte Membrane
PEMEC	Proton-Exchange Membrane Electrolysis
PDEPE	Partial Differential Equations Parabolic Elliptic
RES	Renewable Energy Sources
SBCR	Slurry Bubble Column Reactor
SOEC	Solid Oxide Electrolysis Cell
SOFC	Solid Oxide Fuel Cell
SPD	Slurry Phase Distillate
SRK	Soave Redlich Kwong
STY	Space Time Yield
SMR	Steam Methane Reforming

Appendix

6.1 Winddiesel Technology

Place of Experimental setup: Town of Güssing (Austria)

Winddiesel technology developed by the Technical University of Vienna was tested at an FT demonstration plant based on synthesis gas from biomass steam gasification and steam electrolysis in cases of availability of renewable energy. This system integrated steam electrolysis coupling with surplus Renewable electricity (RES-E) to provide renewable hydrogen for FT synthesis. When it recylces CO_2 to the gasification part (CO_2 gasification), electrolysis is positioned into the process for achieving usage syngas ratio for the inlet of Fischer-Tropsch reactor ($H_2/CO = 2$) [27].

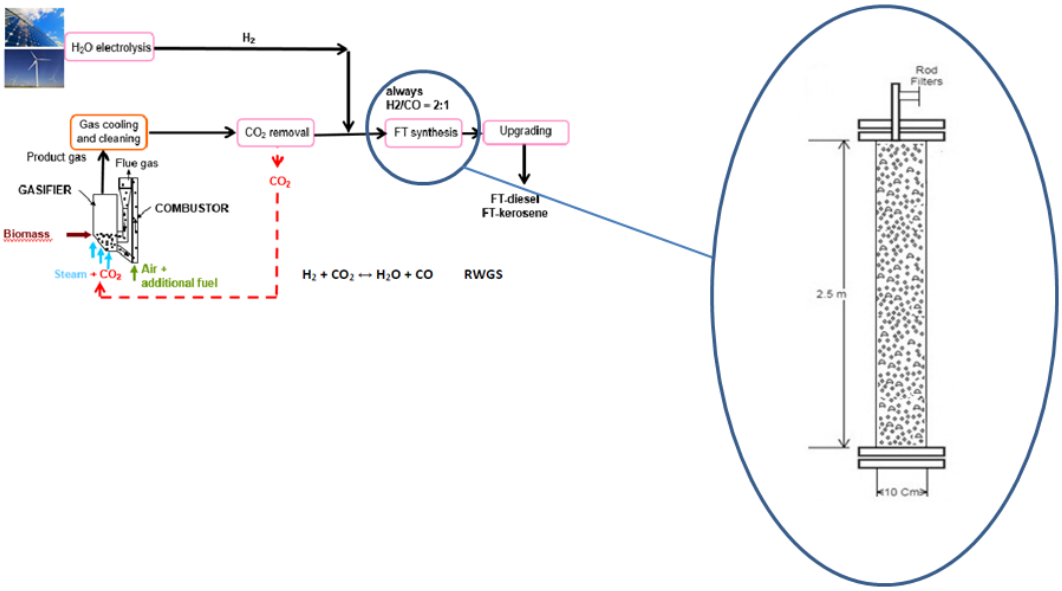

Figure 43: The scheme flow of Winddiesel Technology and schematic view of FT-SBCR [27].

6.2 Experimental data

Place of analysis: Town of Güssing (Austria)

Table 10: Average composition of Inlet/Outlet Gases under BL condition [28].

Inlet/Outlet Gas	N_2	CO_2	CH_4	C_2H_4	C_2H_6	CO	C_3H_6	C_3H_8	H_2
Syngas (vol. %)	4.6	24.2	8.4	2.5	0.3	19.1	~ 0	~ 0	40.1
Off-gas (vol. %)	7.0	39.0	14.4	0.1	4.5	12.1	~ 0	0.1	22.6

Table 11: Average composition of Inlet/Outlet Gases under CL condition [28].

Inlet/Outlet Gas	N_2	CO_2	CH_4	C_2H_4	C_2H_6	CO	C_3H_6	C_3H_8	H_2
Syngas (vol. %)	2.5	25.1	9.5	2.8	0.2	19.2	~ 0	~ 0	40.1
Off-gas (vol. %)	3.6	40.6	16.5	~ 0	5.0	11.7	~ 0	0.1	22.4

Table 12: Mass fraction of the FT products measured by off-line device [28].

Products	C_8	C_9	C_{10}	C_{11}	C_{12}	C_{13}	C_{14}	C_{15}	C_{16}
BL	0.0039	0.0072	0.012	0.0186	0.0271	0.0361	0.0442	0.0506	0.0536
CL	0.0095	0.0167	0.0238	0.0323	0.0405	0.0487	0.0555	0.0606	0.0624

Products	C_{17}	C_{18}	C_{19}	C_{20}	C_{21}	C_{22}	C_{23}	C_{24}	C_{25}
BL	0.0538	0.0524	0.0505	0.048	0.0454	0.0427	0.0395	0.0364	0.0334
CL	0.0604	0.0564	0.0498	0.0415	0.0333	0.0262	0.0206	0.0177	0.016

Products	C_{26}	C_{27}	C_{28}	C_{29}	C_{30}	C_{31}	C_{32}	C_{33}	C_{34}
BL	0.0307	0.0285	0.0265	0.0244	0.0229	0.0214	0.0193	0.0178	0.0158
CL	0.016	0.0161	0.0181	0.0202	0.0218	0.0227	0.0222	0.0213	0.0177

Products	C_{35}	C_{36}	C_{37}	C_{38}	C_{39}	C_{40}	C_{41}	C_{42}	C_{43}
BL	0.0143	0.0127	0.0115	0.0107	0.0098	0.0088	0.0081	0.0072	0.0063
CL	0.0135	0.0128	0.0129	0.0126	0.0122	0.011	0.0103	0.0094	0.0083

Products	C_{44}	C_{45}	C_{46}	C_{47}	C_{48}	C_{49}	C_{50}	C_{51}	C_{52}
BL	0.0059	0.0053	0.0046	0.0043	0.0039	0.0034	0.0031	0.0028	0.0025
CL	0.0075	0.0065	0.0058	0.0049	0.0043	0.0036	0.0032	0.0027	0.0022

Products	C_{53}	C_{54}	C_{55}	C_{56}	C_{57}	C_{58}	C_{59}	C_{60}
BL	0.0022	0.002	0.0018	0.0016	0.0014	0.0012	0.0011	0.0009
CL	0.0018	0.0015	0.0013	0.0011	0.0009	0.0007	0.0006	0.0005

BL: Base Load condition (V_f =5 m^3/hr)

CL: Change Load condition (V_f =3.5, 7.5 m^3/hr)

References

[1] A. Zervos, C. Lins, L. Tesniere, (2011), Mapping Renewable Energy Pathways Towards 2020-EU ROADMAP, Brussels, Belgium.

[2] T Roos, B North, (2016), CO_2 utilization, CSIR power to liquid workshop, CSIR Pretoria

[3] M. Iglesias G.a , C. de Vriesb, M. Claeysb, G. Schauba, (2015) Chemical energy storage in gaseous hydrocarbons via iron Fischer–Tropsch synthesis from H_2/CO_2—Kinetics, selectivity and process considerations, Catalysis Today 242 184–192

[4] W.L. Becker, R.J.Braun, M.Penev, M. Melaina, (2012) Production of Fischer-Tropsch liquid fuels from high temperature solid oxide co-electrolysis units, Energy 47 99-115

[5] Christoph J. Meinrenken and Klaus S. Lackner, (2014), Options to dissociate CO_2 and H_2O for sustainable sunlight-to-fuel pathways: Comparative assessment of current R&D hurdles and future potential, Journal of Natural Sciences, Vol. 2, No. 2, pp. 19-54

[6] Elia, Josephine A., Richard C. Baliban, and Christodoulos A. Floudas. (2010), "Toward novel hybrid biomass, coal, and natural gas processes for satisfying current transportation fuel demands, 2: Simultaneous heat and power integration." Industrial & Engineering Chemistry Research 49.16: 7371-7388.

[7] Alberto Varone, Michele Ferrari., (2015), Power to liquid and Power to gas: An option for the German Energiewende, The journal of renewable and Sustainable Energy Reviews 45: pages 207-218

[8] Jacques de Bucy, (2016) The Potential of Power-to-gas: Technology review and economic potential assessment.

[9] S. Anger, (2014), Potential of thermally integrated high-temperature electrolysis and methanation for the storage of energy by Power-to-Gas, International Gas Union Research Conference,

[10] Markus Lehner, Robert Tichler, Horst Steinmuller, Markus Koppe, (2014), Power to Gas: Technology and Business Models, Springer, ISBN 978-3-319-03995-4

[11] Daniel H. König, Marcel Freiberg, Ralph-Uwe Dietrich, Antje Wörner, (2015), Techno-economic study of the storage of fluctuating renewable, Fuel 159 289–297

[12] Qiang Fei, Michael T. Guarnieri, Lingo Tao, Lieve M.L. Laurens, Nancy Dowe, Philip T., (2014), Pienkos. Bioconversion of natural gas to liquid fuel: Opportunities and challenges, Biotechnology Advances 32 596–614

[13] Sunfire: "Power to liquid", http://www.sunfire.de/en/applications/fuel

[14] Peter M. Maitlis and Arno de Klerk, (2013) Greener Fischer Tropsch Process for Fuels and Feedstocks, Wiley-VCH Verlag & Co. KGaA, Boschstr. 12, 69469 Weinheim, Germany

[15] Kalala, M. G. (2012). Synthesis gas conversion into dimethyl ether and light hydrocarbons via methanol over a hybrid gold-based catalyst (Doctoral dissertation).

[16] W.L. Becker, R.J. Braun, M. Penev, M. Melaina, (2012) Production of Fischer-Tropsch liquid fuels from high temperature solid oxide co-electrolysis units, Energy (47) 99e115.

[17] Nimir O. Elbashira, Buping Bao, Mahmoud M. El-Halwagi, (2009), An Approach to the Design of Advanced Fischer-Tropsch Reactor for Operation in Near-Critical and Supercritical Phase Media, Proceedings of the 1st Annual Gas Processing Symposium.

[18] Duvenhage, D. J., & Shingles, T. (2002). Synthol reactor technology development. Catalysis Today, 71(3), 301-305.

[19] Kohler, M. A. (1986). Comparison of mechanically agitated and bubble column slurry reactors. Applied catalysis, 22(1), 21-53.

[20] Chaudhari, R. V., & Ramachandran, P. A. (1980). Three phase slurry reactors. AIChE Journal, 26(2), 177-201.

[21] Van der Laan, Gerard Pieter, Kinetics, (1999) Selectivity and Scale up of the Fischer Tropsch synthesis , University of Groningen / UMCG research database,.

[22] Ademola O. Odunsi, Tadhg S. O'Donovan, David A. Reay, (2016) Dynamic Modeling of Fixed-Bed Fischer-Tropsch Reactors with Phase Change Material Diluents, Chem. Eng. Technol., 39, No. 11, 2066–2076

[23] Maria Iglesias Gonzalez, Hilke Eilers, Georg Schaub, (2016) Flexible Operation of Fixed bed Reactors for a Catalytic Fuel Synthesis- CO_2 Hydrogenation as Example Reaction, Energy Technol., 4, 90 – 103

[24] González, Marıa Iglesias. (2016) "Gaseous Hydrocarbon Synfuels from H_2/CO_2 based on Renewable Electricity-Kinetics, Selectivity and Fundamentals of Fixed-Bed Reactor Design for Flexible Operation"

[25] Lucero, A. (2009). Improved Fischer-Tropsch Slurry Reactors (No. WRI-09-R005). University Of Wyoming Research Corporation.

[26] Laurent Sehabiague, Romain Lemoine, Arsam Behkish, Yannick J. Heintz, Mariela Sanoja, Rachid Oukaci Badie I. Morsi, (2008), Modeling and optimization of a large-scale slurry bubble column reactor for producing 10,000 bbl/day of Fischer–Tropsch liquid hydrocarbons, Journal of the Chinese Institute of Chemical Engineers 39 169–179.

[27] Sauciuc, A., Potetz, A., Weber, G., Rauch, R., Hofbauer, H., & Dumitrescu, L. (2011). Synthetic diesel from biomass by Fischer-Tropsch synthesis. na

[28] Rima Abulmfalfel, Winddiesel: Power to liquids assisted by biomass steam gasification, Master's Thesis, Karlsruhe Institute of Technology, March 2017.

[29] Domenico Ferrero, Design, (2016) development and Testing of SOEC-based Power-to-Gas systems for conversion and storage of RES into synthetic methane, doctrol thesis.

[30] Gruber, M., Harth, S., Trimis, D., Bajohr, S., Posdziech, O., Brabandt, J., & Koppel, W. (2015). Integrated high-temperature electrolysis and methanation for effective power to gas conversion. Gasfachliche Aussprachetagung, Essen.

[31] Pletcher D, Li X, (2011), Prospects for Alkaline zero gap water electrolysers for hydrogen production. International journal of Hydrogen Energy, 36, 15089-15104.

[32] Mergel, J., Carmo, M. and Fritz D. (2013) Status on Technologies for Hydrogen Production by Water Electrolysis, in Transition to Renewable Energy Systems, Wiley-VCH Verlag GmbH & Co. KGaA, Weinheim, Germany.

[33] Jensen, Søren H., Peter H. Larsen, and Mogens Mogensen, (2007) "Hydrogen and synthetic fuel production from renewable energy sources." International Journal of Hydrogen Energy 32.15: 3253-3257.

[34] Sune Dalgaard Ebbesen, Ruth Knibbe and Mogens Mogensen, (2012) Co-Electrolysis of Steam and Carbon Dioxide in Solid Oxide Cells, Journal of The Electrochemical Society, 159 (8) F482-F489.

[35] G.Botta, M.SOlimeo, P.Leone, P.V. Aravind, (2015) Thermodynamic Analysis of Coupling a SOEC in Co-Electrolysis Mode with the Dimethyl Ether Synthesis, Fuell Cells 15, No. 5, 669-681.

[36] Craig A. Grimes, Oomman K. Varghese, Sudhir Ranjan, Light, Water, (2008) Hydrogen The solar Generation of Hydrogen by Water Photoelectrolysis, Springer Science+Business Media, LLC.

[37] Alhassan Salami Tijani, Nur Afiqah Yusup, A. H. Abdol Rahim, (2014) Mathematical Modeling and Simulation Analysis of advanced alkaline electrolyzer system for hydrogen production, Procedia Technology 15 798-806

[38] Hanna Er-rbib, Chakib Bouallou, (2014) Modeling and Simulation of CO methanation process for renewable electricity storage, Energy 75 81-88

[39] Bajohr, Siegfried, et al. "Storage of regeneratively generated electrical energy in natural gas infrastructure." (2011), Gas water supply Gas natural gas 152.4: 200-210.

[40] Kopyscinski, Jan, Tilman J. Schildhauer, and Serge MA Biollaz. (2010), "Production of synthetic natural gas (SNG) from coal and dry biomass–A technology review from 1950 to 2009." Fuel 89.8: 1763-1783.

[41] Elvers, Barbara. (1989) Ullmann's encyclopedia of industrial chemistry. Eds. Stephen Hawkins, and William Russey. Verlag Chemie.

[42] Koytsoumpa, E. I., Bergins, C., Buddenberg, T., Wu, S., Sigurbjörnsson, Ó., Tran, K. C., & Kakaras, E. (2016). The Challenge of Energy Storage in Europe: Focus on Power to Fuel. Journal of Energy Resources Technology, 138(4), 042002.

[43] Manuel Gotz , Jonathan Lefebvre , Friedemann M€ors , Amy McDaniel Koch , Frank Graf , Siegfried Bajohr , Rainer Reimert, (2016) Thomas Kolb, Renewable Power-to-Gas: A technological end economic review, Renewable energy 85 1371-1390.

[44] Tichler R, (2013) Volkswirtschaftliche Relevanz von power to gas für das zukünftige Energiesystem. Presentation at 8. Internationale Energiewirtschaftstagung an der TU Wien, Wien 13–15 Feb 2013.

[45] Maria Iglesias Gonzalez and Georg Schaub, (2015) Gaseous Hydrocarbon Synfuels from Renewable Electricity via H_2/CO_2-Flexibility of Fixed-Bed Catalytic Reactors, Int. J. Chem. React. Eng; aop

[46] Gassner, Martin, and François Maréchal. "Thermo-economic process model for thermochemical production of Synthetic Natural Gas (SNG) from lignocellulosic biomass." Biomass and bioenergy 33.11 (2009): 1587-1604.

[47] http://www.sunfire.de/en/applications/fuel

[48] James, O.O., Chowdhury, B., Mesubi, M. A., & Maity, S. (2012). Reflections on the chemistry of the Fischer–Tropsch synthesis. Rsc Advances, 2(19), 7347-7366.

[49] van der Laan, G. P. (1999). Kinetics, selectivity and scale up of the Fischer-Tropsch synthesis. Groningen.

[50] Hyun-Seob Song, Doraiswami Ramkrishna, Sinh Trinh and Harold Wright, (2004) Operating Strategies for Fischer-Tropsch Reactors: A Model-Directed Study, Korean J. Chem. Eng., 21(2), 308-317.

[51] Carlo N. Hamelinck, Andre P.C. Faaij, Herman den Uil, Harlod Boerrigter, (2004) Production of FT transportation fuels from biomass; technical options, process analysis and optimization, and development potential. Energy 29 1743–1771.

[52] M. Iglesias, R. Edzang, G. Schaub, (2013) Combinations of CO/CO_2 reactions with Fischer-Tropsch synthesis, Catalysis Today 215 194-200

[53] Triantafyllidis, K., Lappas, A., & Stöcker, M. (Eds.). (2013). The Role of Catalysis for the Sustainable Production of Bio-fuels and Bio-chemicals. Newnes.

[54] Laurent Sehabiague (2012) modeling, scale up and optimization of slurry bubble column reactors for Fischer-Tropsch synthesis, Doctoral thesis.

[55] Dry, M. E., T. Shingles, and L. J. Boshoff. (1972) "Rate of the Fischer-Tropsch reaction over iron catalysts." Journal of Catalysis 25.1: 99-104.

[56] Brötz, Walter. (1949) "On the Systematics of Fischer-Tropsch Catalysis." Reports of the Bunsen Society for Physical Chemistry 53.5 301-306.

[57] Feimer, Joseph L., Peter L. Silveston, and Robert R. Hudgins. (1981) "Steady-state study of the Fischer-Tropsch reaction." Industrial & Engineering Chemistry Product Research and Development 20.4 609-615.

[58] Kölbel, H., Engelhardt, F., Hammer, H., & Gaube, J. (1960). Kinetics and reaction mechanism of the hydrocarbon synthesis from carbon monoxide and water vapor on iron, cobalt, and nickel catalysts. Actes du 2ème Congrès International de Catalyse. Paris, 1, 953-972.

[59] Dry, Mark E. (1976)"Advances in Fishcher-Tropsch Chemistry." Industrial & Engineering Chemistry Product Research and Development 15.4: 282-286.

[60] Deckwer, W. D., Kokuun, R., Sanders, E., & Ledakowicz, S. (1986). Kinetic studies of Fischer-Tropsch synthesis on suspended iron/potassium catalyst-rate inhibition by carbon dioxide and water. Industrial & Engineering Chemistry Process Design and Development, 25(3), 643-649.

[61] Leib, T.B. and J.C.W. Kuo. (1984) Modeling the Fischer-Tropsch Synthesis in Slurry Bubble-Column Reactors. Proceedings of the AIChE Annual Meeting.. San Fransisco, CA.

[62] Thomson, W. J., Arndt, J. M., & Wright, K. L. (1979). Applied Fischer-Tropsch kinetics for a flame sprayed iron catalyst. Am. Chem. Soc., Div. Fuel Chem., Prepr.;(United States), 25(CONF-800303-P3).

[63] Atwood, H.E. and C.O. Bennett, Kinetics of the Fischer-Tropsch Reaction over Iron. (1979) Industrial & Engineering Chemistry Process Design and Development,. 18(1): p. 163-170.

[64] Jess, A., Popp, R., & Hedden, K. (1999). Fischer–Tropsch-synthesis with nitrogen-rich syngas: fundamentals and reactor design aspects. Applied Catalysis A: General, 186(1), 321-342.

[65] Lox, Egbert S., and Gilbert F. Froment. (1993) "Kinetics of the Fischer-Tropsch reaction on a precipitated promoted iron catalyst. 2. Kinetic modeling." Industrial & engineering chemistry research 32.1: 71-82.

[66] Berger, R. J., Stitt, H. E., Marin, B. B., Freek, K., A, M. J., (2001). Chemical reaction kinetics in practice. Cattech 5, 30- 60.

[67] Visconti, C. G., Tronconi, E., Lietti, L., Zennaro, R., & Forzatti, P. (2007). Development of a complete kinetic model for the Fischer–Tropsch synthesis over Co/Al_2O_3 catalysts. Chemical Engineering Science, 62(18), 5338-5343.

[68] Yates, Ian C., and Charles N. Satterfield. (1991) "Intrinsic kinetics of the Fischer-Tropsch synthesis on a cobalt catalyst." Energy & Fuels 5.1: 168-173.

[69] Krishna, R., and S. T. Sie. (2000) "Design and scale-up of the Fischer–Tropsch bubble column slurry reactor." Fuel Processing Technology 64.1: 73-105.

[70] Yang, C.H., et al. (1979), Advances in Chemistry Series. Vol. 178. 35.

[71] Smith, G. V., Brower, W. E., & Matyjaszezyk, M. S. (1980). Proceedings of the 7th International Congress on Catalysis. Tokyo, 355.

[72] Outi, A., I. Rautavuoma, and Hessel S. van der Baan. (1981) "Kinetics and mechanism of the Fischer-Tropsch hydrocarbon synthesis on a cobalt on alumina catalyst." Applied Catalysis 1.5 247-272.

[73] Withers Jr, Howard P., Kenneth F. Eliezer, and John W. Mitchell. (1990) "Slurry-phase Fischer-Tropsch synthesis and kinetic studies over supported cobalt carbonyl derived catalysts." Industrial & engineering chemistry research 29.9 1807-1814.

[74] Keyser, Martin J., Raymond C. Everson, and Rafael L. Espinoza. (2000) "Fischer− Tropsch kinetic studies with cobalt− manganese oxide catalysts." Industrial & engineering chemistry research 39.1: 48-54.

[75] Sarup, B., and B. W. Wojciechowski. (1989) "Studies of the fischer- tropsch synthesis on a cobalt catalyst II. Kinetics of carbon monoxide conversion to methane and to higher hydrocarbons." The Canadian Journal of Chemical Engineering 67.1: 62-74.

[76] Anfray, J., Bremaud, M., Fongarland, P., Khodakov, A., Jallais, S., & Schweich, D. (2007). Kinetic study and modeling of Fischer–Tropsch reaction over a Co/Al_2O_3 catalyst in a slurry reactor. Chemical Engineering Science, 62(18), 5353-5356.

[77] van Steen, Eric, and Hans Schulz. (1999) "Polymerisation kinetics of the Fischer–Tropsch CO hydrogenation using iron and cobalt based catalysts." Applied Catalysis A: General 186.1: 309-320.

[78] Cinti, G., Baldinelli, A., Di Michele, A., & Desideri, U. (2016). Integration of Solid Oxide Electrolyzer and Fischer-Tropsch: A sustainable pathway for synthetic fuel. Applied Energy, 162, 308-320.

[79] Stempien, J. P., Ni, M., Sun, Q., & Chan, S. H. (2015). Thermodynamic analysis of combined solid oxide electrolyzer and Fischer–Tropsch processes. Energy, 81, 682-690

[80] Shim, H. M., Lee, S. J., Yoo, Y. D., Yun, Y. S., & Kim, H. T. (2009). Simulation of DME synthesis from coal syngas by kinetics model. Korean Journal of Chemical Engineering, 26(3), 641-648.

[81] Iliuta, I., Larachi, F., & Fongarland, P. (2010). Dimethyl ether synthesis with in situ H_2O removal in fixed-bed membrane reactor: model and simulations. Industrial & Engineering Chemistry Research, 49(15), 6870-6877.

[82] Azizi, Z., Rezaeimanesh, M., Tohidian, T., & Rahimpour, M. R. (2014). Dimethyl ether: A review of technologies and production challenges. Chemical Engineering and Processing: Process Intensification, 82, 150-172.

[83] Yuanyuan, H. A. N., Zhang, H., Weiyong, Y. I. N. G., & Dingye, F. A. N. G. (2009). Modeling and simulation of production process on dimethyl ether synthesized from coal-based syngas by one-step method. Chinese Journal of Chemical Engineering, 17(1), 108-112.

[84] You, Q., Liu, Z., Li, W., & Zhou, X. (2009). Synthesis of dimethyl ether from methane mediated by HBr. Journal of Natural Gas Chemistry, 18(3), 306-311.

[85] Iliuta, I., Iliuta, M. C., & Larachi, F. (2011). Sorption-enhanced Dimethyl Ether Synthesis-Multiscale reactor modeling. Chemical Engineering Science, 66(10), 2241-2251.

[86] J.W.A de Swart, R. Krishna, (2002), Simulation of transient and steady state behavior of a bubble column slurry reactor for Fischer-Tropsch synthesis, Chemical Engineering and Processing 41, 35–47.

[87] Rados, N., Al-Dahhan, M. H., & Duduković, M. P. (2005). Dynamic modeling of slurry bubble column reactors. Industrial & engineering chemistry research, 44(16), 6086-6094.

[88] Nasim Hooshyar, Shohreh Fatemi, Mohammad Rahmani, (2009) Mathematical Modeling of Fischer-Tropsch Synthesis in an industrial Slurry Bubble Column, Chemical Reactor Engineering Volume 7 Article A23.

[89] R.Krishna, (2000) A scale up Strategy of a commercial scale bubble column slurry reactor for Fischer Tropsch Synthesis, Vol. 55, No. 4, pp. 359-393.

[90] PRATT, Joseph W. (2012) A Fischer-Tropsch synthesis reactor model framework for liquid biofuels production. Sandia National Laboratories, California.

[91] Laurance Alistair Watson, (2011). Solar-Boosted Biomass-to-liquid (BtL) Process Modeling, A bachelor thesis in Australian National University

[92] John J. Marano, Gerald D. Holder, (1997) Characterization of Fischer-Tropsch liquids for vapor-liquid equilibria calculations, Fluid Phase Equilibria,.

[93] Shah,Y.T.; Dassori, C.G.; Tierney, J.W. Multiple steady states in non-isothermal FT slurry reactor. Chem. Eng. Commun. 1990, 88, 49–61.

[94] Marano, John J., and Gerald D. Holder, (1997) "General equation for correlating the thermophysical properties of n-paraffins, n-olefins, and other homologous series. 2. Asymptotic behavior correlations for PVT properties, Ind. Eng. Chem. Res.

[95] Lau, R., Peng, W., Velazquez-Vargas, LG, Yang, GQ, & Fan, LS, (2004) Gas-liquid mass transfer in high-pressure bubble columns. Industrial & engineering chemistry research, 43, 1302–1311.

[96] Jürgen Loipersböck, Gerald Weber, Hannes Gruber, Jan Kratky, Raphael Capistrano, Hermann Hofbauer, Reinhard Rauch, (2017) Upscaling and operation of a biomass-derived Fischer-Tropsch pilot plant producing one barrel per day, 25th European Biomass Conference and Exhibition, 1088–1093.

[97] Behkish, A. (2005). Hydrodynamic and mass transfer parameters in large-scale slurry bubble column reactors (Doctoral dissertation, University of Pittsburgh).

[98] Sehabiague, L.; Morsi, B.I. Modeling and Simulation of Fischer-Tropsch Slurry Bubble Column Reactor Using different kinetic rate expressions for Iron and Cobalt Catalysts. Int. J. Chem. React. Eng. 2013, 11, 309–330.

[99] Eric, H.; Iglesia, E. Slurry Bubble Column (C-2391). U.S. Patent No. 5,348,982, 20 September 1994.

[100] Farias FE, Silva FR, Cartaxo SJ, Fernandes FA, Sales FG. (2007) Effect of operating conditions on Fischer-Tropsch liquid products. Latin American applied research. Oct;37(4):283-7.

[101] Komvokis, V. G., Karakoulia, S., Iliopoulou, E. F., Papapetrou, M. C., Vasalos, I. A., Lappas, A. A., & Triantafyllidis, K. S. (2012). Upgrading of Fischer–Tropsch synthesis bio-waxes via catalytic cracking: Effect of acidity, porosity and metal modification of zeolitic and mesoporous aluminosilicate catalysts. Catalysis today, 196(1), 42-55.

[102] P. Gross, R. Rauch, H. Hofbauer, C. Aichering, R. Zweiler, (2015) Winddiesel Technology- An alternative to power to gas systems, 23rd European Biomass Conference and Exhibition, Vienna, Austria.

[103] Hu, J., Yu, F., & Lu, Y. (2012). Application of Fischer–Tropsch synthesis in biomass to liquid conversion. Catalysts, 2(2), 303-326.